HURRICANE BONNIE WIND FLOW CHARACTERISTICS

by

JOHN L. SCHROEDER, B.S.C.E., M.S.

A DISSERTATION

IN

CIVIL ENGINEERING

Submitted to the Graduate Faculty
of Texas Tech University in
Partial Fulfillment of
the Requirements for
the Degree of

DOCTOR OF PHILOSOPHY

Approved

Accepted

December, 1999

ACKNOWLEDGEMENTS

I would like to express my deepest thanks to Dr. Douglas Smith, chairman of my committee, for the advice, and encouragement he gave to me throughout my graduate career. I would also like to thank Dr. Kishor Mehta, Dr. Richard Peterson, Dr. James Dunyak, and Dr. Joseph Minor for reviewing this manuscript, as well as their helpful suggestions throughout the completion of my dissertation.

A sincere appreciation is expressed towards the countless individuals who spent time in the field with me during the experimental phase of this project, and the students who gave me encouraging words when they were needed the most. I also owe a word of thanks to the office staff in the Wind Science and Engineering Research Center who offered their help in logistical support for this project. Above all, I thank my wife whose love, support, and patience has made the completion of my doctorate degree possible.

The project was supported by the Idaho National Environmental and Engineering Laboratory (INEEL) and the National Institute of Science and Technology (NIST).

CONTENTS

ABSTRACT

Whether convective influences result in localized areas of increased wind speeds and different turbulent structure than expected in a normal high wind situation has been debated for years. The question has been especially active concerning landfalling hurricanes. Given a lack of high-resolution wind speed data from within hurricanes necessary to resolve the debated questions, a field experiment was designed and conducted by Texas Tech University to acquire the necessary data.

The Wind Engineering Mobile Instrumented Tower Experiment (WEMITE), the first successful field experiment to place a reinforced, self-powered, instrumented tower directly in the path of several hurricanes, successfully gathered high-resolution wind speed data from within Hurricane Bonnie as it made landfall near Cape Fear, North Carolina, on 26 August 1998, at 5:00 PM.

These data are used to inspect the variations in turbulent characteristics of the wind during the passage of the storm. Specifically, turbulence intensities, integral scales, gust factors, and spectrograms are evaluated with respect to the surrounding meteorological events, such as the passage of rainbands. Comparisons are drawn between turbulence intensity and integral scale values present in Hurricane Bonnie, and those employed in the determination of the gust effect factor in ASCE 7-98. Wavelet analysis was also used to examine the incoherent model assumption employed in wind engineering.

LIST OF TABLES

LIST OF FIGURES

CHAPTER I

INTRODUCTION

In 1992, Hurricane Andrew made landfall in south Florida as a category 4 hurricane on the Saffir-Simpson Scale. The result was large-scale wind-induced damage to the man-made environment. Following the storm, engineers and meteorologists openly discussed the magnitude of wind speed produced by Andrew. Controversy swirled at that time, and disagreement still continues today. Fortunately, Powell et al. (1996b) have attempted some scientific quantification of Andrew's wind speeds. Powell's analysis represents the state-of-the-art in the determination of boundary layer wind speeds within hurricanes during and following an event. Unfortunately, even Powell's results are based on several assumptions including that the hurricane is semi-steady state, and the reduction of the wind speed with height is equivalent and equally predictable in different areas of the storm. Of course, the controversy surrounding Hurricane Andrew could have been reduced if most of the surface wind speed sensors had not failed during the event.

Recently new findings about the hurricane planetary boundary layer (HPBL) have occurred through the use of field instrumentation and remote sensing devices (Franklin et al., 1999; Wurman and Winslow, 1998). These discoveries include the presence of apparent boundary layer rolls (or wind streaks) and wind speed profiles that do not follow the anticipated reduction with height (Log-Law). This deviation from the expected wind speed profile is especially apparent in the most convectively active portions of intense hurricanes such as Hurricanes Georges and Mitch (1998) leading to the question of whether convective influences may result in localized areas of increased wind speeds and different turbulent structure than what is

expected in a normal high wind situation (different from neutrally stratified boundary layer flow which can be predicted by using Monin-Obukhov similarity theory). The importance of this to forecast meteorologists is obvious, but changes in the wind speed and/or wind speed characteristics such as turbulence intensity can also affect the mean and peak wind loads felt by structures. Thus the wind engineering community also has an inherent interest in developing a full understanding of the HPBL.

It is therefore the goal of this research to start to unravel the mysteries surrounding HPBL wind structure. The research objectives are to:

1. develop and construct a mobile apparatus to collect high-resolution wind speed data from within harsh environments;
2. collect high-resolution wind speed data from within hurricanes during the 1998 Atlantic Hurricane Season; and
3. complete a case study from the collected wind speed data focusing on variations in hurricane wind flow throughout the event.

The development of a rugged, mobile system is necessary due to the fact that there are a limited number of observation systems along the coast of the United States which are able to sample high-resolution wind speed data. Even with a technically capable system, most systems fail in extreme events due to inadequate instrument durability or mounting, or the data are not recorded due to a lack of backup power supply on the data acquisition system.

The 1998 Atlantic Hurricane Season was active, allowing the Wind Engineering Mobile instrumented Tower Experiment (WEMITE) to deploy the mobile apparatus in four different tropical systems: Tropical Storm Charlie (22 August, Rockport, TX), Hurricane Bonnie (26-27 August, Wilmington, NC), Hurricane Earl (3 September, Panama City, FL), and Hurricane Georges (27-29 September, Gulfport, MS). The case study presented here only uses the Hurricane Bonnie data set. Hurricane Bonnie

represents the best deployment and most complete data set from the 1998 season. Unfortunately, all of the deployments were for storms which had weak convective activity at landfall and can be classified as "stratiform." Therefore, the collected data do not represent an intense active hurricane at landfall, but one which is "winding down."

Regardless of the hurricane's state at landfall, the data provide an excellent opportunity to conduct a case study. The analysis of the case study focuses on two central issues:

1. whether or not there are storm-scale influences on the HPBL wind structure in Hurricane Bonnie; and
2. the validity of the incoherent model assumption which has traditionally been employed by the wind engineering community.

Certain material will have an immediate impact on the wind engineering community such as a statistical description of a "hurricane" wind for use in wind tunnels, and building codes. Included in this analysis is a comparison between this description of Hurricane Bonnie's wind flow and that currently incorporated in ASCE 7-98. More importantly, the research generates additional understanding of the interaction between storm processes and HPBL wind structure; this will result in a greater, long-term impact for wind engineering. The study employs data collected from the WEMITE tower, the National Weather Service (NWS) Automated Observation System (ASOS) in Wilmington, NC, and the Doppler radar data from the NWS Next Generation Radar (NEXRAD) in Morehead City, NC.

The achievement of these objectives is described in the following chapters. Chapter II gives the background used to complete this case study, including an up-to-date description of what we do and do not understand about the HPBL, and a description of the statistical techniques used in this study. Chapter III provides a detailed summary of the WEMITE apparatus.

Chapter IV offers a description of the Hurricane Bonnie deployment. Chapter V summarizes the analysis performed. Chapter VI contains conclusions from the aforementioned objectives and recommendations for future efforts.

CHAPTER II

BACKGROUND AND HISTORICAL RESEARCH

2.1 Hurricane Planetary Boundary Layer

In general, the boundary layer (BL) is the lower portion of the atmosphere affected by the earth's forcing (friction, heat) and responds on time scales less than 24 hours (Garrat, 1992). In the BL, there are two main sources of turbulence: mechanical mixing due to the interaction of the moving air with the earth's surface (friction), and convection (thermal buoyancy). Normally in high wind situations (>10 m/s), mechanical turbulence is expected to dominate over convectively generated turbulence (EDSU, 1982), and a neutrally stratified atmosphere is assumed, leading to the assumption that in the high wind environment of a hurricane with limited sunlight ground initiated convectively generated turbulence is limited.

While this assumption may be true, thunderstorms within a hurricane create updrafts and downdrafts that can penetrate into the HPBL. These convectively generated air motions created by the eyewall and rainbands may be responsible for most of the damage (Fujita, 1980) in certain hurricanes, and are the cause for 'miniswirls' or 'streaks' of severe winds (Fujita, 1992; Wakimoto and Black, 1993). Given that air from the upper portions of the HPBL or above is able to sustain itself to the lowest portions of the atmosphere within a downdraft, we cannot expect the airmass to have the same turbulent properties as if it were present in the lowest levels of the atmosphere from the start (Powell et al., 1996a). This scenario allows for localized areas with different wind speed magnitudes and characteristics. This results in peak gusts at the surface which are longer in duration and size than those encountered under the influence of mechanical mixing alone. The remaining unanswered questions are: how often might this scenario

occur; does this process only occur in intense eyewall convection or in other locations in the storm; is the process enhanced by eyewall meso-vortex activity; how efficient is the momentum transfer; and how much does it change the HPBL characteristics. It is thought that most of the updrafts and downdraft maintained within a hurricane are of limited magnitude, usually less than 3 m/s (Houze, 1993), although intense downdrafts do occur on a very limited extent. Black and Marks (1991) documented a downdraft in Hurricane Hugo (1989) of 9 m/s and an updraft greater than 20 m/s.

Recently, new technologies have arrived which allow for the acquisition of wind speed data from GPS dropsondes released from hurricane hunter aircraft (Franklin et al., 1999). Although highly controversial, the data obtained from these instruments during the 1997 and 1998 Atlantic Hurricane Seasons indicate that we understand little about the wind speed profile within the most convective portions of intense hurricanes. Wind speed profiles such as those found in the eyewall of Hurricane Guillermo depicted in Figure 2.1, show multiple wind maxima below 1 km occurring within a shallow boundary layer (Powell et al., 1999a), and vertical wind velocities on the order of –3 m/s (not shown), indicating the possibility of convective scale gusts, as there is a lack of surface induced friction (shear) evident in the profile. In addition, boundary layers have been observed to be as shallow as 200 m, providing for higher momentum air residing much closer to ground level than normally anticipated.

Ratios between the lowest dropsonde wind speed reading and the mean boundary layer (MBL) wind derived from the lowest 500 m taken within eyewalls shows a range from 0.6 to 1.0. But on average this ratio increases as the hurricane intensity increases, indicating shallower boundary layers are present in more intense hurricanes, and/or the presence of efficient momentum transfer associated with convective scales in the lowest portions

of the HPBL. These factors could yield higher gust factors within the eyewalls of more intense hurricanes than in moderate or minimal hurricanes and extratropical midlatitude weather systems.

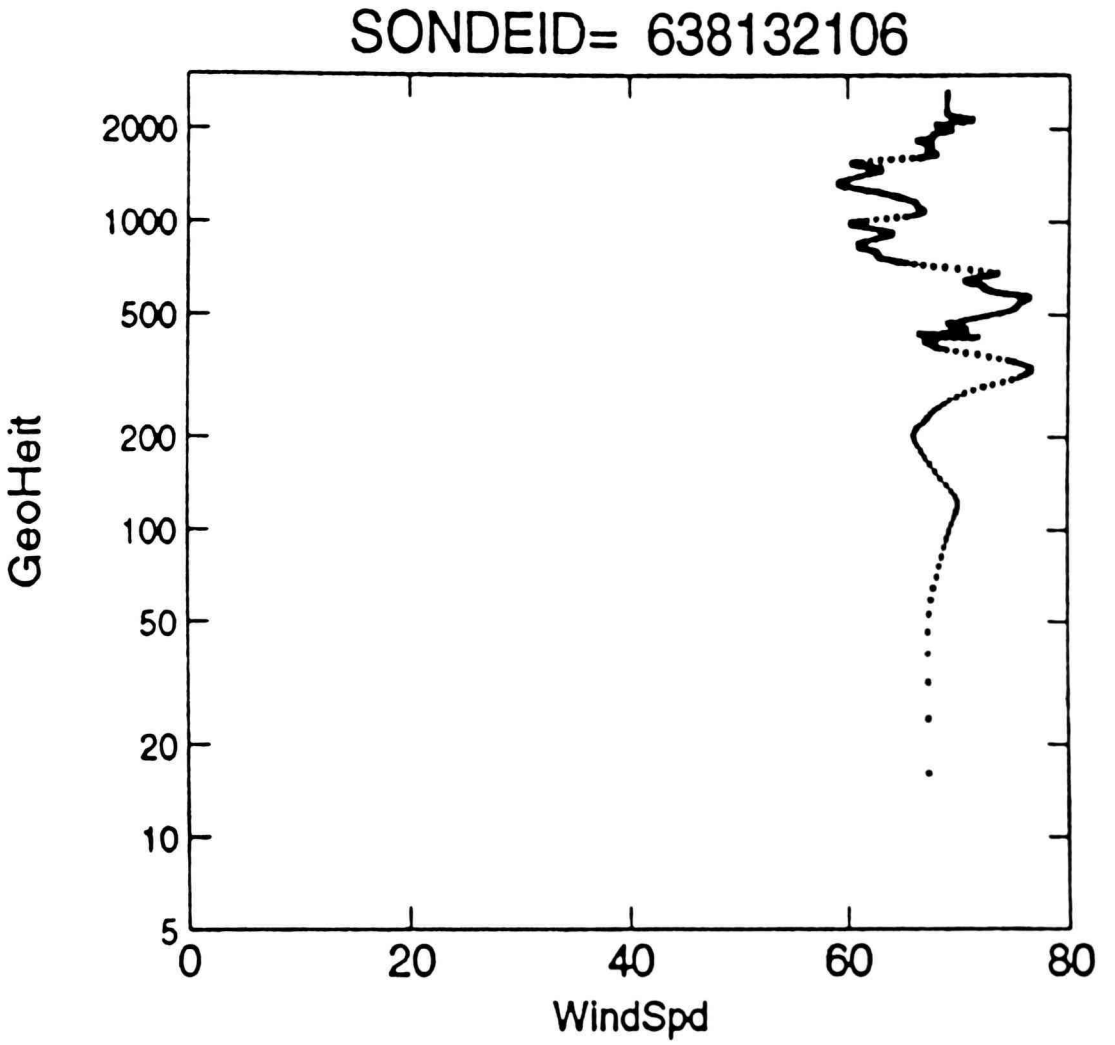

Figure 2.1. Hurricane Guillermo eyewall wind speed profile from GPS dropsonde (Powell et al., 1999).

These developments are a concern for wind engineers, as the governing wind load provisions may not account for the increased gust factors that may be present in certain instances such as these intense eyewalls. Also, the turbulent characteristics of the wind in an intense eyewall may differ from that expected in a normal high wind situation because the origin of the air mass may be from an elevated level.

Another recent technological advancement was the development of the mobile Doppler Radar on Wheels (DOW). Recently the DOW's have been deployed in the path of three landfalling hurricanes (Fran, Bonnie, and Georges). The data from these DOW deployments indicate the presence of linear wind streaks or rolls in the HPBL (Wurman and Winslow, 1998). While the origin of these streaks - most likely a shear instability (Frank Marks, Personal Communication) - is still unknown, their presence may indicate a fundamental deviation between the HPBL compared to that present in a west Texas "mixing down" event sampled at the Wind Engineering Research Field Laboratory (WERFL) at TTU. These streaks resulted in wind shear as high as 30 m/s over 300 m, as shown in Figure 2.2, and occurred in the lowest 500 m in Hurricane Fran. They were aligned essentially parallel to the mean wind flow and were only present when the mean wind speed reached a threshold value of about 50 m/s at 1000 m. An example of the high-resolution DOW data from Hurricane Fran is shown in Figure 2.3.

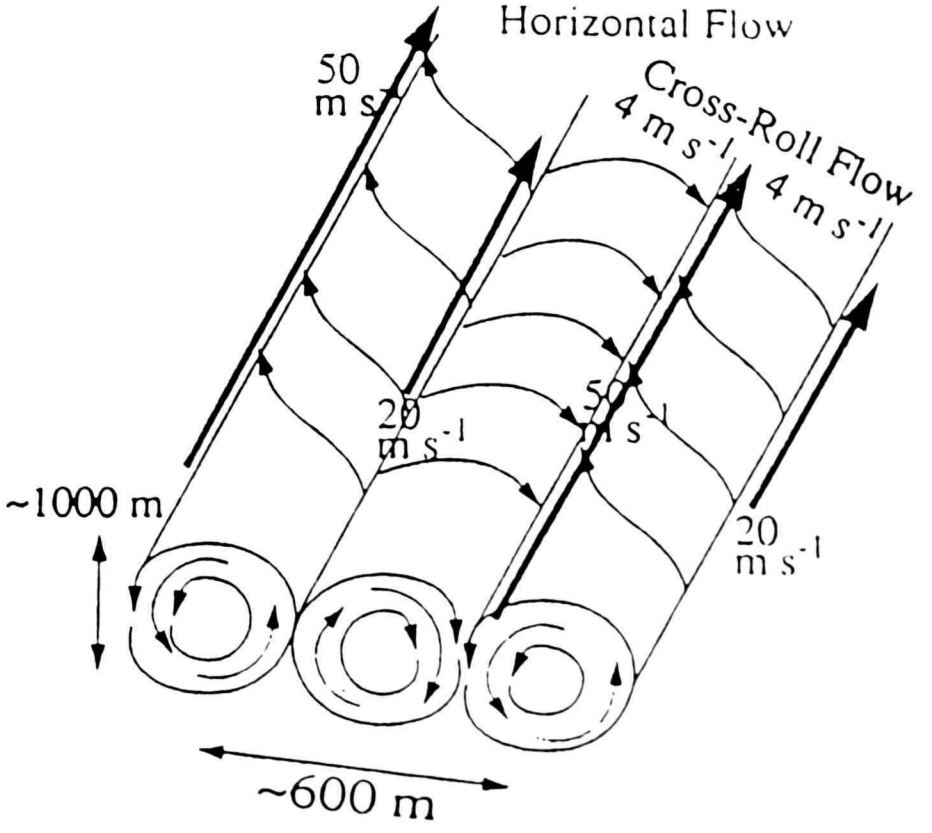

Figure 2.2. Schematic representation of HPBL roll structure in Hurricane Fran (Wurman and Winslow, 1998).

Time scales of these streaks are on the order of 2.5 to 8 seconds, and they result in gust factors of approximately 1.5. It is plausible that these streaks are related to some of the localized damage streaks noted in some post disaster investigations (Wakimito and Black, 1993; Fujita, 1992). However, Wurman concluded that the streaks are likely unrelated to the convective scale motions because thunderstorms within the hurricane are on the order 5 km or greater in scale.

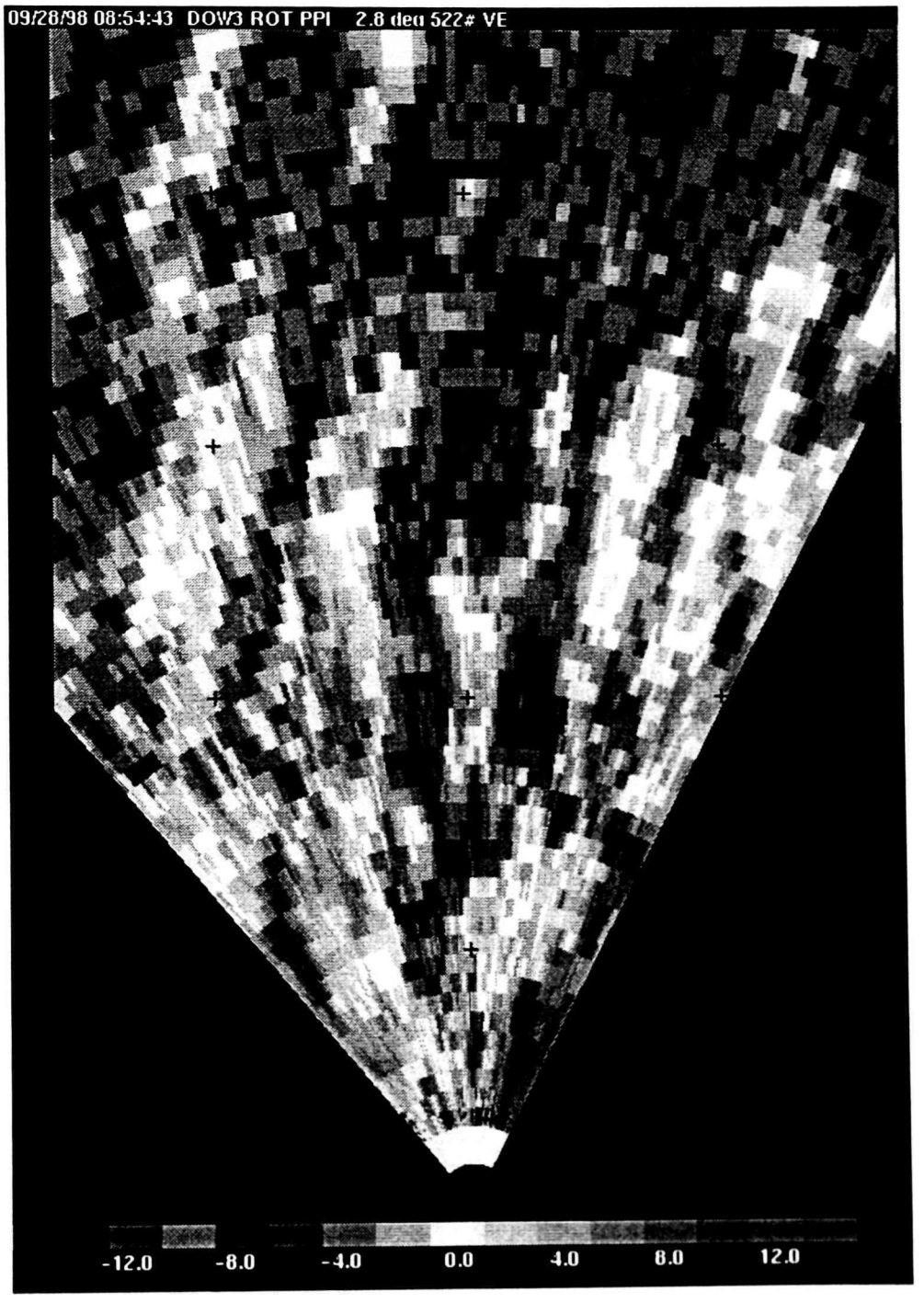

Figure 2.3. HPBL roll structure in Hurricane Fran as seen by the Oklahoma University DOW (DOW Internet Site).

2.2 Stationarity

Traditionally, wind has been considered a random process that is weakly stationary. This criterion allows for simpler evaluation methods to be used, but may not be fully accurate in most cases for winds which are of interest to wind engineers such as hurricane and thunderstorms. For a signal to be classified as weakly stationary the first two moments (mean and variance) of the signal must be independent of time (Bendat and Peirsol, 1986).

In a hurricane, wind direction changes and wind speed trends (ramp up and down) are inherent to the passage of the storm. Therefore, over a moderate length of time, the wind direction signal is nonstationary in the first moment; the same is true for the wind speed record. Complicating the issue, different upstream exposures can occur for different wind directions so the second moment (variance) of the wind speed record can vary with direction and thus time. Other complicating issues such as downdrafts can also increase the wind speeds or change the wind direction on a shorter time scale.

The majority of these issues can be handled in two ways: the signal can be detrended to remove the general trends found during the passage of a storm, or the signal can be broken into multiple data segments (smaller pieces) for evaluation. Since, wind is essentially viewed as a random process, multiple estimates of the same parameter are necessary to obtain reasonable confidence in distribution properties of the parameter. Therefore, using multiple data segments is beneficial. The other benefit to breaking the data into smaller segments is the ability to find changes in a parameter's value with time.

There are three traditional ways to evaluate the stationarity of a time series. These include simple visual observation, the run test and the reverse

arrangements test (Zao, 1992). The last two are non-parametric statistical tests. The run test is employed in this case study.

2.3 Wind Engineering Relevant Turbulent Flow Characteristics

2.3.1 Turbulence Intensities

The peak wind loads on a building or building component are affected by a parameter known as turbulence intensity (TI). This parameter is determined by normalizing the standard deviation contained in the wind speed record by the mean wind speed. Several studies have compared TI's determined from hurricane or typhoon records to those determined from extratropical winds or monsoon winds (Chuen, 1971; Choi, 1978, 1983; Ishizaki, 1983; Schroeder et al., 1998; Sparks and Huang, 1998). These studies have revealed no clear answer as to whether the TI is different within a hurricane or not; some have indicated increased TI's within hurricanes, while others have not.

TI's in high wind situations are dependent on several factors including the height of the anemometer and the upstream terrain conditions. Increases in anemometer height will normally decrease the TI, because the source of mechanical turbulence is the earth's surface. Therefore, more distance between the anemometer and the earth's surface reduces the variance in the wind record, and increases the mean wind speed resulting in a reduction of TI. Rougher terrain conditions will also increase TI for the same reasons; thus, some relationships can be drawn between roughness lengths, instrument height, and turbulence intensity, assuming neutral stability (Cermak et al., 1983).

Normally in wind engineering, the wind speed record is separated into longitudinal (along wind) and lateral (across wind) components, and TI's are calculated with respect to each of these components. It is important to realize that nonstationarities which may exist (first or second moments) in

the record may "artificially" increase the TI's. Schroeder et al. (1998) found just such a nonstationary data segment that inflated the lateral TI by approximately 300%, as shown in Figure 2.4. At the root of this artificial rise in lateral TI was a sharp change in wind direction coupled with a small trend in the wind speed record, inflating the lateral variance in the data segment and yielded a high TI. Nonstationarities in the first moments can have a remarkable effect on the TI, and changes in the second moments with time inherently change the variance and the TI. Therefore, stationarity can play a major role in the determination of TI's calculated from individual data segments. In general, however, the TI statistic is very stable even when calculated from data segments that are of length 5 minutes or less.

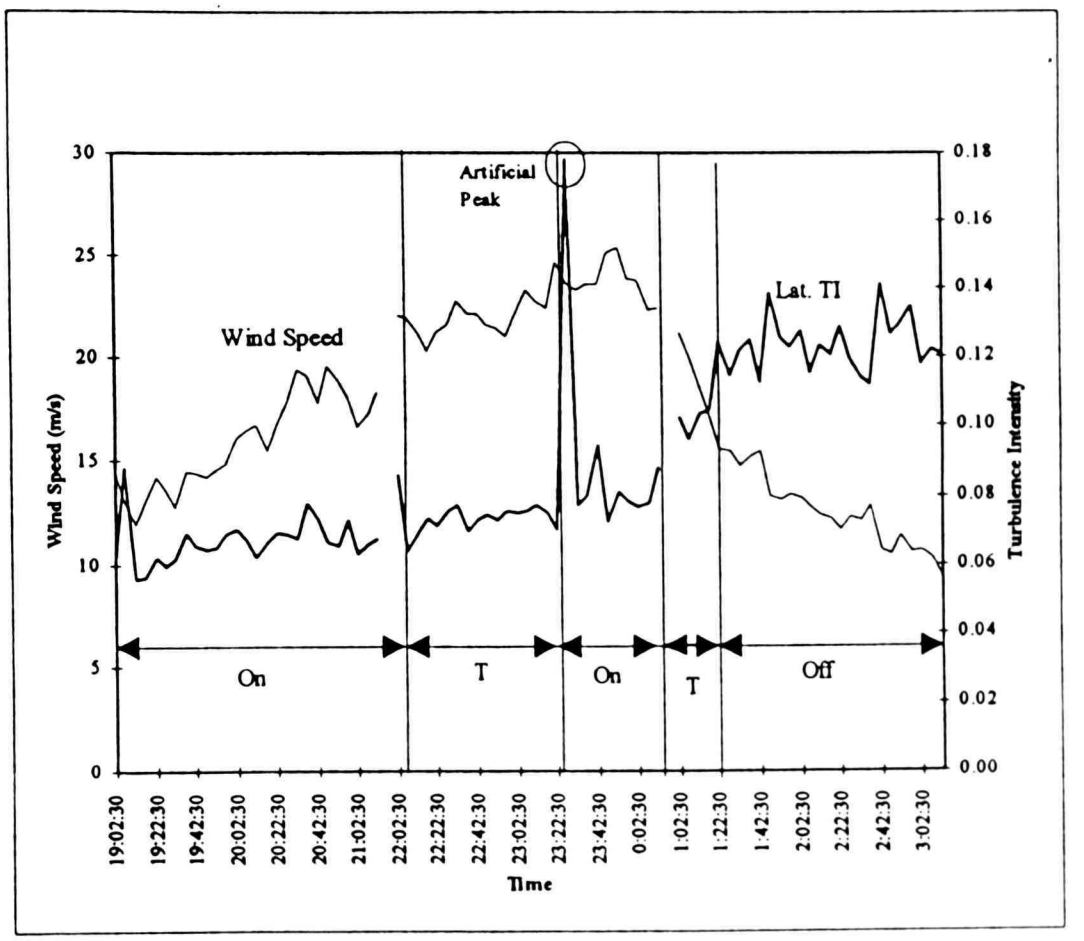

Figure 2.4. Time series of lateral TI's determined from Hurricane Bob (1991) (Schroeder et al., 1998).

Only a few people (Schroeder et al., 1998; Sparks and Huang, 1998) have evaluated the variations of TI with convective activity. These studies

involved looking at the evolution of TI's during the storm's passage, and whether or not TI's increased or decreased in the most convective portions of the storm. Given there are only limited data used in the studies, there is no evidence to suggest that TI's are affected by convective regions of the storm such as the eyewalls or the rainbands. However, TI's by themselves do not comprehensively describe the flow. In fact, two different signals can yield the exact same TI, even though they appear drastically different and contain different scales. This is shown in Figure 2.5 as each signal contains the same mean and standard deviation yielding identical turbulence intensity.

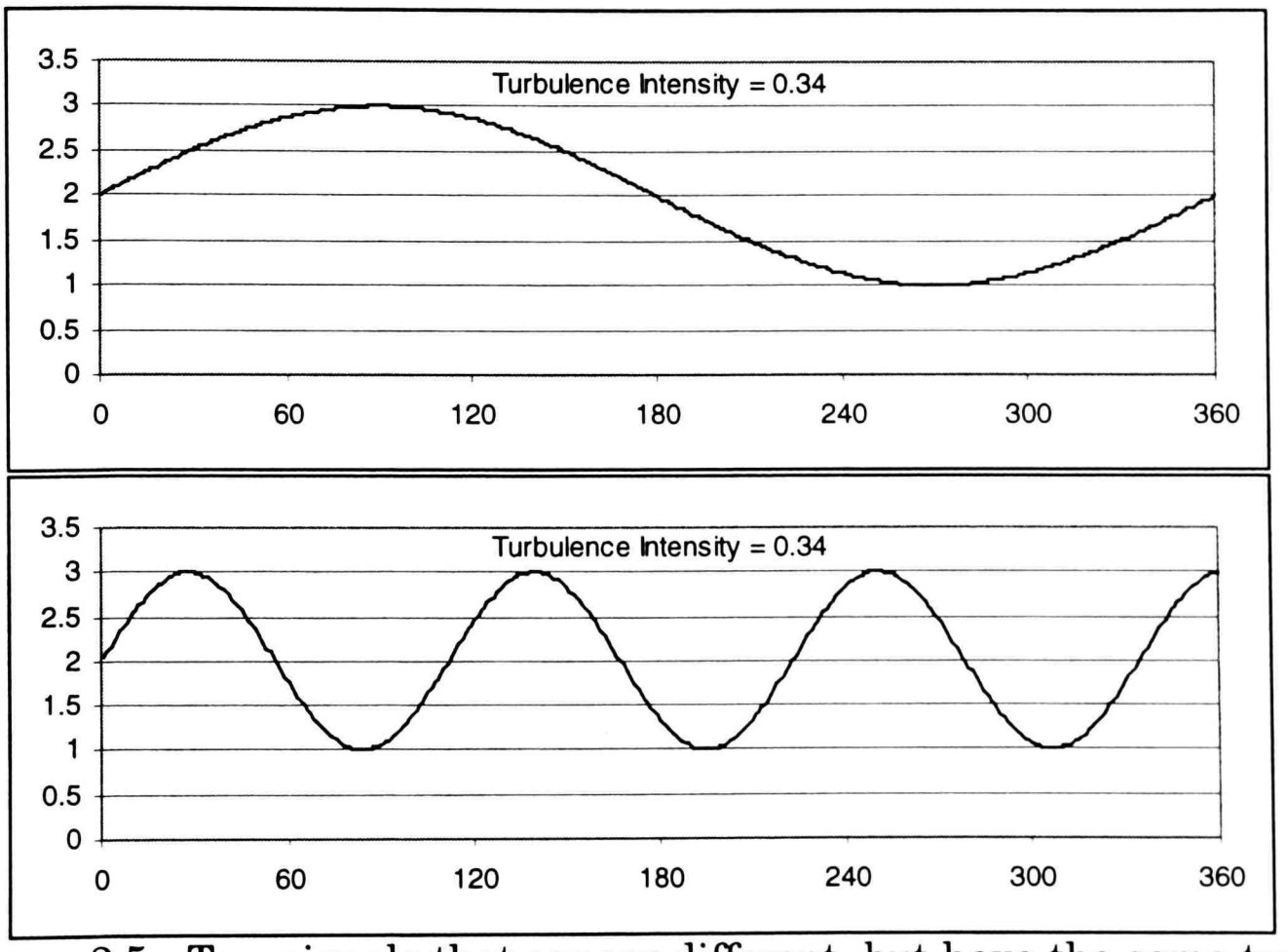

Figure 2.5. Two signals that appear different, but have the same turbulence intensity.

2.3.2 Gust Factors

A gust factor (GF) is defined as the ratio between the peak and mean wind speeds from a given data segment. Several recent studies have included analysis of GF in hurricanes including Mitsuta and Tsukamoto (1989), Powell

and Black (1990), Black (1992), Marshall and Krayer (1992), Bradbury et al. (1994), Maeda (1996), Sparks and Huang (1998, 1999), and Schroeder and Smith (1999). These studies have yielded conflicting results. Marshall and Krayer (1992), noting higher GF's within hurricanes than compared with extratropical winds, and Sparks and Huang (1998, 1999) indicating little difference between hurricanes and extratropical systems.

Marshall and Krayer standardized wind speed records from numerous hurricanes with respect to exposure (open terrain, roughness length = 0.03 m), and height (10 m) and compared the resultant GF's with Durst's (1960) and Cook's (1985) analysis. The results, as shown in Figure 2.6, indicate there are higher GF's for hurricane winds when considering peak wind gusts of duration less than approximately 90 seconds (using a mean hourly wind to normalize). In fact, the average GF (2-second peak to 10-minute mean) was found to be 1.55 within hurricanes compared to 1.40 as determined by Durst for extratropical cyclones. These higher GF's would then need to be accounted for in the design of structures and structural components in hurricane prone areas. Little reason was hypothesized for the increase in GF, but convective scale motions were mentioned.

Sparks and Huang (1998, 1999), on the other hand, examined numerous wind speed records from offshore and onshore sites, and concluded that there was little evidence of an increase in GF's generated within hurricanes compared to their extratropical counterparts. They concluded that Marshall and Krayer's results, which were generated from numerous airport sites, resulted from differences in roughness compared to those determined by Durst from data collected at Cardinton in the United Kingdom, and that a hurricane wind was essentially the same as any other wind. Sparks and Huang (1999) concluded that there is little evidence that deep eyewall convection affects GF's either; and that, in fact, there is a

reduction in the magnitude and variability of GF's found within the eyewalls of hurricanes.

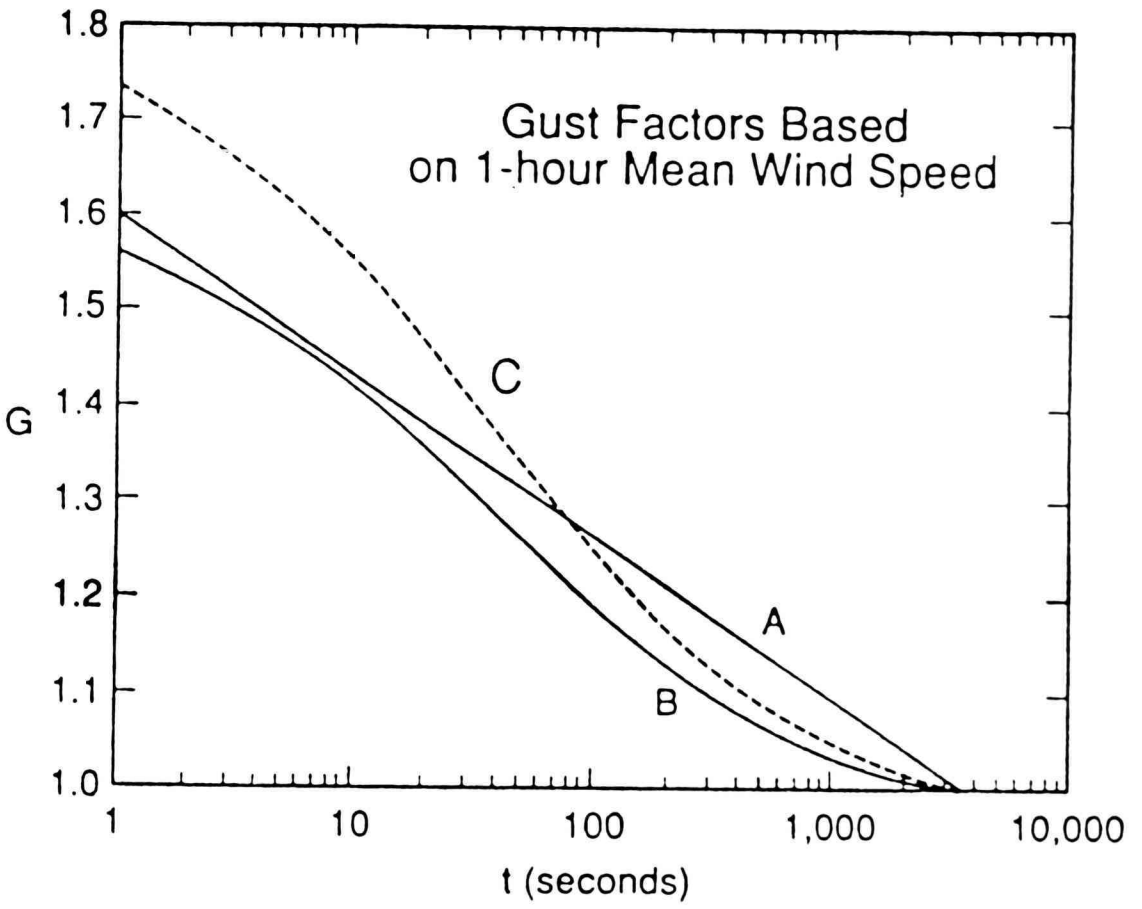

Figure 2.6. Cook (A), Durst (B), and Marshall-Krayer (C) GF curves based on mean hourly wind speeds and gusts of various durations (Marshall and Krayer, 1992).

GF's do increase with increasing surface roughness. The increased friction allows for more mechanical mixing (increasing variance), and reduces

the mean wind speed. These factors both promote increasing GF's. It is interesting to note that as a hurricane makes landfall, and the wind flow makes the transition from sea to land, the mean flow is expected to slow, but the GF's are actually increasing. One remaining question is: how fast does the onshore wind in the HPBL modify for changing roughness at the coastline? Currently, this is being openly debated; as Powell and Houston (1999b) indicate most of the changes occur within the first 1-mile of the coastline, while some numerical studies (Zhang et al., 1999) indicate that the changes occur much more slowly. If the numerical studies are correct, higher momentum air is reaching much further inland than once thought, and would need to be considered in the determination of the exposure categories within the national building codes and standards for the design of structures.

A reduction in GF's with height has also been found in hurricanes (Black, 1992). Given the mean wind speed is increasing with height, the peak wind speeds were actually found to be invariant with height. This invariance was attributed to the mixing of undiluted air to the surface (i.e., convection).

2.3.3 Integral Scales

Integral scales are effectively an average measure of the gust size along a particular dimension contained in the wind. They are usually calculated to determine the lateral, longitudinal and vertical extent of the longitudinal component of the wind (ESDU 74030, 1974). Integral scales are important to wind engineers because they offer a representation of the area on a building or structural component impacted by a wind gust, and thus are related to peak and mean wind loads.

Lateral and vertical integral scales are evaluated by employing the cross correlation between adjacent anemometers. Given the instrument

setup in WEMITE (no lateral spacing of anemometers and limited vertical spacing), only longitudinal integral scales are determined reliably. Of course calculation of the integral scales in the longitudinal direction assumes that Taylor's hypothesis is valid, which assumes that the turbulence field is "frozen" as it passes over the anemometer. This is usually a good assumption when the TI's are less than 50% (Willis and Deardorf, 1976). This criterion is met throughout this Hurricane Bonnie case study. Longitudinal integral scales can be calculated in several ways (Teunissen, 1980), including:

1. Integrating the autocorrelation function (ACF) generated from a wind speed record and multiplying the result by the mean wind speed to obtain a distance. Sometimes, the ACF is fitted with an exponential curve to facilitate the integration process;
2. Fitting a model spectral density such as the von Karman model to the determined normalized spectral density from the wind speed data, and then evaluating the peak in the model spectral density by employing an empirical equation. Conceptually, the peak in the spectrum represents a wavelength related to the longitudinal integral scale. Others such as Tieleman (1992) have suggested other spectral methods which do not require fitting a model to the data.

Only a few studies have been completed comparing typhoon and nontyphoon winds; these include Choi (1978) and Chuen (1971). Both of these studies found smaller length scales present in typhoon winds compared to monsoon winds. However it is plausible that larger integral scales would be expected in regions where convective-scale motions are active and unmodified air is effectively transported to the surface. Only one study (Schroeder et al., 1998) has compared integral scales for the same exposure and height within different portions of a hurricane. Although the data were

limited, the results indicated that larger integral scales may have been associated with the passage of some rainbands.

Just as with TI's, integral scales are affected by changes in exposure and height; therefore, they can vary with changing wind direction and anemometer location. As is the case with any other turbulence statistic, integral scales can only be compared within the same terrain regime, and at the same height. Increasing height yields increasing sizes of turbulence and integral scales, and increasing surface roughness increases mechanical friction effectively reducing the size of turbulent eddies and the corresponding integral scales.

As with TI's, stationarity of the record is again a concern when determining integral scales. When employing a spectral technique to determine integral scales, stationarity of the data record is assumed. Any localized changes in the variance content of the wind will be spread equally throughout the window. Nonstationarities in the record will also affect the ACF curve with trends inflating the right hand side of the curve, which can increase the resulting magnitude of the calculated integral scales. Given these issues, it becomes apparent that integral scales can be sensitive to the method employed to calculate them, and that care should be used when comparing one researcher's work to another. The focus of this case study is to look for variations in turbulence parameters throughout the record; the main concern is to calculate the integral scale uniformly. Therefore, changes can be evaluated with a constant baseline.

2.4 Signal Processing Techniques

2.4.1 Nonparametric Power Spectral Density Estimate

Traditionally wind engineers have examined wind records with the assumption that the signal is incoherent meaning that the phase information

contained in the signal is independent and uniformly (0 to 2π) distributed, and that for a stationary data segment, techniques such as a conversion to the frequency domain is a useful way of evaluating the signal. In completing a power spectral density (PSD), the energies contained in the signal at different frequencies are assumed to occur equally across the window. Therefore concentrations of energies at one location in time (coherent structures) are not resolvable by employing this time-to-frequency technique; these concentrations of energy are effectively averaged out of the resulting PSD. The method employed in this case study to determine the nonparametric estimate of the PSD (Bendat and Piersol, 1986):

1. Divide the data record into n_d blocks, each containing N data points;
2. Compute the N-point Fast Fourier Transform (FFT) for each data block;
3. Compute the PSD from the n_d blocks of data, where S_{xx} is the estimated power at an arbitrary frequency, Δt is the sampling interval, and X_i is the FFT of the original data segments, using

$$S_{xx}(f) = \frac{2}{n_d N \Delta t} \sum_{i=1}^{n_d} |X_i(f)|^2 \quad (2.1)$$

In employing such a technique the signal is assumed to be stationary, and any nonstationarities contained in the record will influence the resulting PSD. For instance, marked trends in the data will increase the amount of energy located in the low frequency bands of the PSD.

There are other considerations in using a PSD to evaluate a wind record, including the fact that anemometers with rotating components act as a mechanical filter to the data, effectively reducing the frequency content found in the high frequency end of the PSD (Thomas, 1996). To avoid this problem one can use a sonic or hot wire anemometer, but most of these

technologies are not conducive to harsh environments such as those found within hurricanes. Given the propeller-vane anemometers (used on the WEMITE tower) have rotating components, the resolvability of high frequency energies in the wind is limited. For instance, the R. M. Young Company Marine Wind Monitor anemometer can only respond at 5 Hz given a 13.5 m/s wind (distance constant = 2.7 m). Any increase in wind speed above that 13.5 m/s threshold increases its resolvability and decreases in speed reduce it.

Another problem, which sometimes occurs, is aliasing, where high frequency energy that can be resolved by the anemometer is wrapped into the PSD about the Nyquist frequency. The Nyquist frequency represents the highest resolvable frequency and is equal to the sampling frequency divided by two. For instance, a 10 Hz sampling frequency yields a 5 Hz Nyquist frequency. If the signal contains energies at the 7.5 Hz frequency, then this energy is wrapped back into the PSD at the 2.5 Hz level. This concept is shown in Figure 2.7. This problem is usually minimized for wind if the anemometer and sampling rate are chosen judiciously. Given that wind is assumed to have minimal energy below a frequency of 1 Hz, if the sampling rate is chosen at 5-10 Hz, yielding a Nyquist frequency of 2.5-5 Hz, the amount of energy available to "wrap" in via aliasing is minimal.

It is common in the wind engineering literature to use a normalized semilog plot for the PSD. This normalization process reduces the horizontal axis to reduced frequency. Reduced frequency is a nondimensional quantity in which the frequency is multiplied by the height of the anemometer and divided by the mean wind speed of the record. The vertical axis is the power multiplied by the frequency and divided by the variance. The advantage of employing such a technique is that PSD's generated from records with

different mean wind speeds and from different anemometer heights can be easily compared.

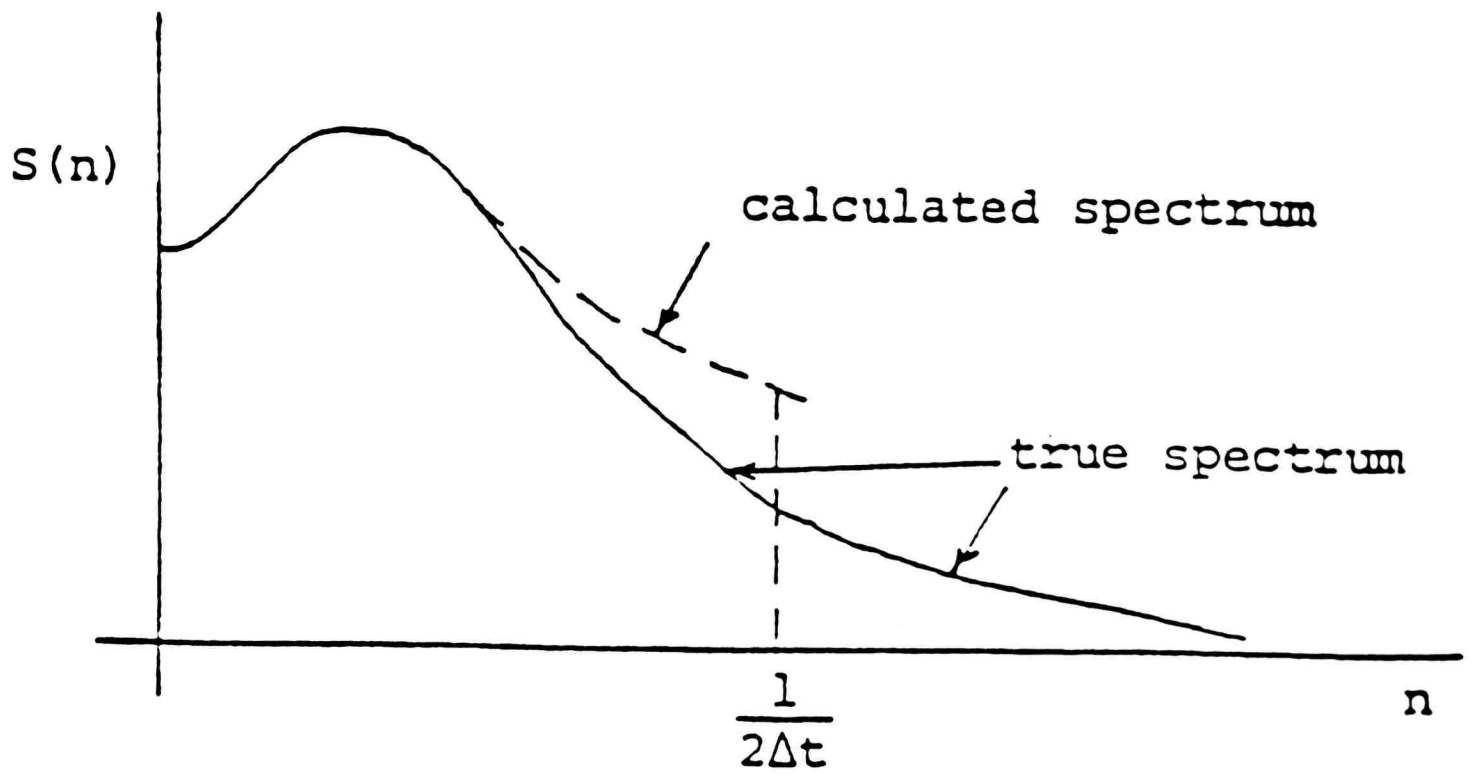

Figure 2.7. PSD illustrating the effect of aliasing (Holmes, 1989).

Very little work has been completed in comparing PSD generated from hurricane and non-hurricane winds, largely due to a lack of high-resolution data available for analysis. The little work which has been completed with hurricane wind speed data (Choi, 1978) indicates a higher amount of high frequency energy found in the record and (Powell et al., 1992) the presence of a convective peak shown in Figure 2.8 due to the passage of rainbands. Tieleman (1995) has developed several sets of universal spectra for high wind situations; some of these are shown in Figure 2.9 and used for comparison in this case study.

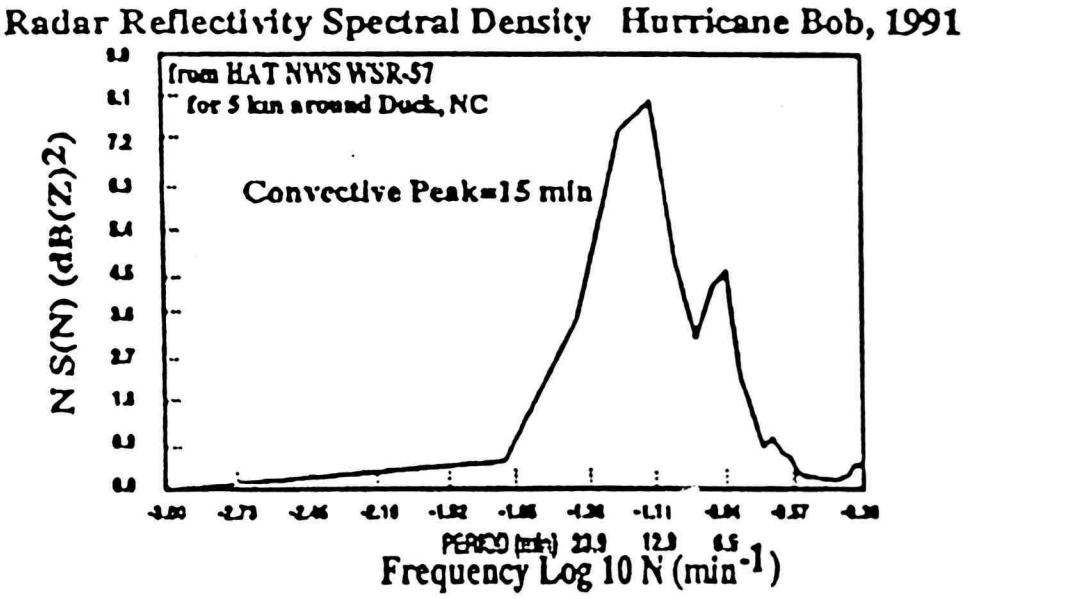

Figure 2.8. PSD's for wind speed and radar reflectivity from Hurricane Bob (Powell et al., 1992).

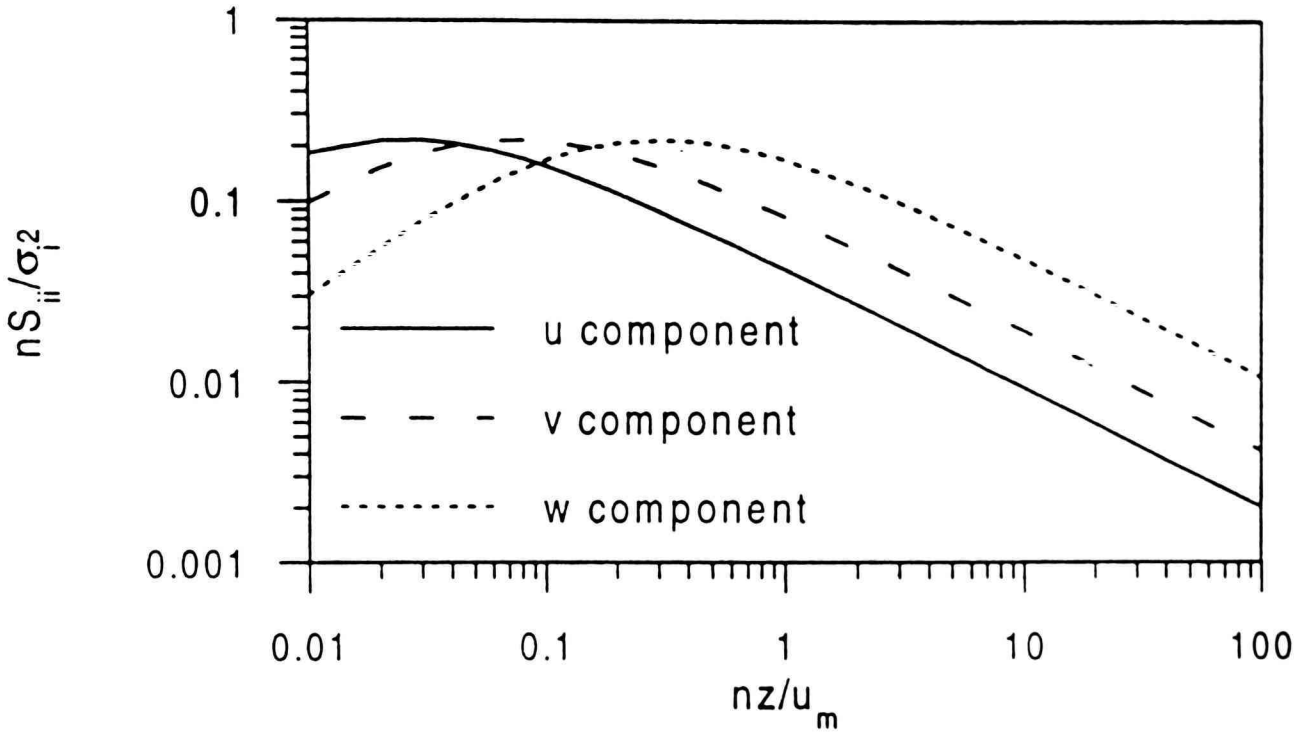

Figure 2.9. Perturbed terrain spectra developed by Tieleman (Geurtz, 1997).

2.4.2 Autoregressive Power Spectral Density Estimate

Another method of estimating the PSD of a given wind speed record is by fitting an autoregressive (AR) model to the time series. To do this several assumptions need to be made (Smith, 1993):

1. the wind speed observations are equally spaced in time;
2. the observations are a random variable;

3. the white noise used in the model is assumed to be Gaussian;
4. the index set for the process is time, T = ...,-2, -1, 0, 1, 2,...;
5. the time series represented by the AR model is stationary with zero mean.

In general, the AR model assumes that at a given point in time, the value of the stochastic process can be represented by a linear relationship between the previous terms in the time series and an error function represented by white noise. The order of the model is established by how many terms are used. For instance if the AR model is of order 3, then AR(3) is

$$X_t = \phi_1 X_{t-1} + \phi_2 X_{t-2} + \phi_3 X_{t-3} + Z_t \quad (2.2)$$

AR models of minimal order (2 or less) have been shown to represent a time series of high wind well (Reed and Scanlan, 1984). Once the model coefficients are obtained the PSD can be directly obtained from (Brockwell and Davis, 1991)

$$f_x(\lambda) = \frac{\sigma^2}{2\pi}\left|1 - \phi e^{-i\lambda}\right|^{-2} \quad (2.3)$$

where $(1-\phi e^{-i\lambda})$ represents the modulus of time.

The AR method provides for reliable estimates of the PSD for wind speed time histories even for short window lengths. This is advantageous, because it yields a less "noisy" estimate than its nonparametric counterpart. For more detailed information about AR models, the reader is directed to Smith (1993), Box and Jenkins (1976), or Brockwell and Davis (1991). Both the nonparametric and parametric methods are used in this case study.

2.4.3 Spectragram

Given the true focus of this case study is to evaluate changes in time of the wind speed record (i.e., changes in process) due to storm-scale influences, the utility of the frequency domain is limited. This is because strictly making a conversion to the frequency yields no information about changes may have occurred in time throughout the window. In fact, drastic changes in the process with time may make the time series nonstationary. To elevate the usefulness of the frequency domain in addressing the objectives of this study, another step must be taken. This step involves breaking the original time series into segments (Cohen, 1995), determining the nonparametric or parametric PSD for each segment, and plotting each PSD centered in time on the middle of the data window, as shown in Figure 2.10. The result is a 3-dimensional plot in which brighter colors indicate higher energy content, at a specific frequency and location in time. The generated spectragram can then be used to evaluate changes in frequency content of the wind with time.

The peak (brightest colors) in the PSD occurs at a frequency that is linearly related to the wind speed. This is because the plot does not employ reduced frequency, and increases in mean wind speed are represented, on average, by increases in energy content. Conceptually this makes sense; if the process remains the same and the wind speed doubles, then the "eddies" contained in the wind are passing by the instrument at twice the rate, and the resulting frequency content indicated on the spectragram is effectively doubled. Another change can occur if there is a change in upstream roughness. An increased level of mechanical mixing would yield a shift in the frequency content to higher frequencies on the spectragram.

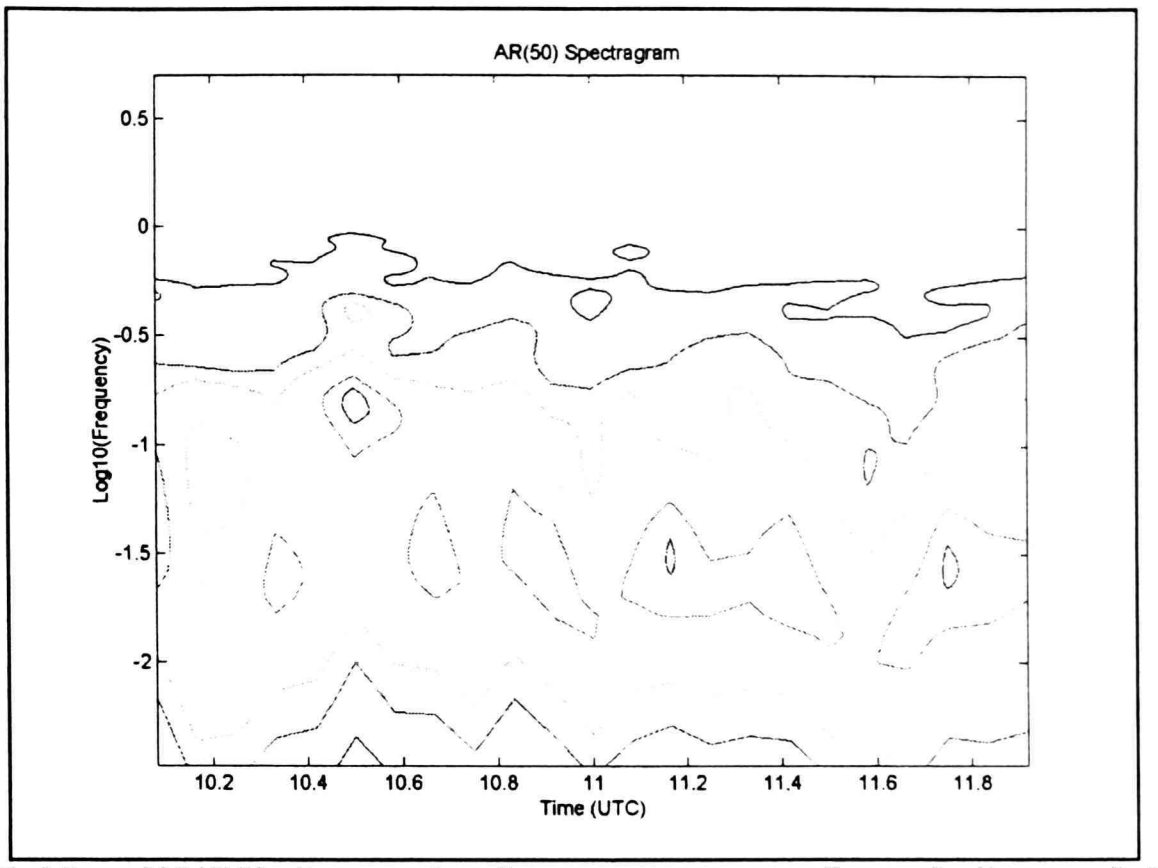

Figure 2.10. AR(50) determined spectragram of a wind speed time series. The time series is two hours in length and is broken up into 10-minute data segments for purposes of calculating the power spectrum.

2.4.4 Wavelets

Perhaps an even better approach to look for changes in the frequency or "scale" content of the wind with time is wavelets. Wavelets can be used as a bank of matched filters, which means the choice of the mother wavelet used in the analysis is important, because its shape is correlated with the original time series. Physically the shape may have some meaning; for instance, if we are trying to evaluate localized areas of increased turbulence we may want to use the Morlet wavelet shown in Figure 2.11. On the other hand, if we are trying to locate sharp directional change we may use the Haar wavelet, shown in Figure 2.12. These mother wavelets have been used to evaluate wind and other atmospheric phenomena (Acevedo et al., 1997; Meyers et al., 1993).

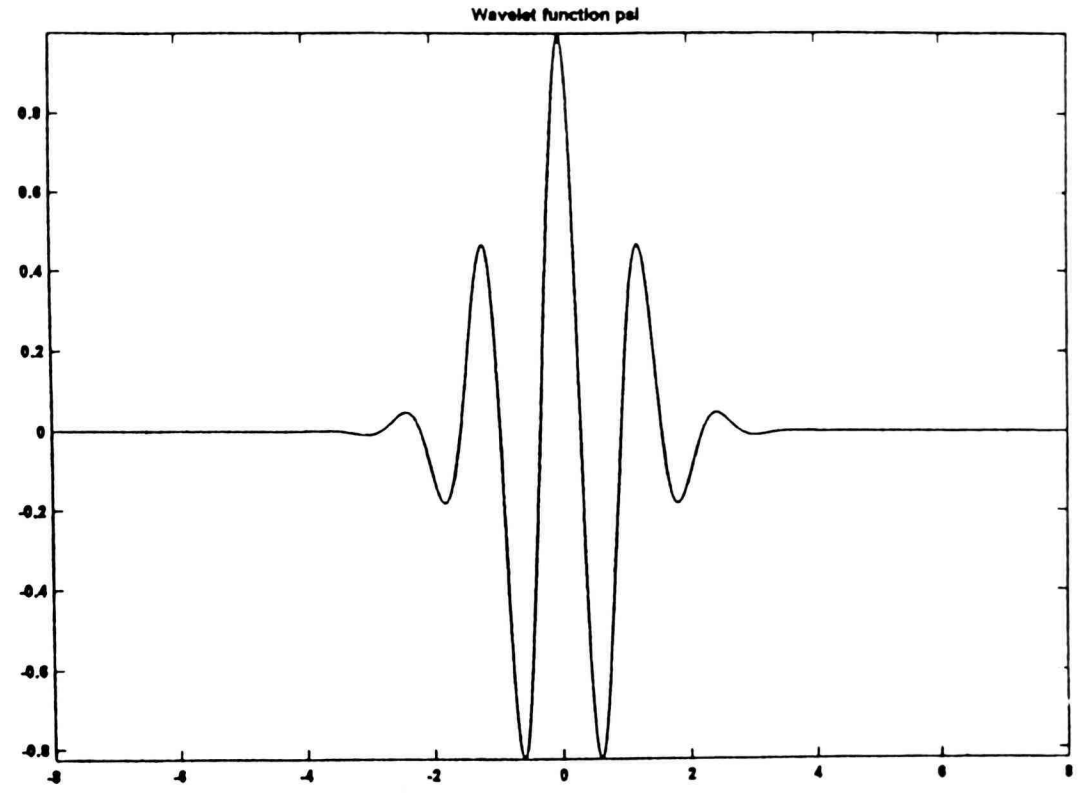

Figure 2.11. Morlet mother wavelet.

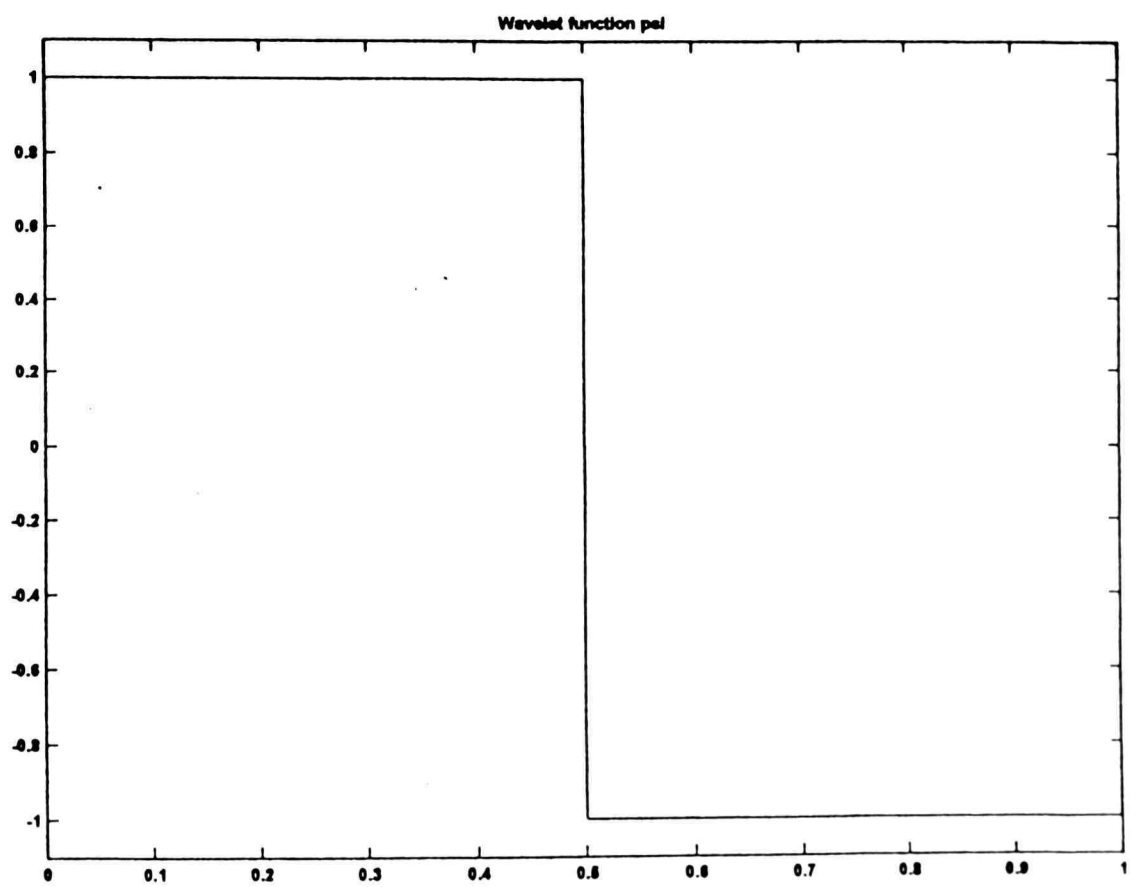

Figure 2.12. Haar mother wavelet.

The wavelet transform is defined as (Gilliam, 1998)

$$W_x(b,a) = a^{-1/2} x(t) * \overline{\Psi(\frac{t-b}{a})} \qquad (2.4)$$

where x(t) is the detrended signal, a is the scale, b is the position and ψ is the analyzing function. A continuous wavelet transform is performed by selecting a mother wavelet, producing scaled versions of the shape, individually offsetting the scaled shapes through the existing time series, and calculating the correlation between the individual scaled versions of the mother wavelet and the time series. These correlation coefficients are then displayed on a plot as a function of time and scale (amount of stretching or dilation) such as that shown in Figure 2.13.

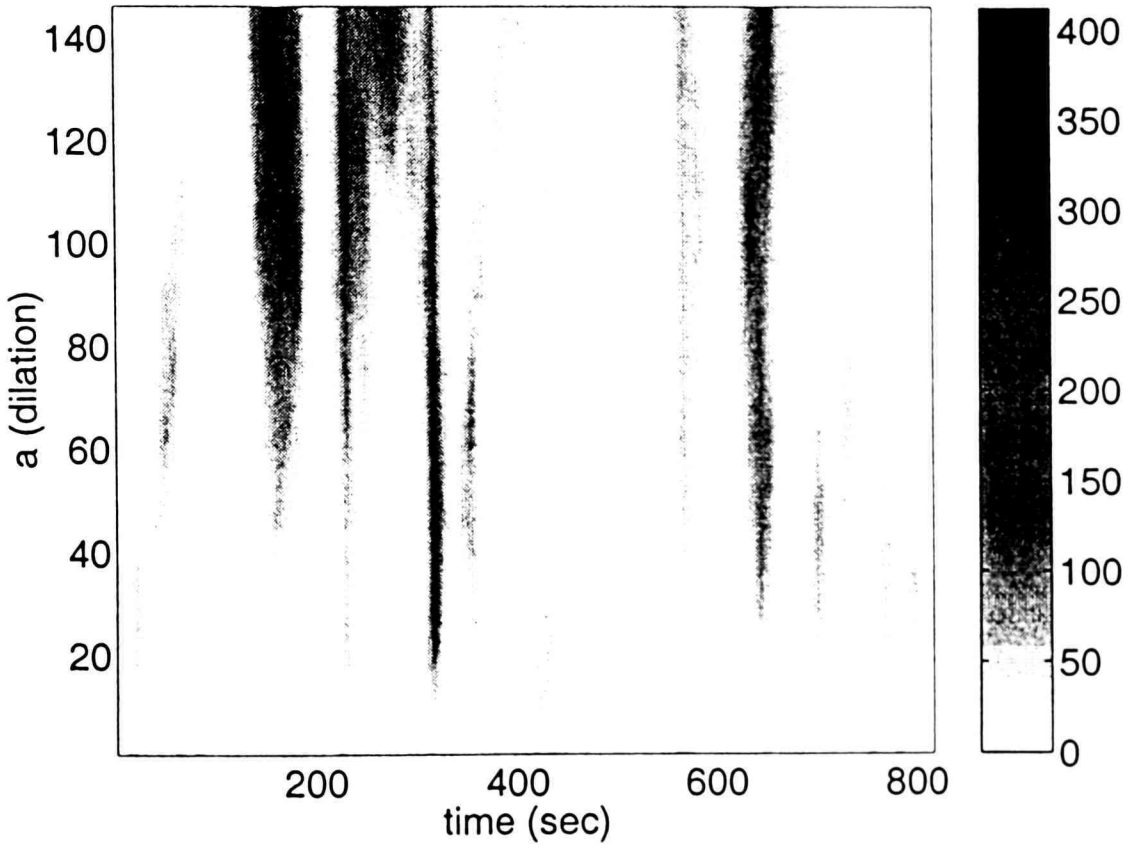

Figure 2.13. Plot of energy versus scale and time employing the Haar wavelet on a wind speed time series (Gilliam, 1998).

Given that coherent structures do exist in a record, spectral analysis would have a limited usefulness because it assumes the signal is incoherent and that the phase information is uniform and independent. It essentially averages out any concentrations in energy in time. Another important advance was made by (Dunyak et al., 1999) with the development of the coherent structure detector (CSD). The CSD uses a selected wavelet over a particular record to evaluate for the intermittent presence of coherent structures as did previous research, but the CSD also determines the likelihood that the occurrence of a given coherent structure occurred due to chance. To do this a PSD is evaluated for the given record, then assuming the record is incoherent and the phase information is random and uniform, additional time series are generated by using the same amplitudes determined from the original PSD, but randomizing the phase. These additional time series are called exemplars. A statistic is built based on all of the exemplar time series (which are incoherent by definition). This statistic can then be compared to the original energies determined using the mother wavelet, and a p-value can be determined for frequencies of interest. Conceptually, this p-value is related to the likelihood that the concentration of energy (identified coherent structure) really occurred, and was not just a random combination of energies which could be represented by an incoherent process. If the threshold value is chosen to be 0.05 for a given data segment such as is shown in Figure 2.13, and the plot is reduced to only statistically significant coherent structures, Figure 2.14 results. This represents the statistically significant areas of coherence.

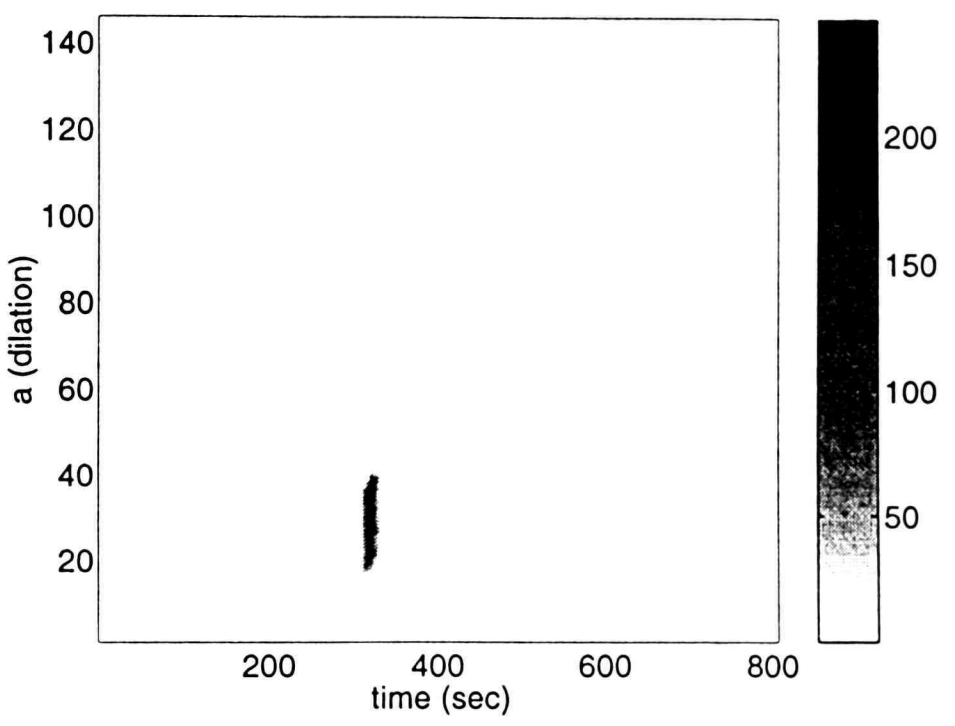

Figure 2.14. Results following application of the CSD at a threshold of 0.05.

CHAPTER III

WEMITE

Historically, hurricane wind speed data from conventional meteorological sites has been limited because in extreme events:

1. the mast fails;
2. the instrument fails; or
3. the power to the data acquisition system fails.

Unfortunately, even when the system survives, the wind speed is rarely sampled at rates high enough to improve understanding of the turbulent characteristics of the wind. These turbulent characteristics affect the static and dynamic wind loads on structures. Therefore creating a database of hurricane wind speed information is important, if one wants to reproduce a "hurricane" wind within a wind tunnel, full-scale, or CFD. The purpose of developing the WEMITE apparatus was to accomplish this specific goal, namely, to collect high-resolution wind speed data from within hurricanes. Therefore WEMITE focused on quickly deploying a properly instrumented, structurally reinforced, mobile tower in the path of U.S. landfalling hurricanes.

3.1 WEMITE Design Criteria

The WEMITE system was developed adhering to several key concepts including easy transport, quick deployment, protection of acquired data, and ruggedness. This led to the development of the following design standards:

1. the tower should withstand approximately a 67 m/s (150 mph) sustained wind (a strong category 4 storm on the Saffir Simpson scale);
2. the instruments should be rated to withstand approximately a 67 m/s (150 mph) sustained wind speed with higher gusts;

3. the data acquisition system should be protected from windborne debris and water intrusion;
4. the power supply should be protected and long lasting;
5. the entire system should take 1 hour or less to deploy;
6. the tower should be at least 10 meters in height;
7. the system should be able to collect high-resolution wind speed and other meteorological data for long periods of time continuously;
8. the system should contain duplicate instrumentation.

The tower and instrument survival rates are comparable, as one without the other is useless. The power supply was designed to run at least three days, allowing for complete data collection even for a slow moving or stalled hurricane. The power supply is also protected from water intrusion and the chance occurrence of "shorting out" the system. Overall, the protection of the collected data took the highest priority. Even if the tower fails in an extreme event, the data collected up to that point should be preserved for review and analysis. The minimum tower height is based on the World Meteorological Organization standard of 10 m, and most ASOS stations abide by this standard.

High-resolution temporal sampling of the data is required to establish the wind's turbulent characteristics. NWS ASOS stations provide some data including peak and average wind speeds, but not a time series necessary to calculate TI's or integral scales, not to mention performing signal-processing techniques useful in identifying coherent structures or a lack thereof. Some buoy data can also include the measured variance in the wind record over a given time period and can be used to calculate TI, but again no high-resolution time series is provided for detailed examination. From previous research (Tieleman, 1995) it has been shown that the wind has little energy above a reduced frequency of 1 Hz. The reduced frequency is a function of

wind speed so the actual energy content could be relevant even below 1 Hz within extremely high wind events such as hurricanes, but little is known about this regime (see Chapter II). Given this lack of information, and understanding that the final instrument selection would be a compromise between durability and response, a target sampling frequency of 5-10 Hz was established.

To create the most efficient apparatus it was decided to retrofit an existing 15.2 m (50 ft) mobile tower that was already in the possession of the TTU Department of Civil Engineering. Given the dimensions of the members for the existing tower were known, the final retrofitted tower design was developed by using a finite element analysis program called STARDYNE and applying wind loads as prescribed by ASCE 7-95. Complications of deploying the modified 15.2 m tower in moderate wind speeds became apparent and the tower height was reduced to 10.7 m (35 ft). Complementing the tower is a heavy, rugged trailer. Again TTU retrofitted an existing piece of equipment to efficiently accomplish the goal and used STARDYNE to arrive at the final design.

3.2 WEMITE Construction

3.2.1 Tower Construction and Details

In order for the WEMITE tower to withstand 67 m/s (150 mph) wind loads, several methods were utilized. The tower is guyed from the 10.7 m (35-ft) and 6.1 m (20 ft) level to the ground. The tower's three main legs, as shown in Figure 3.1, which were connected by 0.64 cm (¼ in) steel lattice to form a truss, were filled with 2 cm (¾ in) cold rolled solid steel bars that were slot welded by TTU personnel. Every effort was made to minimize any dynamic response of the tower to the wind, as any dynamic movement of the tower would be reflected in the collected wind speed data. Stiffening the

tower during construction and guying it in its final deployment state accomplish this objective.

Instrument arms at the 3, 6.1, and 10.7 m levels (10, 20, and 35 ft), as shown in Figure 3.2, are provided by welding 2.54 cm (1 in) diameter pipe to the tower. Cross bracing (adding static and dynamic resistance) is provided by 0.64 cm (¼ in) solid steel bars. The tower has three sections which telescope to reach the 10.7 m (35 ft) level.

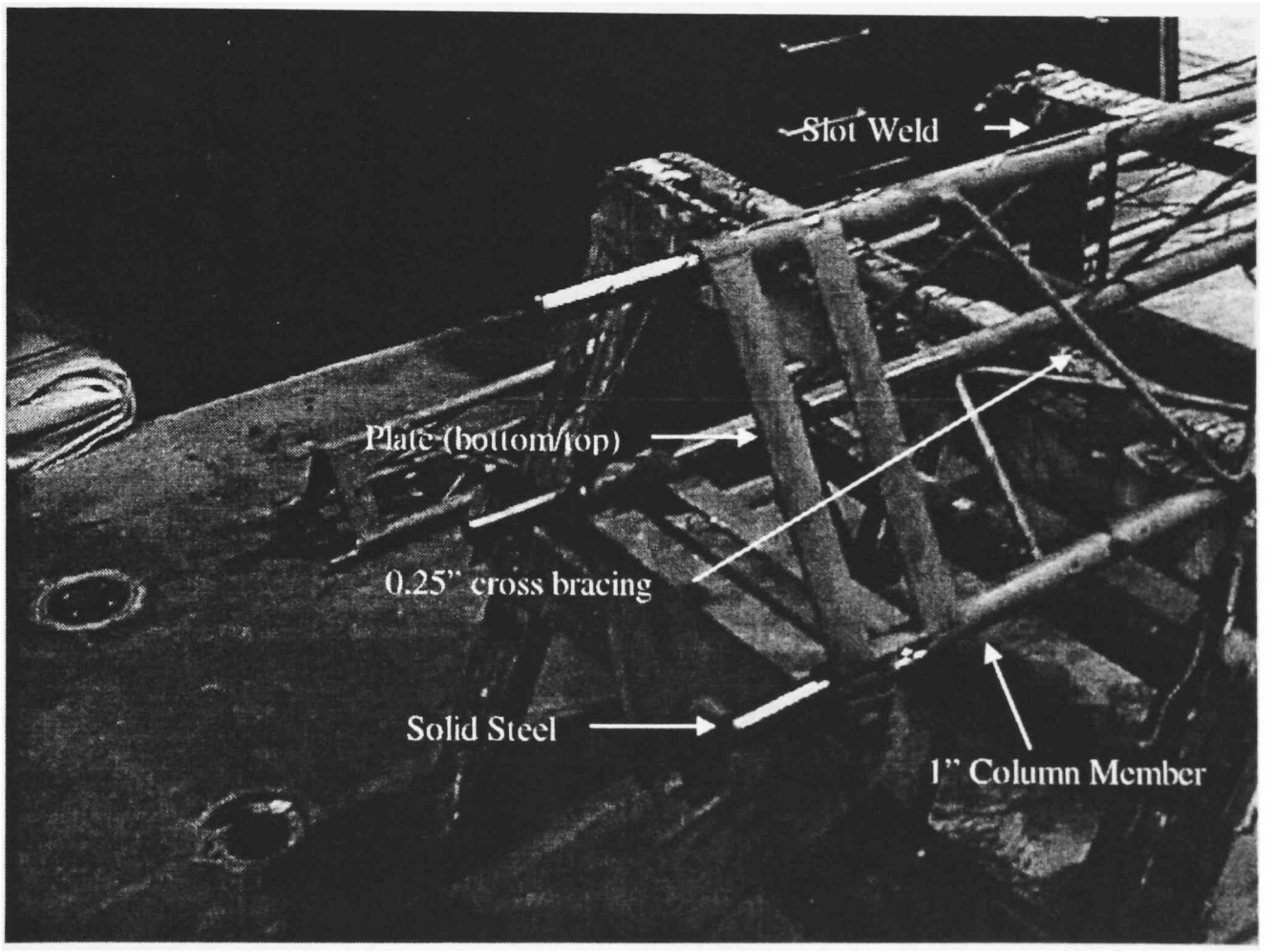

Figure 3.1. WEMITE tower structure details.

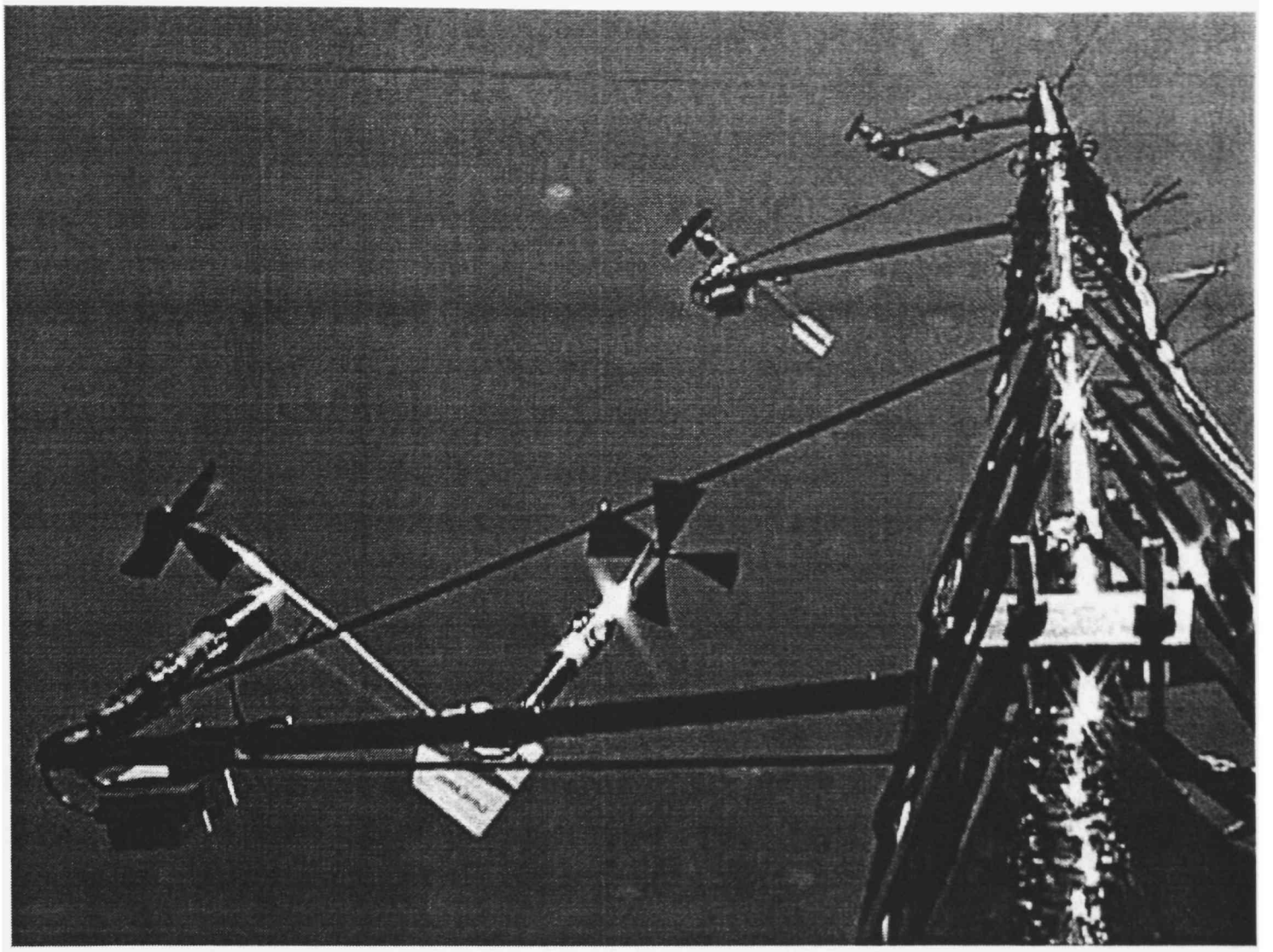

Figure 3.2. WEMITE instrument arms located at the 3, 6.1, and 10.7 m levels.

3.2.2 Trailer Construction

The original trailer was constructed of small channel (C4 X 5.4) sections. For the trailer to resist the forces developed in it by the attached tower, the structural frame had to be modified. The frame was strengthened by continuously butt welding small wide flange sections (W4 X 13) to the existing channel sections. Furthermore, 3.175 cm (1¼-in) thick plate was added across the entire width of the trailer at the front and back where the outrigger arms were mounted. Additional channel sections were also added to provide mounting brackets for the boxes that house the computer, multiplexer, and batteries.

Using a 7.62 cm (3 in) pipe as a focal point, the connection harness was created. At the top of the pipe a fulcrum was created for the tower to rotate

from horizontal to vertical. Cross bracing is provided by a series of 2.54 cm (1 in) pipes that stabilize and transmit the forces developed in the 7.62 cm pipe to the trailer. Bolts accomplish the connection of the harness to the trailer, allowing it to be removed for future changes. The trailer with the attached outriggers is shown in Figure 3.3.

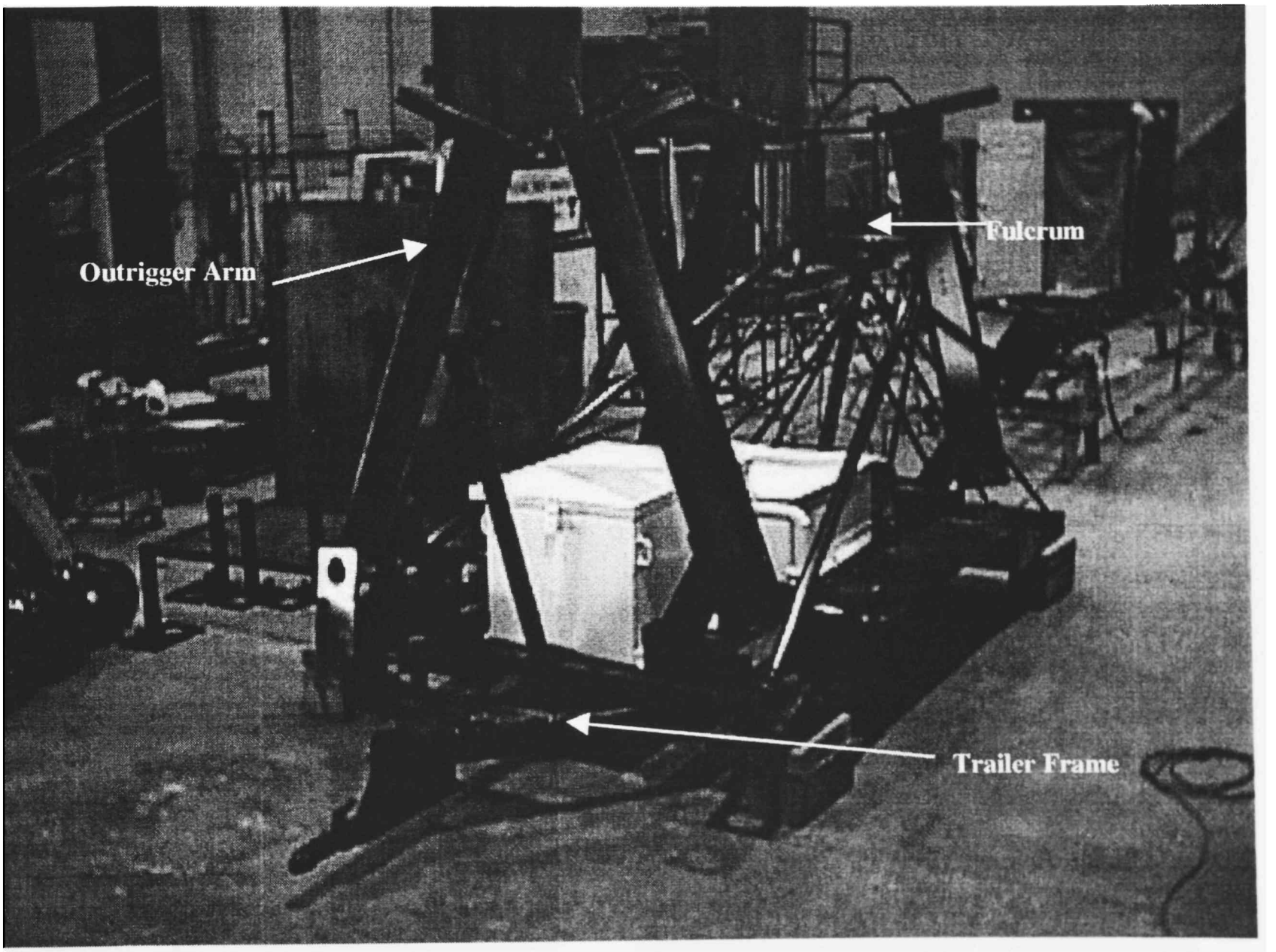

Figure 3.3. WEMITE trailer with attached outriggers.

3.2.3 Anchoring and Outriggers

Anchoring of the tower and trailer to the earth's surface was accomplished by modifying standard mobile home anchors, as shown in Figure 3.4. Two sets of anchors were constructed. The first set is 0.76 m (2.5 ft) long whereas the second set is 0.3 m (1 ft) long. By using two different sets of anchors it is possible to deploy the tower and trailer within many different types of soil conditions. Eight anchors are used during deployments, five for the trailer and three for the guy wires.

A typical outrigger arm is made of a 1.83 m (6 ft) long wide flange (W8 X 13) section with a modified jack placed on the end. The modifications made to the jacks include placing a 40 cm x 3.5 cm x 1.25 cm plate on the end and placing two pieces of all thread bolts between the foot and wide flange section. By placing the all thread bolts between the foot and beam section the outrigger arm gained the ability to resist tensile forces, as the jacks themselves could only support compression. A typical outrigger arm is shown in Figure 3.5.

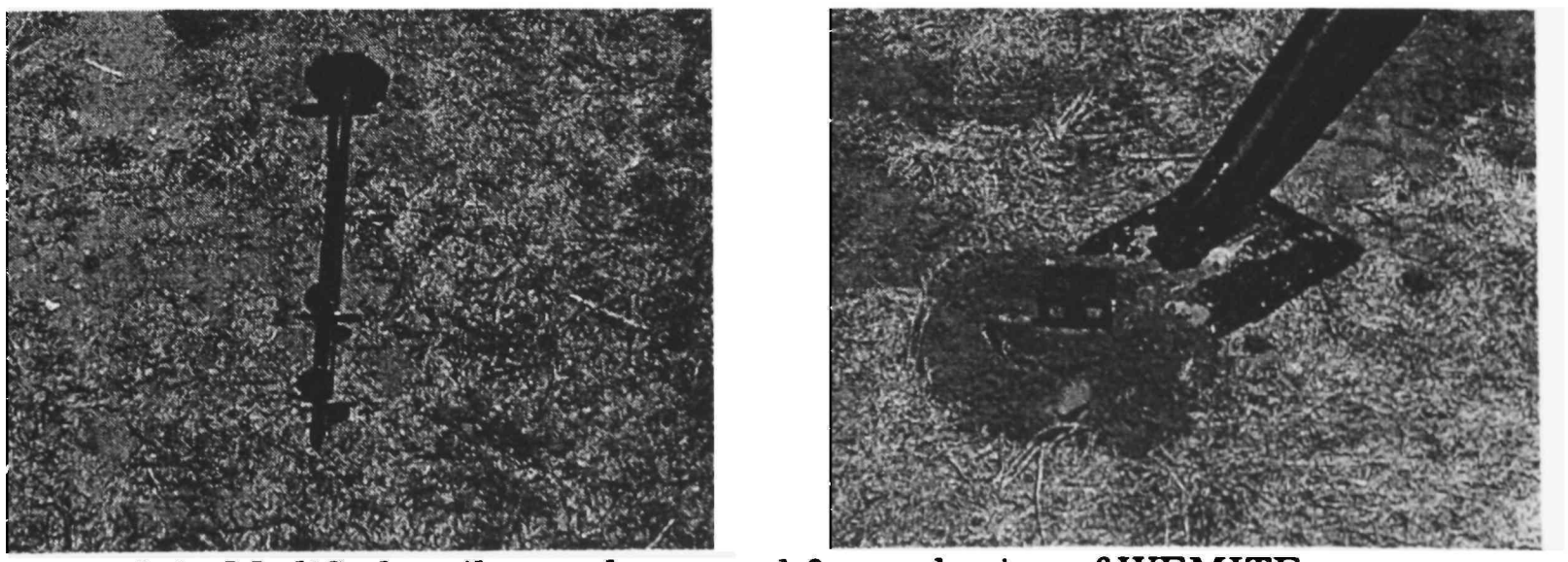

Figure 3.4. Modified trailer anchors used for anchoring of WEMITE.

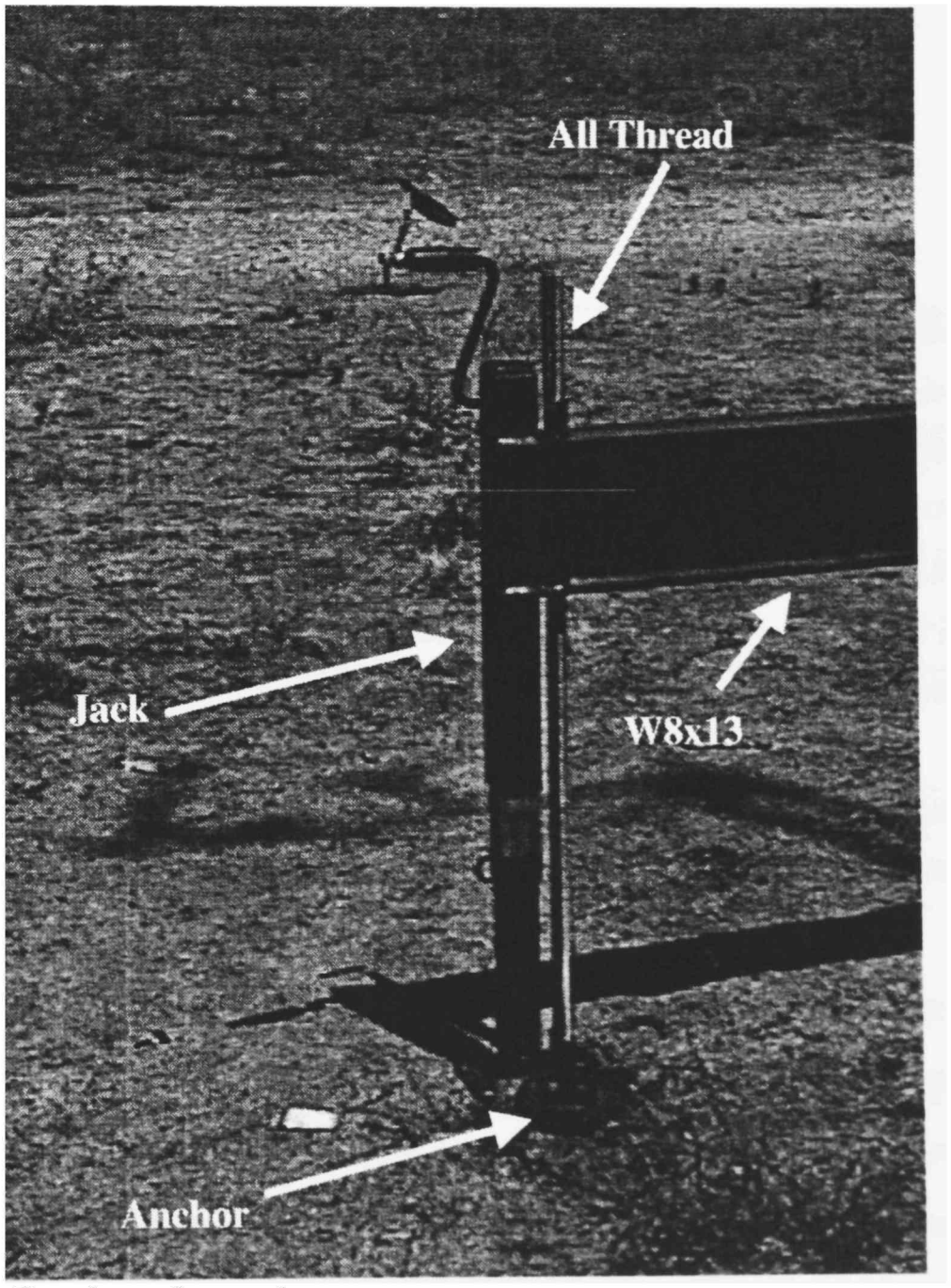

Figure 3.5. Deployed outrigger arm.

3.3 Instrumentation

Several types of meteorological data are collected by the system. Horizontal wind speed and direction at the 3, 6.1, and 10.7 m levels; vertical wind speed at the 3 and 10.7 m levels; and temperature, relative humidity, and barometric pressure are obtained at the 1 m level. The instrumentation employed on the WEMITE tower is based on a compromise between collecting high-resolution data, and providing the necessary durability to survive most hurricane winds. The WEMITE tower is instrumented at four levels as indicated in Table 3.1.

Table 3.1 WEMITE instrumentation.

Instrument Height	Sensor Type	Model Number
1.0 m	R.M. Young Barometric Pressure Sensor	61201
(3.3 ft)	R.M. Young Temperature/Relative Humidity Sensor	41372VC
3 m	R.M. Young Wind Monitor	05106 MA
(10 ft)	R.M. Young Propeller Anemometer	27106R
6.1 m	R.M. Young Wind Monitor	05106 MA
(20 ft)		
10.7 m	R.M. Young Wind Monitor	05106 MA
(35 ft)	R.M. Young Propeller Anemometer	27106R

Currently, all of the indicated instrumentation is available "off the shelf." According to its specifications, the instrumentation provides for wind speed data collection at 5 Hz given wind speeds are greater than approximately 13.5 m/s (for full response) as the distance constant is 2.7 and 1.3 m for the propeller and vane, respectively. The R.M Young Wind Monitor offers a rugged instrument rated at 60 m/s sustained and capable of surviving gusts to 100 m/s.

One complication to employing a propeller-vane anemometer is the dynamic resonance of the vane. Its natural wavelength is approximately 7.2 m which yields a natural frequency of about 0.36 s^{-1} in a 20 m/s wind. This additional energy will reside in the PSD of the wind direction; and since the lateral wind speeds are calculated in conjunction with the wind direction, this overshoot phenomenon will also be present in the PSD of the lateral wind speeds.

Accompanying each Wind Monitor is a serial interface box. These interface boxes convert the AC sine wave generated by the Wind Monitor into a DC voltage ranging from 0-1 volts. This DC voltage is proportional to the frequency of the AC sine wave and the wind speed. This voltage can then be read directly by the data acquisition hardware. The wind direction output is also 0-1 volts, but comes directly from the potentiometer located in the Wind Monitor. Therefore, although the wiring routes the wind direction signal from the Wind Monitor through the interface box, no further conversion or modification is made to the signal.

Vertical wind speeds are measured via a propeller anemometer. These anemometers provide for moderate durability (45 m/s sustained) and increased frequency response (distance constant = 2.1 m) compared to the Wind Monitors. Survivability in extreme winds is not an issue for vertically mounted anemometers, except for the windborne debris, as the mean wind speed is approximately equal to zero.

Barometric pressure, temperature, and relative humidity sensors are also sampled at 5 Hz, although their actual response times vary. The barometric pressure sensor, along with its accompanying pressure port will almost instantaneously measure the variations in atmospheric pressure, while the temperature/relative humidity sensor take approximately 42 seconds to fully respond. The temperature/relative humidity sensor has been

placed in a protective cover, shown in Figure 3.6, made from plastic pipe to guard against water intrusion in high wind environments. This plastic pipe has openings at the bottom and a small electric fan at the top to pull air through the system. The meteorological instruments provide valuable background information about the general nature of the storm, and may be important in linking storm-scale processes to surface layer wind characteristics. None of the instrumentation can survive significant windborne debris, but given the multiple levels of instrumentation and good siting procedures these problems are minimized.

3.4 Data Acquisition (DAQ) System

The DAQ system for WEMITE consists of a multiplexer board, analog to digital conversion (A/D) card, and a computer system. Analog signals are carried from the instruments via shielded, grounded wire to the National Instruments AMUX-64T multiplexer. The multiplexer is connected to the National Instruments #DAQCard-AI-16XE-50 PCMCIA A/D card using a shielded National Instruments #PSHR68 cable. The system provides for 16-bit resolution.

A Fujitsu Lifebook laptop computer is used as the control center for the entire data acquisition system. Lab View version 5.0 software is used to direct the data collection effort. Custom, streamlined programs have been configured within Lab View thereby allowing WEMITE to sample at various sampling rates. Plots are displayed in real time on the laptop screen allowing for the user to verify instrument output and validate the data upon deployment.

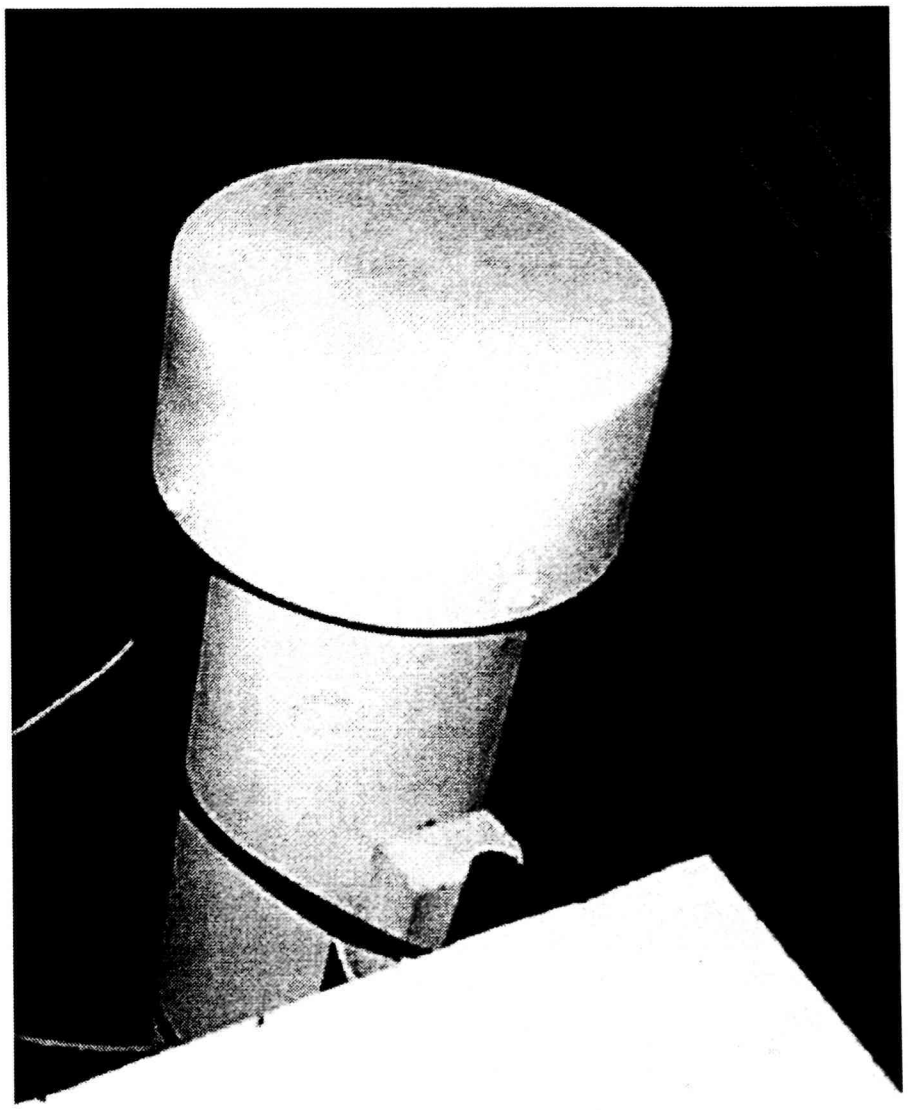

Figure 3.6. Plastic protective housing for the temperature/relative humidity sensor.

3.5 Power Supply Systems

A battery bank and wind generator supplies the power for WEMITE. When fully charged the battery bank provides a continuous 100-hour period of data collection capability without aid from the wind generator. The battery supply consists of four deep cycle marine batteries. The wind generator, as shown in Figure 3.7, is a Windseeker 502 and rated to 54 m/s (120 mph). When running it cannot only power the system, but simultaneously charge the batteries.

The system outputs 12 VDC power that is routed into a power inverter. The inverter converts the DC input into a 110 VAC output that can be used by the computer. Once converted, a DC regulator is connected to the 110 VAC supply and converts it back to approximately 15 VDC for use in all of the instruments that require power. The system is about 90% efficient, and is highly regulated. A diagram of the power supply and DAQ system is provided in Figure 3.8.

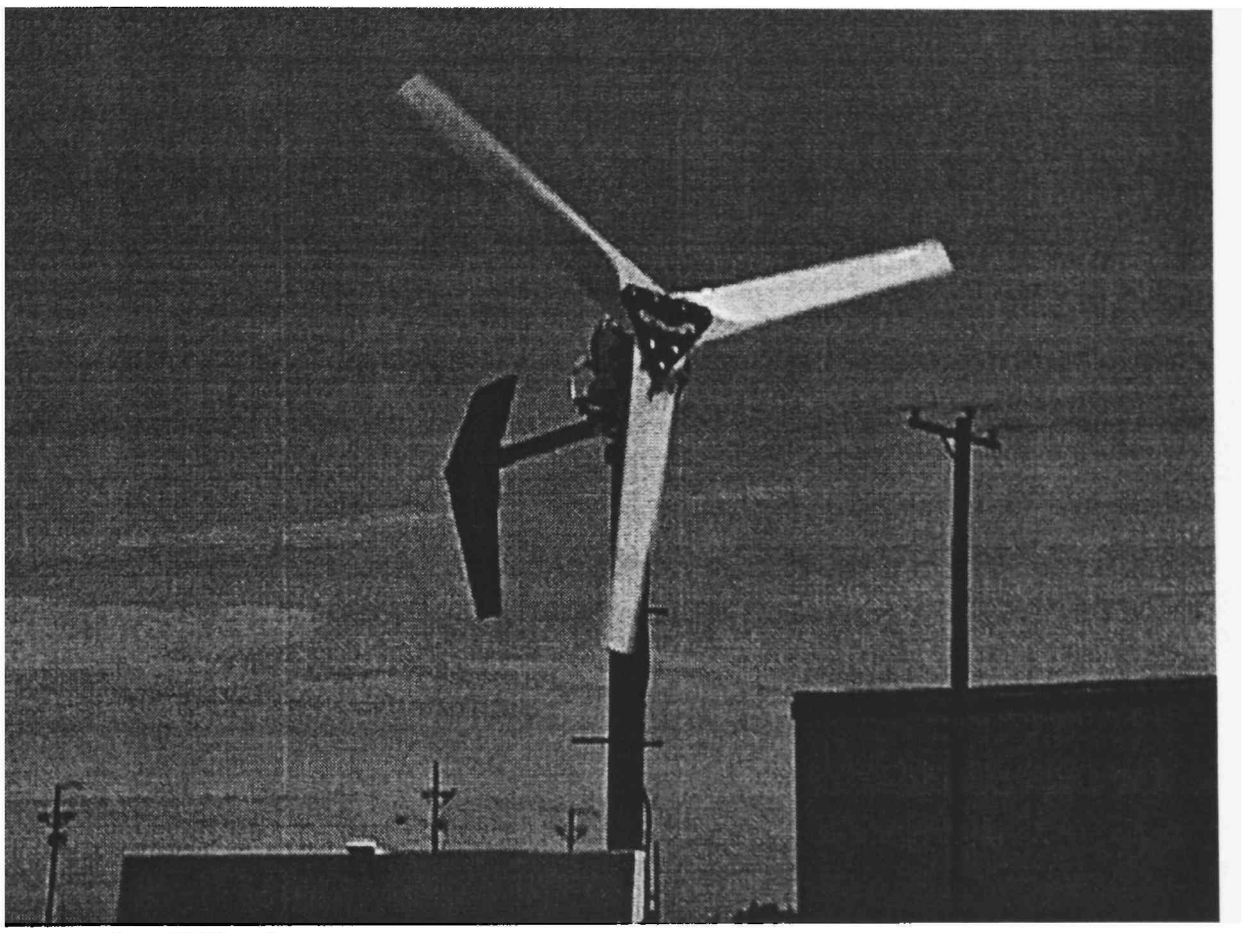

Figure 3.7. Wind generator.

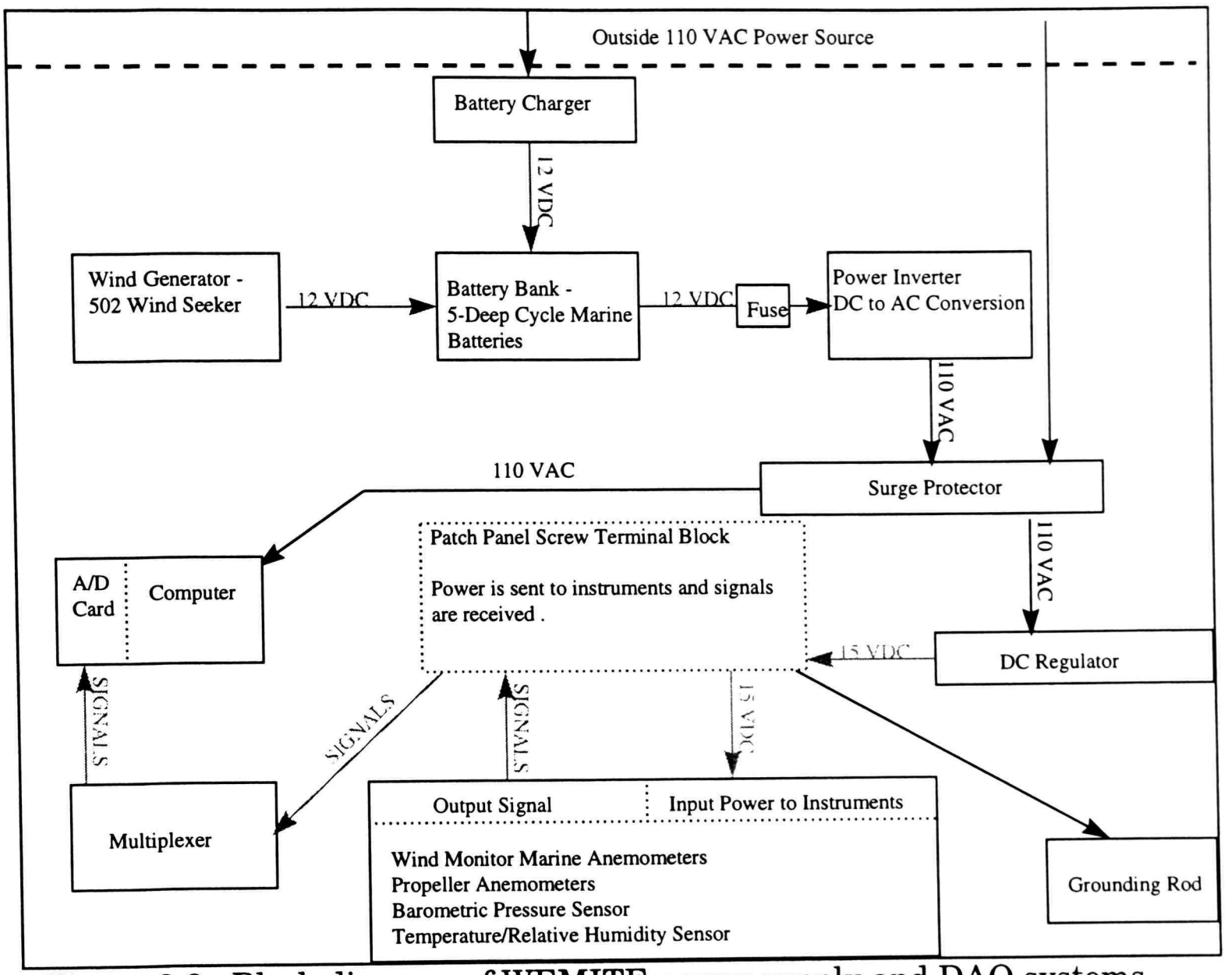

Figure 3.8. Block diagram of WEMITE power supply and DAQ systems.

3.6 Protection from Windborne Debris

In order to provide protection from windborne debris and water intrusion for the computer, multiplexer board, and the battery supply, special housing units were constructed. The computer and multiplexer board housing unit was designed to be a double-walled waterproof box, whereas the battery supply chamber was a single-walled waterproof unit. The inner wall of the computer/multiplexer unit is 0.32 cm (1/8 in) steel, and the outer wall is 0.95 cm (3/8 in) steel. The purpose of the double-wall system is to provide a dead air space to act as insulation for thermal reasons and also to supply a dynamic shock barrier from flying debris during an event. The outer covering

was found to be adequate by testing a steel section of the same dimensions and restraint. The test consisted of firing a 67 Newton (15 pound) wooden 5 x 10 cm (2 x 4 in) plank at 51 m/s (115 mph) at the section and noting damage.

3.7 Systems Integration and Testing

Within the computer/multiplexer protective box, a patch panel was installed. The patch panel enables power to be distributed throughout the system and also provides a means of organizing wires before entering into the multiplexer board. The multiplexer board was permanently affixed to the 2 cm (¾ in) plywood lining, unlike the computer system. The computer system is installed, but removable from its cradle for easy viewing and retrieval of collected data. The completed DAQ system box without the laptop computer is shown in Figure 3.9.

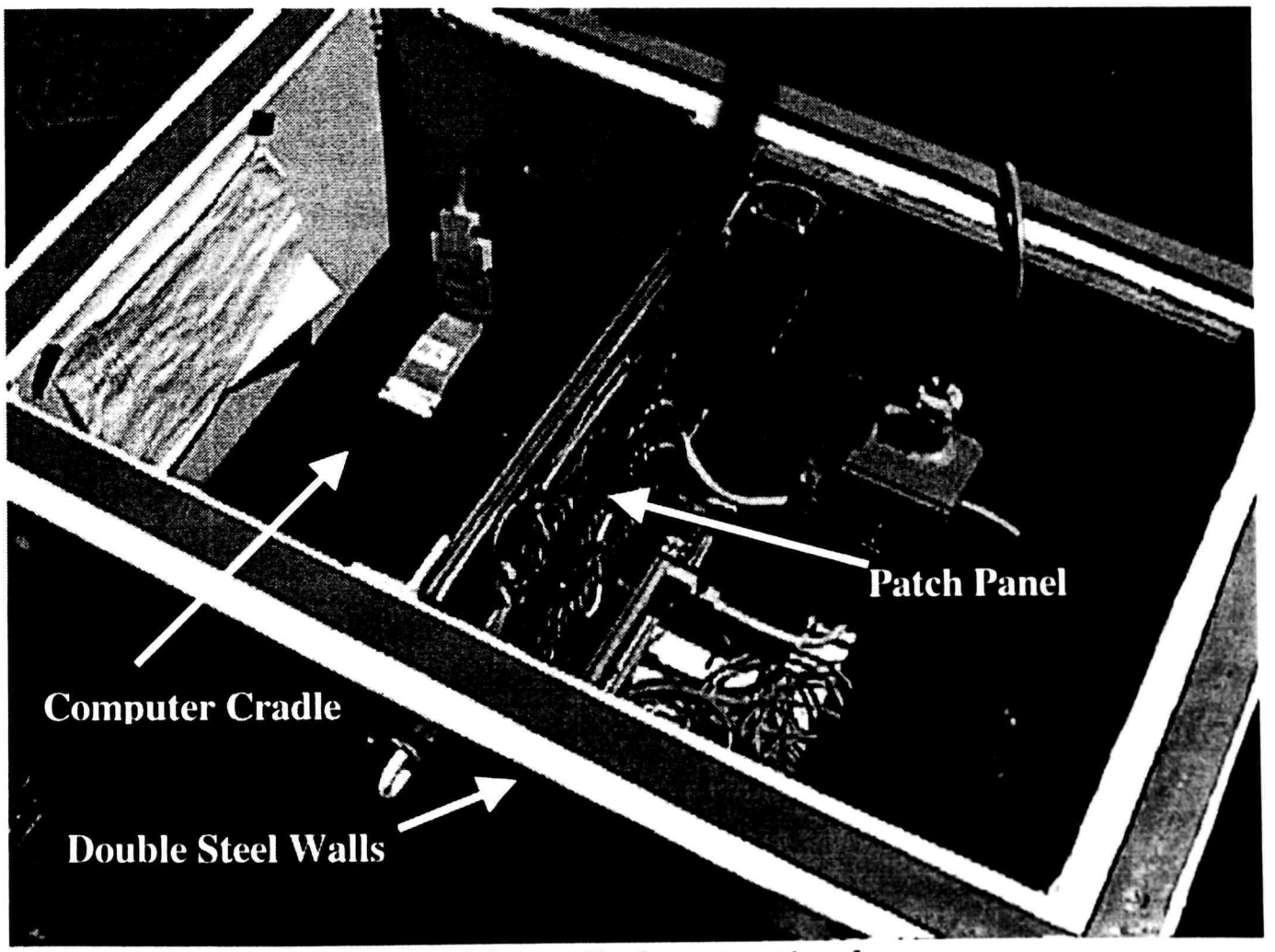

Figure 3.9. DAQ system in double walled protective box.

In mid May 1998, testing of the system began. Testing included running the system until the power was depleted, without the aid of the wind generator. The system collected data for approximately 96 hours continuously, very close to the anticipated 100 hours. Additionally, comparing data collected from the WEMITE tower to the Wind Engineering Research Field Laboratory at TTU completed validation of the wind speed data. A road test was completed to ensure the integrity of all structural and electrical connections, and practice deployments were made to ensure that the team was prepared for the 1998 Atlantic hurricane season.

3.8 Deployment Scheme

The overall goal of WEMITE in 1998 was to collect high-resolution wind speed data from hurricanes in order to gain a better understanding of surface layer winds and their characteristics. Although successful deployments are the goal of the project, personnel safety was always maintained as the highest priority.

3.8.1 Forecasting

The participating Texas Tech University atmospheric science students constantly performed forecasting of tropical storm development and progression. Once a storm of interest was located, the group intensified its monitoring efforts and usually had a meeting prior to making the final activation decision.

Once the WEMITE team was activated, the atmospheric science students, who remained in Lubbock, continued to provide forecasting and logistical information until the event was complete. Sam Houston, Mark Powell, and Frank Marks, from the Hurricane Research Division also contributed forecasting and logistical help once the team was in the field. Location of the final deployment was extremely important. Therefore, track

forecasting and time of landfall became the two most important questions once the team was activated.

3.8.2 Location

The final location of the deployment was selected based on several factors. The location must be:

1. an open (no trees or buildings), flat, grassy area with dimensions of at least 75x75 feet;
2. not threatened by flooding or storm surge;
3. as close as possible to the estimated landfall location of the storm or in an area that will receive extreme winds (normally north or east of the center); and
4. on public property or on private property with the owner's permission before arrival.

While this may seem fairly straightforward, trying to locate a suitable location in the middle of the night can be extremely difficult. Some examples of suitable locations are airports, city parks, schoolyards, etc. Logistical help was provided to the WEMITE deployment team via our home base operations in Lubbock, Texas, or through established contacts in certain areas of the country.

3.8.3 Deployment

Once a location was specified and the WEMITE team arrived, the deployment of the entire system was completed by a 4-5 member multidisciplinary team in about 1-hour. The plan was to complete deployment before the onset of tropical storm force winds, although the tower can be deployed in winds as high as 20 m/s (45 mph). The deployment procedure consisted of:

1. extending, bolting, and anchoring the outriggers to stabilize the trailer/tower;
2. telescoping the tower to its full length of 10.7 m and then securing it using U-bolts;
3. unwrapping the instrumentation from its transit bags and securing all loose wires;
4. attaching the guy wires to the tower and raising it to its vertical position, followed by bolting in the bottom connection;
5. leveling of the tower/trailer;
6. anchoring the guy wires;
7. starting the wind generator by extending it to its full height (about 2.75 m), and attaching its vane;
8. turning the power on and starting the DAQ;
9. recording the location via a Global Positioning System (GPS) and reporting the location to HRD for coordination with other institutions.

3.8.4 Post-Deployment

Following deployment, the team retreated inland to a hotel or shelter. Due to the minimal severity of the 1998 hurricanes, shelter was usually taken within a few miles of the deployment site. Again, safety of the WEMITE personnel was our first priority. Once the event was over, we conducted a small-scale survey to record the surrounding buildings or tree lines as well as small hills and other terrain features that can affect the wind flow. The direction of the instrument arms was also recorded and pictures taken. The team then returned home.

CHAPTER IV

HURRICANE BONNIE DEPLOYMENT

Hurricane Bonnie made landfall near Cape Fear, North Carolina, at 5:00 PM EDT on 26 August 1998. The storm developed in the Atlantic Ocean about 1100 km (675 miles) east of the Leeward Islands (Avila 1999). Bonnie continued west-northwest across the Atlantic reaching its maximum intensity with a central pressure of 954 mb on 24 August. After this point, Hurricane Bonnie slowed in forward motion and the storm began to weaken. Upon making landfall, Bonnie had weakened to a minimal category 3 hurricane "officially" with maximum sustained (1-minute) wind speeds in a marine exposure estimated to be near 45 m/s (100 mph) by Powell (HRD WWW Site). Bonnie continued to slowly move north with the northwest portion of the eye passing over the Wilmington area.

The WEMITE tower was deployed at the New Hanover County Airport near Wilmington by a group of undergraduate and graduate students from the TTU departments of Civil Engineering and Geosciences (Atmospheric Science) at 4:15-5:15 AM EDT with data collection initiating at 5:15 AM EDT (9:15 UTC). The approximate location of the WEMITE tower was 34° 16' 30" N and 77° 54' 30" W. Also located at the airport was the University of Oklahoma with its DOW and the NWS with its ASOS station and nearby WSR-88D.

Unfortunately, the Wilmington WSR-88D had mechanical difficulty during the passage of the storm and recorded little in the way of storm-relevant data. Luckily, the Moorehead City WSR-88D also provides coverage of the area, a 0.5-tilt angle base reflectivity image of Bonnie's landfall is provided in Figure 4.1. The Morehead City WSR-88D allows for comparisons to be made between the acquired WEMITE data and the radar, but is not

close enough to the deployment site to resolve the BL rolls/wind streaks. The ASOS station is located at 34° 16' 06" N and 77° 54' 22" W and remained operational during the entire event. Comparison of the wind speed data from WEMITE and ASOS sites, as shown in Figure 4.2, is excellent, as the separation between the two locations is less than ½ km. Other comparisons (Conder et al., 1999) between the data acquired from the WEMITE and ASOS platform indicate similar results. Maximum sustained and gust wind speeds for Hurricane Bonnie as recorded by the different platforms are shown in Table 4.1 for comparison. Hurricane Bonnie did not generate 1-minute sustained hurricane force winds at the ASOS or the WEMITE tower locations. However, it did generate 5-second gusts over hurricane force as recorded by ASOS and WEMITE and a peak gust (0.2-second) of almost 38.2 m/s as recorded by the WEMITE tower. Following the storm, TTU personnel noted only minimal damage in and around the Wilmington vicinity.

The WEMITE apparatus was deployed in an open field, but a dense forest was located approximately 300 m to the northwest, as seen in Figure 4.3. Therefore, as the wind direction changed with the passage of the eye, winds from a second, rougher regime were measured. This rougher regime is reflected in Figure 4.2 at the end of the record as the wind speeds recorded by ASOS and WEMITE start to differ. This northwest approach direction produced a transitional flow regime (Arya 1988; Simiu and Scalan 1986; Powell et al. 1996a), as determined by the referenced method. Thus, the boundary layer profile and turbulence characteristics were not in equilibrium with either the upstream densely forested roughness or the open grassy roughness immediately surrounding the WEMITE deployment location. Figure 4.4 indicates the WEMITE determined roughness lengths as calculated using the wind speed profile assuming the log-law (employing all 3 anemometer heights) and the TI from the 10.7 m (35 ft) level.

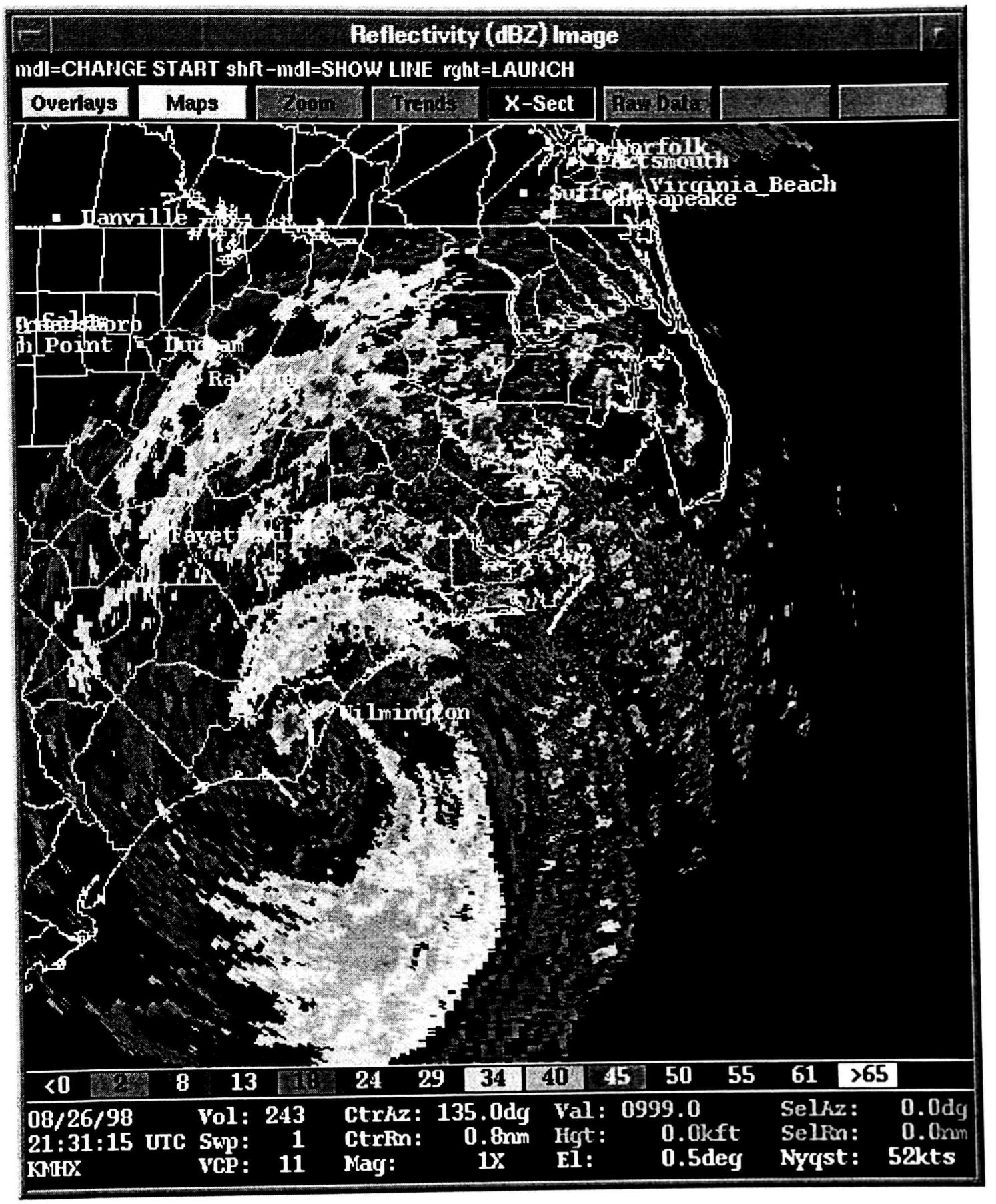

Figure 4.1. Base reflectivity image of Hurricane Bonnie's landfall near Wilmington, NC as seen from the Morehead City NWS WSR-88D.

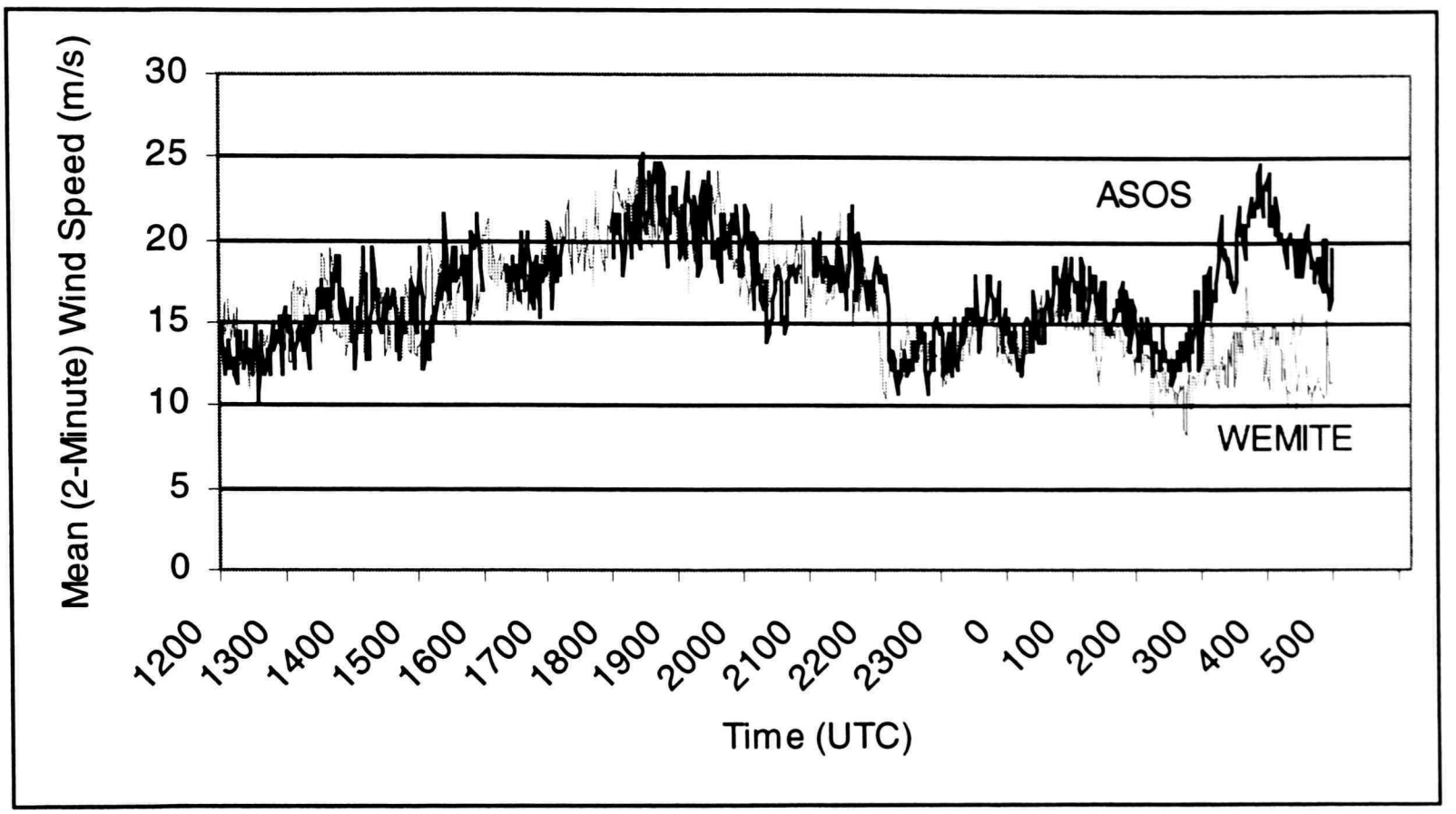

Figure 4.2. Comparison of ASOS and WEMITE wind speed data collected during the passage of Hurricane Bonnie.

Table 4.1. Comparison of wind speeds as obtained via WEMITE and ASOS for Hurricane Bonnie

	ASOS Station	WEMITE
0.2-Second Gust (m/s)	NA	38.2
3-Second Gust (m/s)	NA	33.6
5-Second Gust (m/s)	32.9	33.5
1-Minute Sustained (m/s)	NA	25.0
2-Minute Sustained (m/s)	25.2	24.4

Figure 4.3. Arial photograph of the Wilmington International Airport which served as the deployment site for Hurricane Bonnie (Conder et al., 1999)

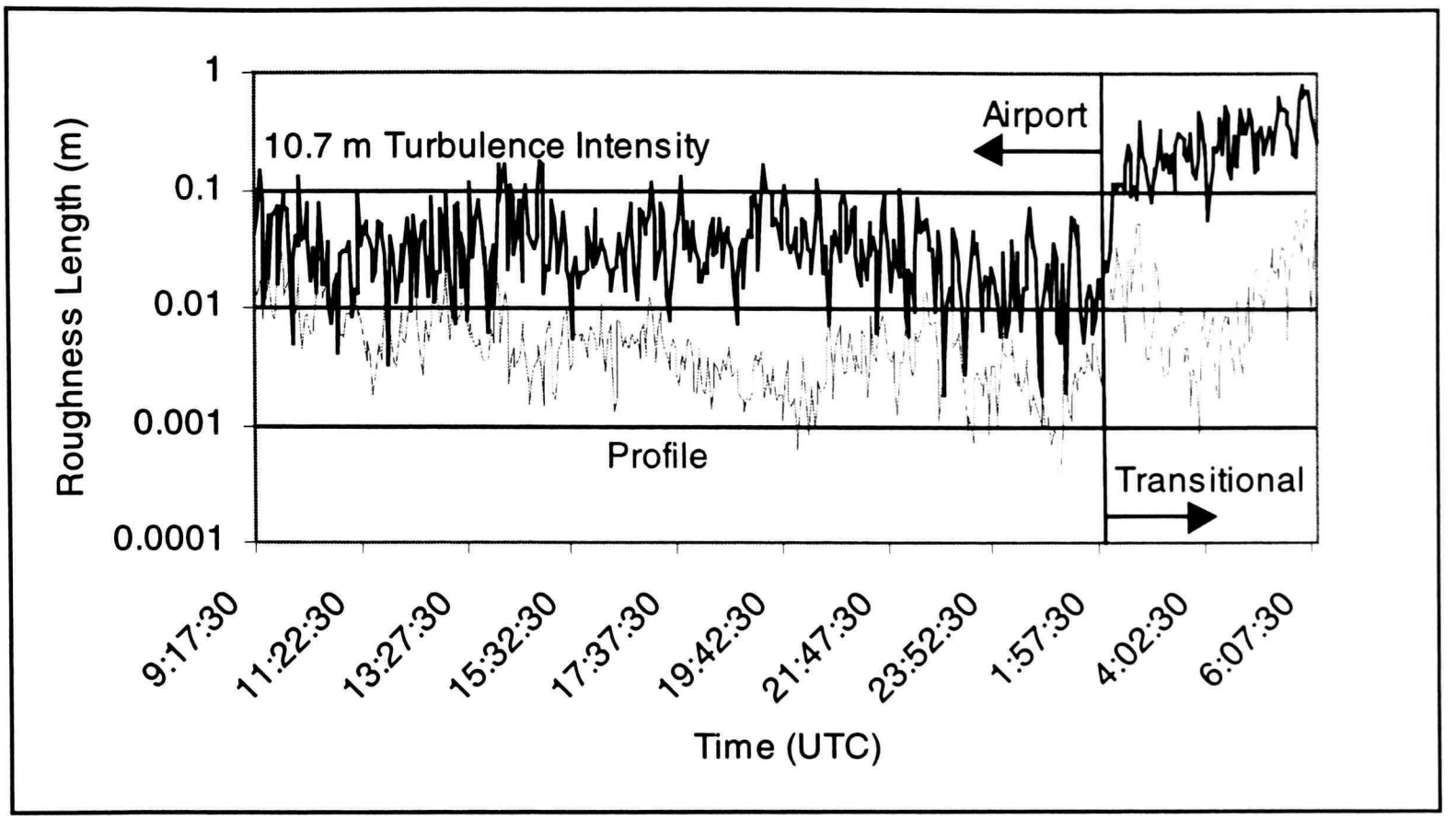

Figure 4.4. Comparison of the roughness lengths determined via the wind speed profile and turbulence intensities during the passage of Hurricane Bonnie employing 5-minute data segments.

At landfall, Hurricane Bonnie was a slow-moving, weakening storm with a double eyewall structure. It was classified as stratiform by most hurricane researchers, as active convection was limited in the storm. This conclusion is supported by WEMITE personnel observing no lightning in the storm as it made landfall; also few, if any, pressure perturbations were found in the record due to convective activity (Figure 4.5). However, the pressure trace does indicate the double eyewall structure.

A total of 630,000 data points were collected from each instrument in Hurricane Bonnie at 5 Hz starting at 5:15 UTC and ending at 17:15 UTC the following day. The horizontal and vertical wind speed records from 10.7 m anemometers are shown in Figures 4.6 and 4.7, respectively. They also indicate the different roughness regimes, as one can observe the calculated

roughness increases at the end collection period. The increased stability within the eye is also noticeable in the plot of vertical wind speeds, as the variance found in the record is reduced within the eye compared to other adjacent periods with the same mean wind speed and roughness.

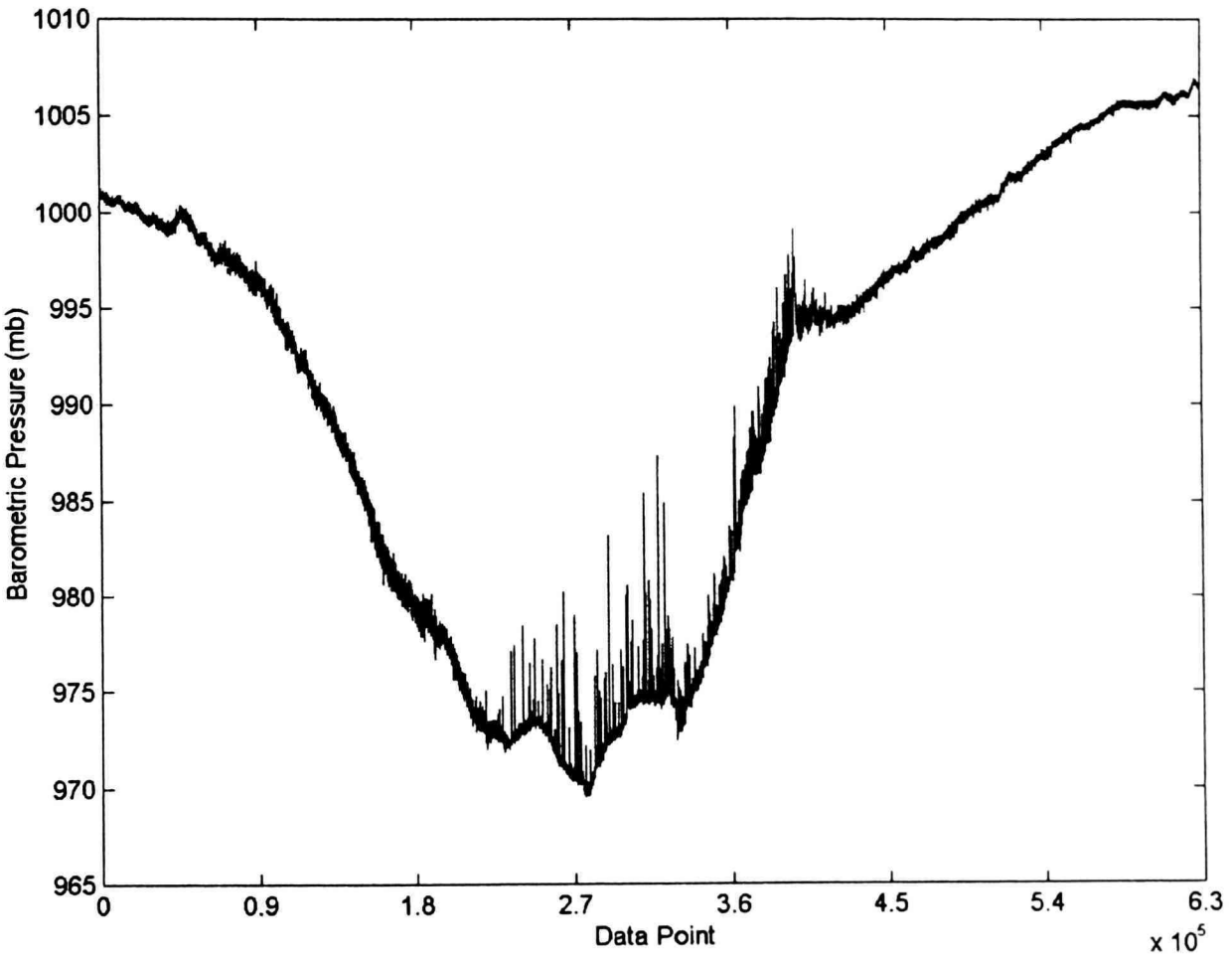

Figure 4.5. WEMITE obtained pressure trace from the passage of Hurricane Bonnie.

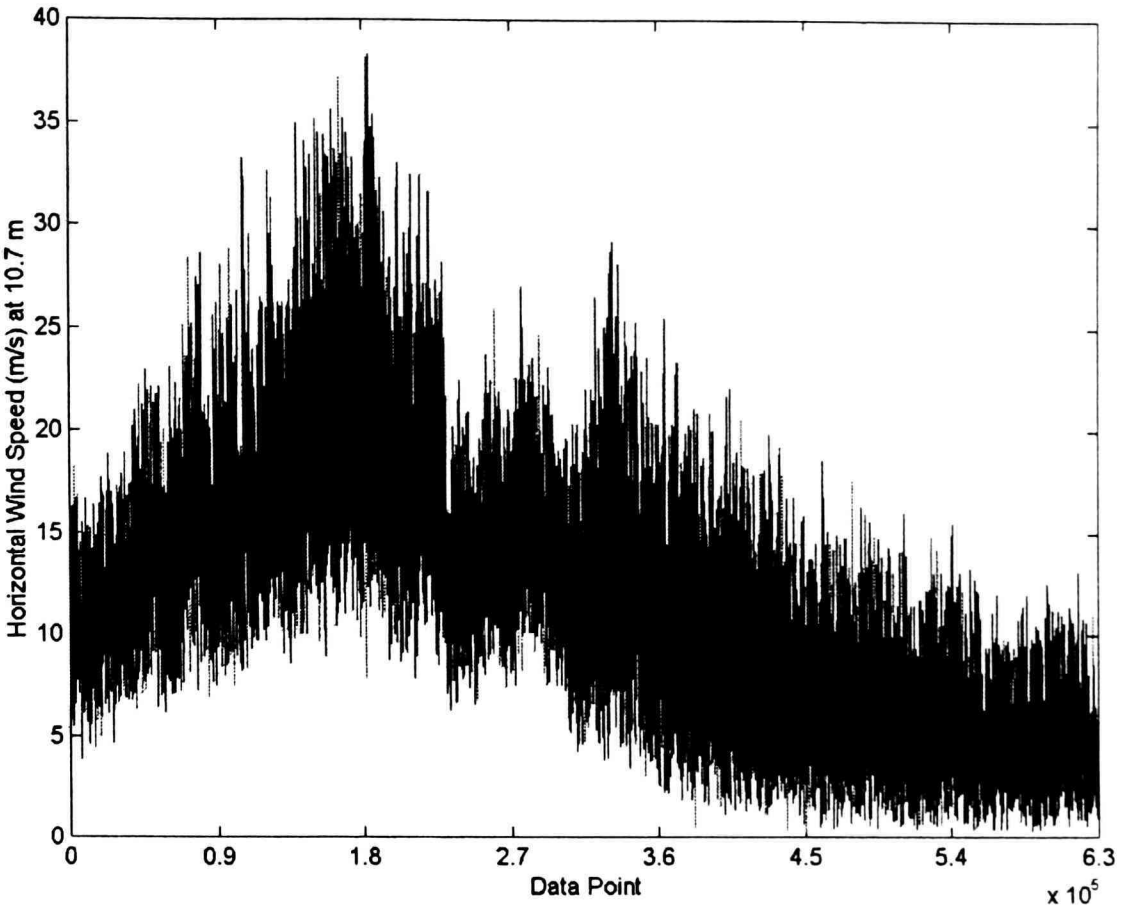

Figure 4.6. WEMITE obtained horizontal wind speed record from the passage of Hurricane Bonnie.

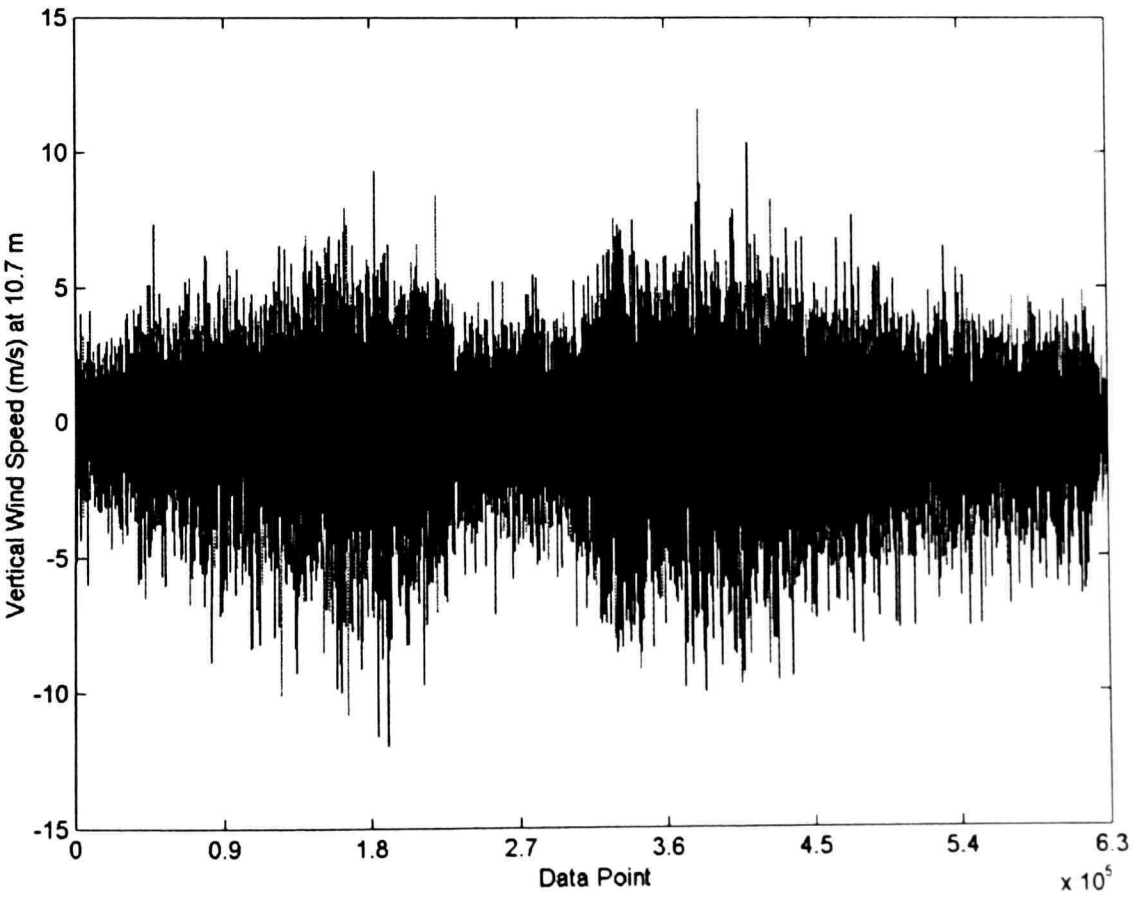

Figure 4.7. WEMITE obtained vertical wind speed record from the passage of Hurricane Bonnie.

A time history of the composite reflectivity over the deployment site as constructed from the Morehead City NWS WSR-88D is provided in Figure 4.8. There are several rainbands that affect the deployment site, the first, centered on 12:15 UTC, provided for the reflectivity values of approximately 45 dBZ. Another larger band followed at 14:45 UTC, and a smaller band passed at approximately 15:55 UTC. These bands are easily identified by examination of the radar data. Other bands exist further into the record, and numerous interactions with the eyewalls occur. The time history becomes more complicated further into the record due to Bonnie's slow forward motion at landfall, and less than aggressive reflectivity values associated with some of the bands and eyewall features located closest to the center of the storm. These issues complicate analysis efforts.

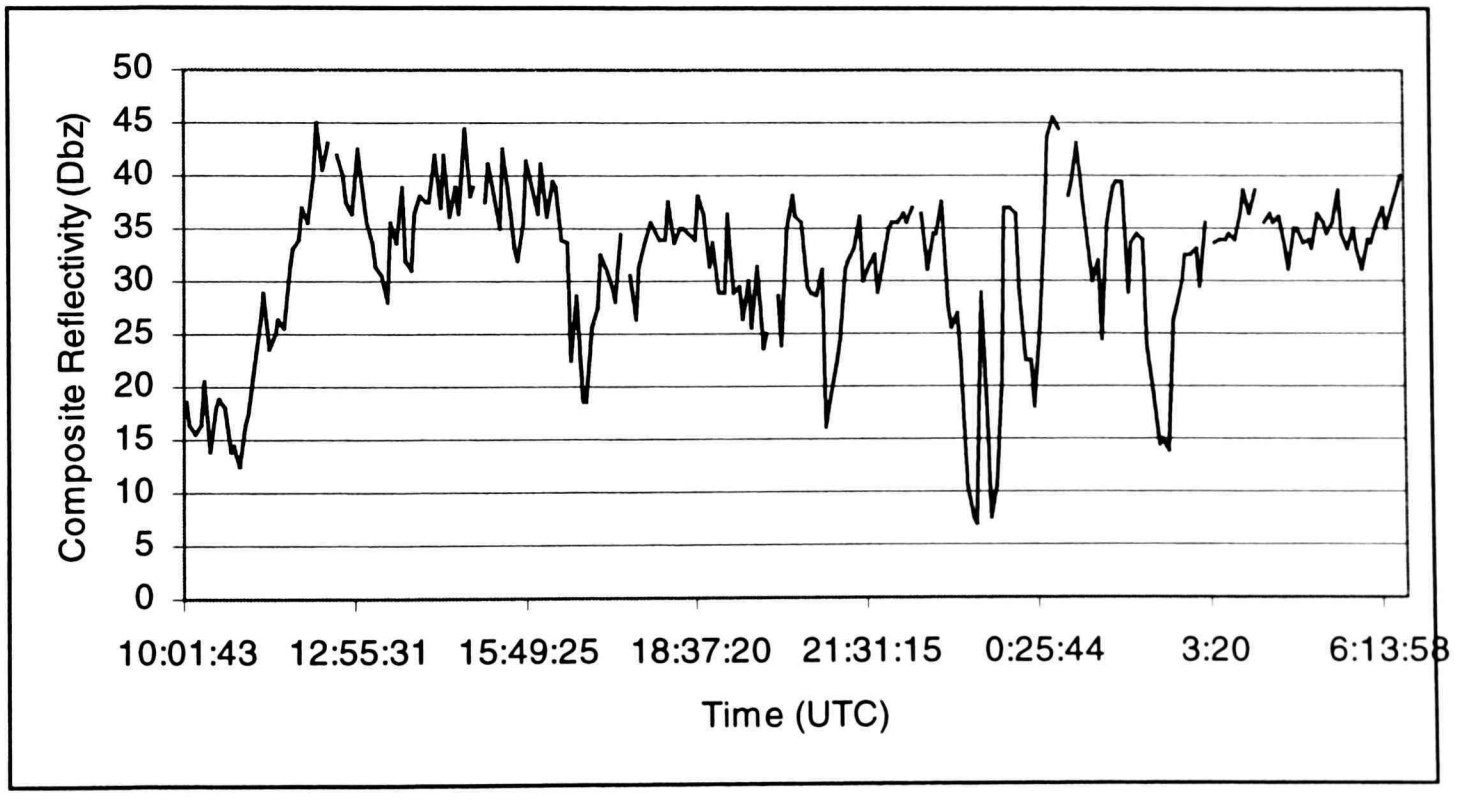

Figure 4.8. Composite reflectivity time history for the WEMITE deployment site as seen by the NWS WSR-88D in Morehead City, NC.

CHAPTER V
ANALYSIS

The main focus of this case study is to evaluate changes in the flow characteristics that may occur in different portions of a hurricane due to storm-scale processes such as the passage of a rainband, eyewall, embedded meso-vortex, updrafts and downdrafts, or other even smaller features like convective gusts. Other items to address include the difference between a "normal" design wind (such as that presented in building codes and standards) and that found within Hurricane Bonnie's wind field. These foci are evaluated by examining changes in the wind speed characteristics with time and by making comparisons to ASCE 7-98 where applicable.

This evaluation can be completed by simply evaluating parameters such as TI with time as different portions of the storm passed by the deployment site, and noting when extreme values or significant changes occured. Other more complicated comparisons include contrasting the intermittence of coherent structures in different locations of the storm with other meteorological data such as radar and barometric pressure. The overall goal is to examine the records with a methodology that will allow for changes in wind flow characteristics in time to be highlighted; and then, given these changes due in fact occur, try to align or correlate them with inherent meteorological events within the hurricane.

5.1 Turbulence Intensities

TI is one of the parameters "matched" in the wind tunnel and present in building codes and standards such as ASCE 7-98. This inclusion is because the intensity of the turbulence in the upstream wind affects the overall static load on a building, not to mention the dynamic excitation

present on flexible buildings and components. TI varies in different terrain and stability conditions, increasing for rougher and unstable conditions.

The TI will differ when calculated using different averaging times, as shown in Figure 5.1 and will be affected by nonstationarities that exists in the record. However, the nonstationary effects are usually minimal without the presence of an abrupt change in wind speed and direction as found in Schroeder et al. (1998). For purposes of this case study, a 5 minute averaging time with a 50% offset between data segments was employed to determine the TI's. It can be seen in Figure 5.1, that the mean TI as determined using the Hurricane Bonnie data becomes fairly stable at approximately 3 minutes with only a modest increase of 2.7% indicated between 5 and 10 minutes. Hence, the mean calculated TI has little dependency on averaging time once above 5 minutes. With 5 to 10 minute averaging times acceptable, a choice of 5 minutes allows for the best comparison to WSR-88D radar data that is taken in approximately 5 minute volume scans.

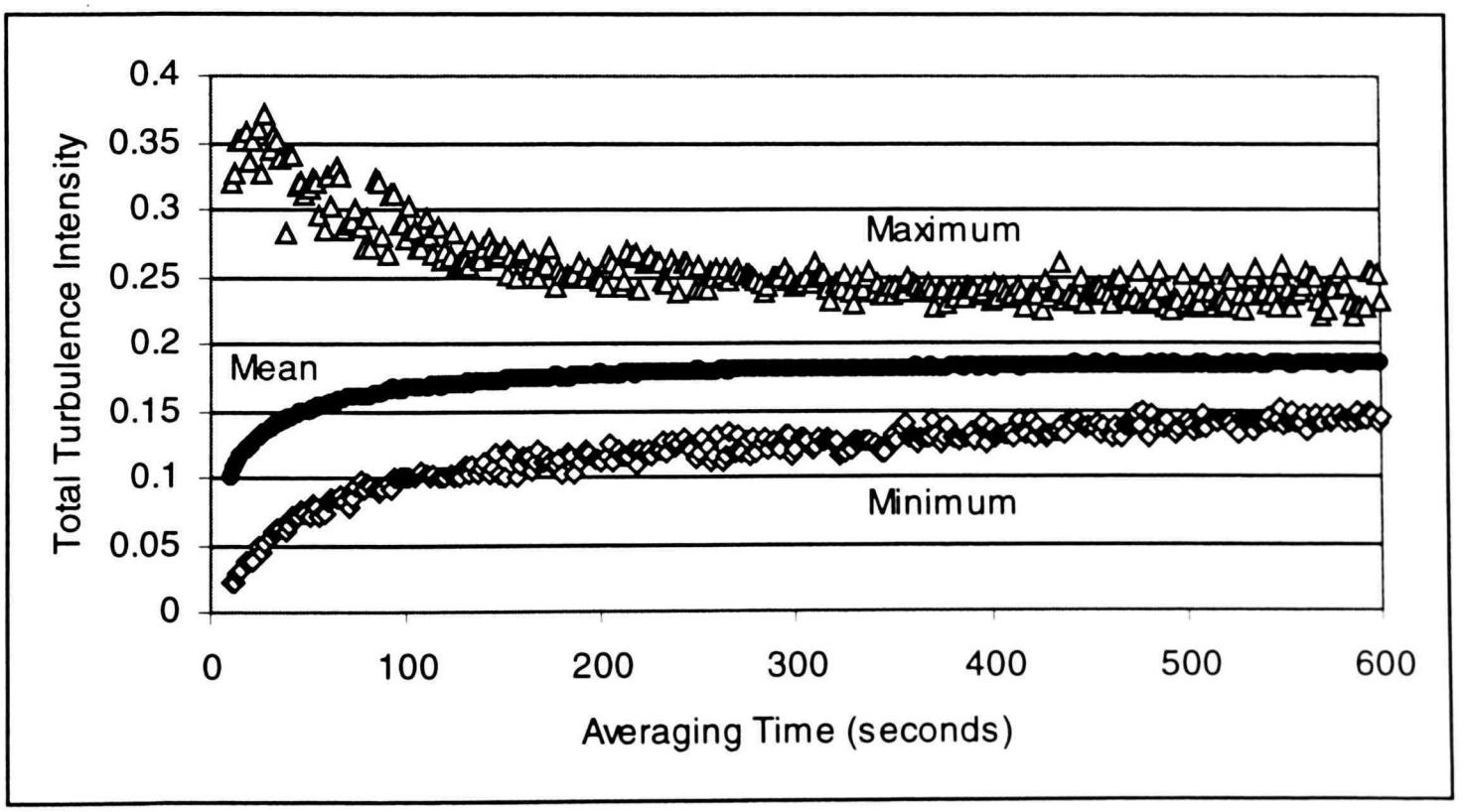

Figure 5.1. Time dependence of turbulence intensity.

5.1.1 Turbulence Intensity Statistics

The longitudinal TI's as determined using the data from the 10.7 m WEMITE anemometer range from 12 to 35% for the airport exposure during the first portion of the storm and increase to 17 to 41% for the remaining (transitional) portion of the storm. Except for one sharp peak near 22:03 UTC in Figure 5.2, only subtle changes with time are noted in the record. The lateral TI's have the same pattern with one sharp peak at 22:03 UTC varying from 12 to 42% for the airport exposure and 16 to 35% for the transitional roughness regime. A time history of lateral TI's is provided in Figure 5.3. Vertical TI's range from 7 to 11% for the airport exposure and 7 to 22% for the transitional exposure; however, there is no large peak in the time history. A time history of the vertical TI's is provided in Figure 5.4.

Examination of the 5 minute time segment containing the sharp peak in lateral and longitudinal TI's indicates a sharp and temporary wind direction change. This change induces an intense "artificial" peak in the TI's due to the nonstationarity of the record. This sharp direction change occurs over a time period of approximately 15 seconds and only occurs at the 10.7 m (35 ft) level. Its physical meaning is unknown, if in fact it is real. Interaction of the anemometer with debris (paper, plastic, etc.) may have caused the abrupt change; on the other hand a temporary instrument malfunction is more likely the cause. The temporary change is shown in Figure 5.5. All of the calculated TI's are summarized in Tables 5.1, 5.2, and 5.3, where stationarity is determined with respect to the longitudinal, lateral, and vertical wind speeds by employing the nonparametric run test at a 0.95 significance level. Only a minimal increase in the mean TI is noted between the stationary and nonstationary data segments. Tables 5.4, 5.5, and 5.6 show the same statistics, but with stationarity defined in terms of the second moment (variance) of each of the wind speed components. Table 5.7 shows

statistics based on the records which are entirely stationary for each wind component (longitudinal, lateral, and vertical) with respect to the mean and variance in the record.

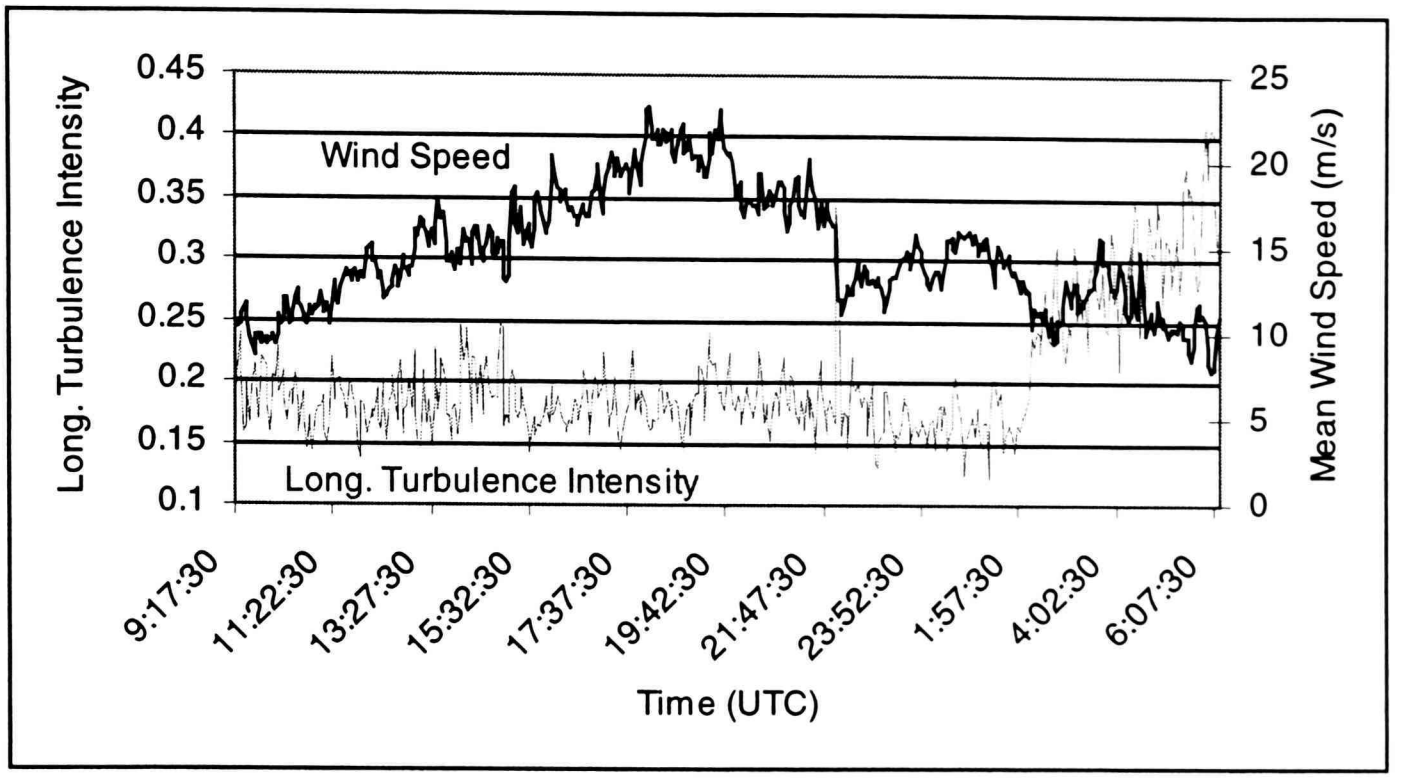

Figure 5.2. Time history of longitudinal turbulence intensity as determined from the 10.7 m WEMITE data during the passage of Hurricane Bonnie.

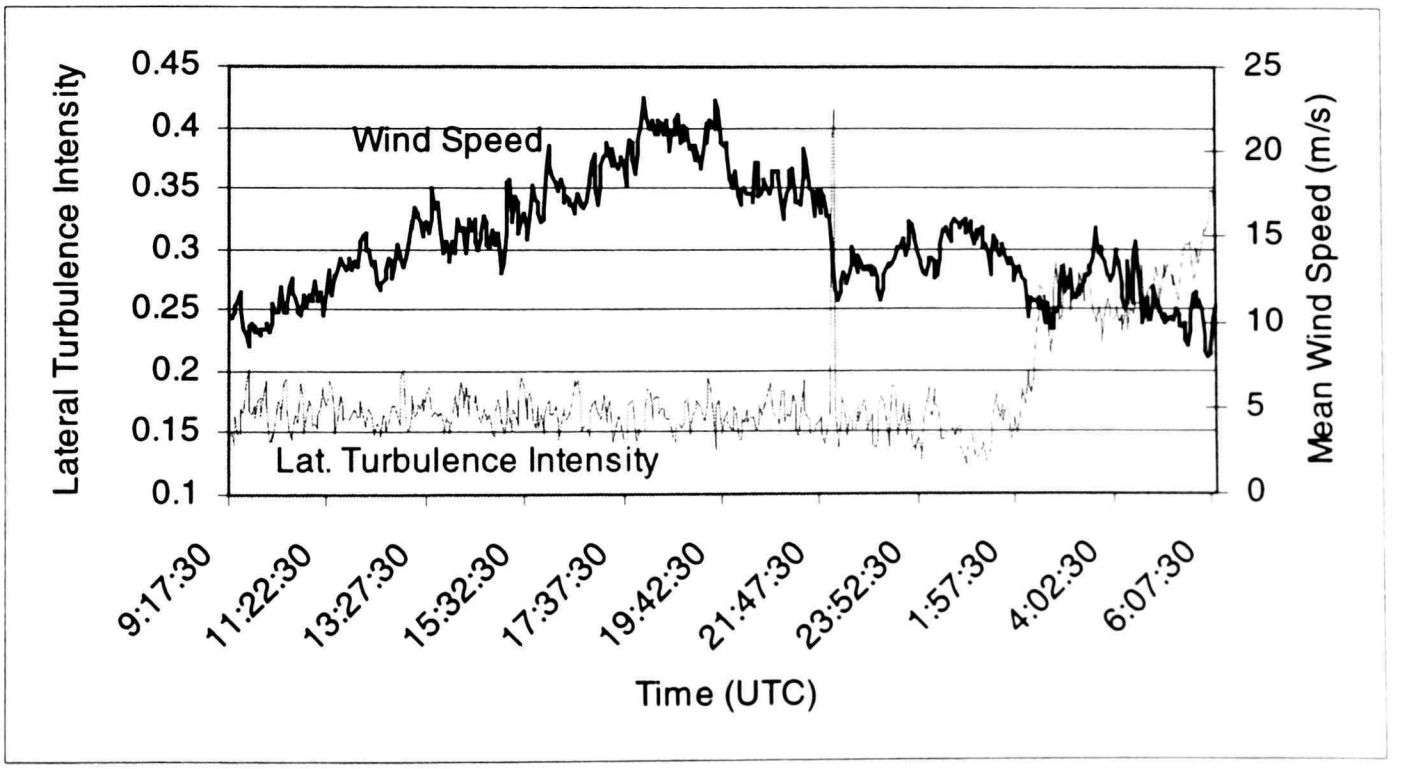

Figure 5.3. Time history of lateral turbulence intensity as determined from the 10.7 m WEMITE data during the passage of Hurricane Bonnie.

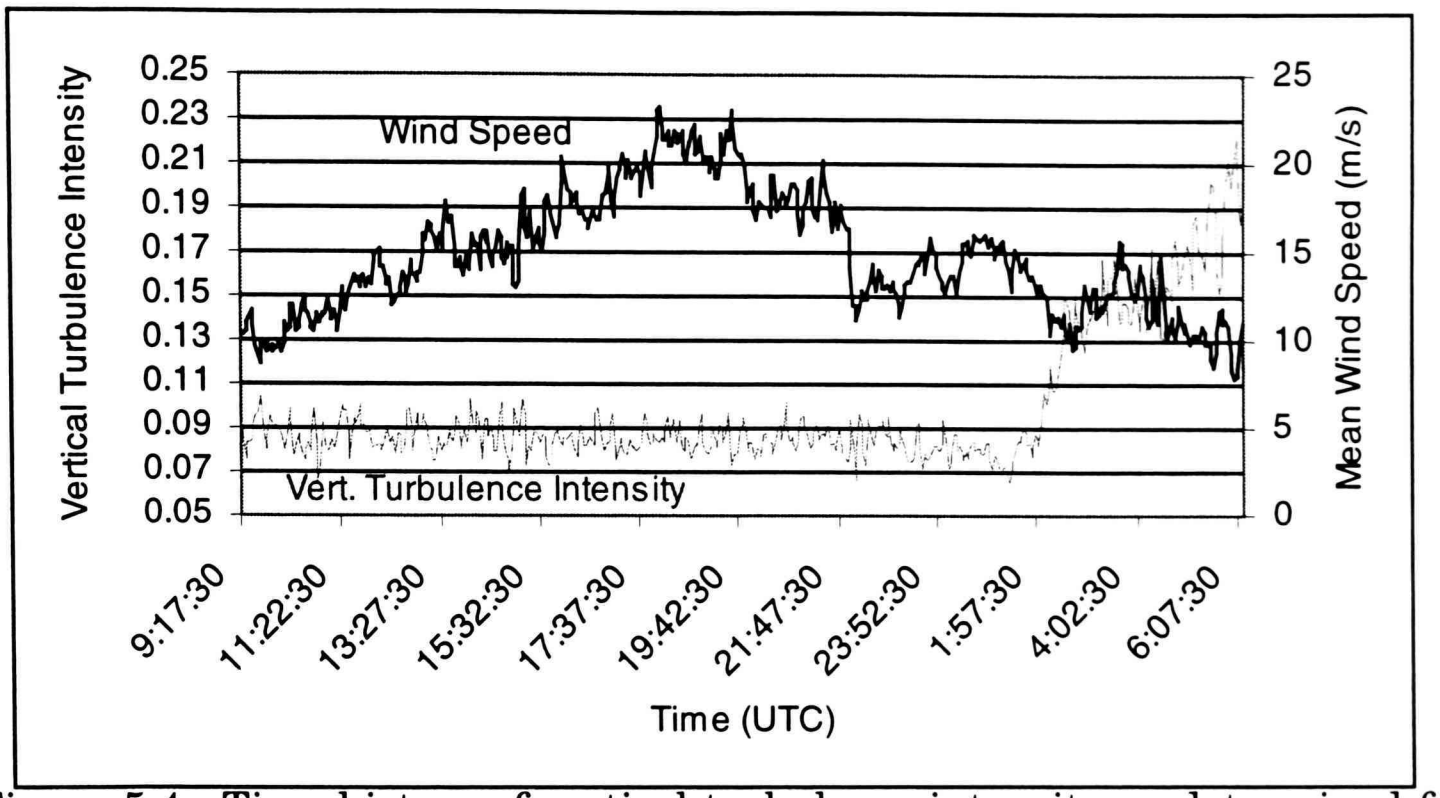

Figure 5.4. Time history of vertical turbulence intensity as determined from the 10.7 m WEMITE data during the passage of Hurricane Bonnie.

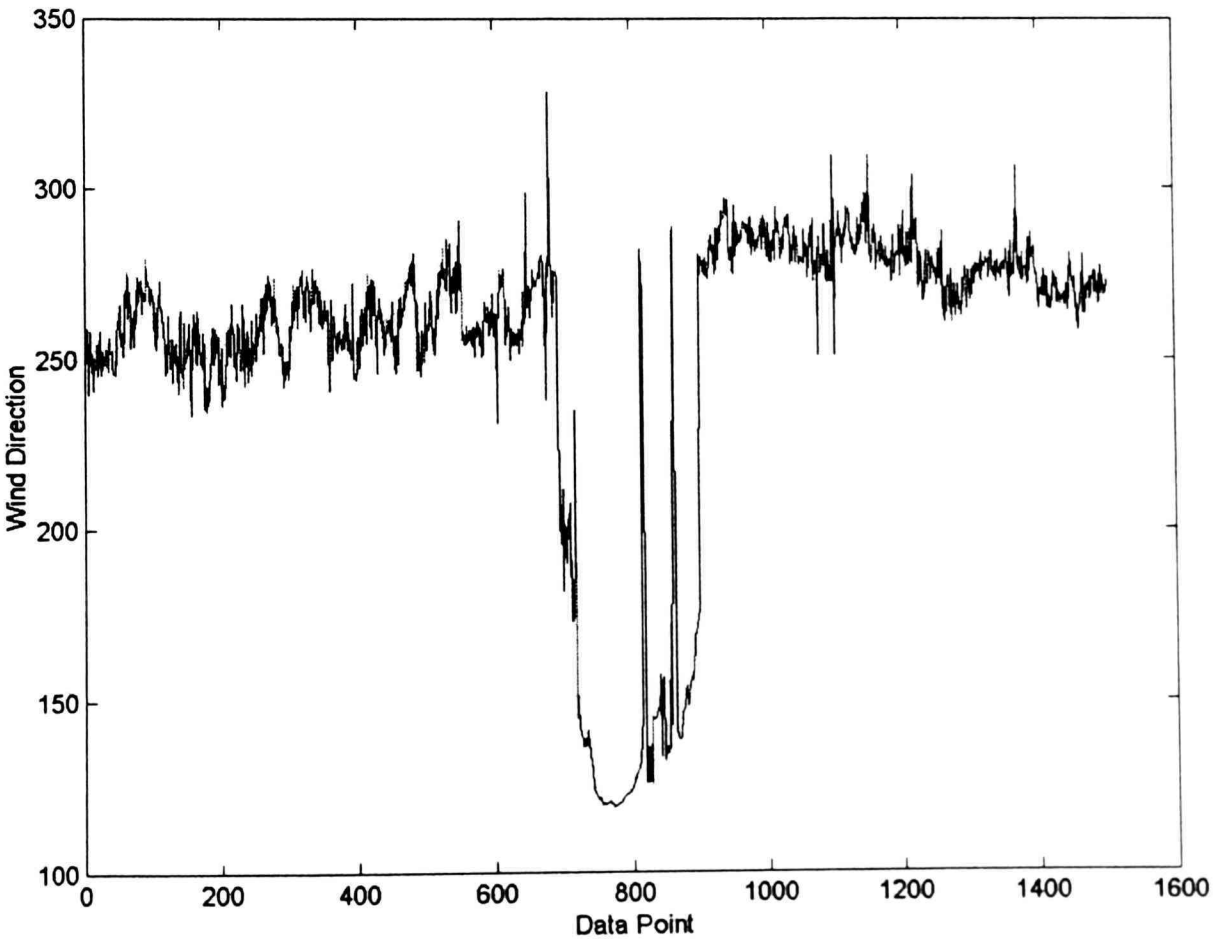

Figure 5.5. Time history of wind direction indicating a temporary change resulting in an artificial inflation of the lateral and longitudinal turbulence intensity.

Table 5.1 Longitudinal turbulence intensity statistics for Hurricane Bonnie classified in terms of stationarity with respect to the longitudinal mean wind speed.

	Stationary		Nonstationary	
	Airport	Transitional	Airport	Transitional
No. 5-min. Segments	269	74	133	27
Mean	17.6%	28.0%	19.4%	29.9%
Maximum	24.4%	40.7%	34.6%	41.0%
Minimum	12.2%	17.3%	13.0%	17.8%
Standard Deviation	0.020	0.048	0.028	0.053

Table 5.2 Lateral turbulence intensity statistics for Hurricane Bonnie classified in terms of stationarity with respect to the lateral mean wind speed.

	Stationary		Nonstationary	
	Airport	Transitional	Airport	Transitional
No. 5-min. Segments	355	95	47	6
Mean	16.4%	26.2%	16.6%	25.0%
Maximum	41.8%	34.7%	20.1%	26.7%
Minimum	12.3%	16.0%	13.7%	23.9%
Standard Deviation	0.036	0.036	0.016	0.012

Table 5.3 Vertical turbulence intensity statistics for Hurricane Bonnie classified in terms of stationarity with respect to the vertical mean wind speed.

	Stationary		Nonstationary	
	Airport	Transitional	Airport	Transitional
No. 5-min. Segments	393	101	9	0
Mean	8.5%	15.4%	8.1%	N/A
Maximum	10.5%	22.3%	8.9%	N/A
Minimum	6.5%	6.5%	7.3%	N/A
Standard Deviation	0.007	0.026	0.006	N/A

Table 5.4 Longitudinal turbulence intensity statistics for Hurricane Bonnie classified in terms of stationarity with respect to the variance in the longitudinal wind speed record.

	Stationary		Nonstationary	
	Airport	Transitional	Airport	Transitional
No. 5-min. Segments	393	97	9	4
Mean	18.2%	28.3%	18.7%	32.6%
Maximum	34.6%	41.0%	22.2%	39.9%
Minimum	12.2%	17.3%	14.7%	28.7%
Standard Deviation	0.025	0.050	0.028	0.052

Table 5.5 Lateral turbulence intensity statistics for Hurricane Bonnie classified in terms of stationarity with respect to the variance in the lateral wind speed record.

	Stationary		Nonstationary	
	Airport	Transitional	Airport	Transitional
No. 5-min. Segments	381	93	21	8
Mean	16.4%	26.2%	15.7%	25.5%
Maximum	41.8%	34.7%	17.3%	27.2%
Minimum	12.3%	16.0%	14.3%	23.9%
Standard Deviation	0.036	0.036	0.009	0.012

Table 5.6 Vertical turbulence intensity statistics for Hurricane Bonnie classified in terms of stationarity with respect to the variance in the vertical wind speed record.

	Stationary		Nonstationary	
	Airport	Transitional	Airport	Transitional
No. 5-min. Segments	393	96	9	0
Mean	8.5%	15.4%	8.8%	N/A
Maximum	10.5%	22.3%	10.1%	N/A
Minimum	6.5%	6.5%	7.0%	N/A
Standard Deviation	0.007	0.026	0.010	N/A

Table 5.7 Longitudinal, lateral, and vertical turbulence intensity statistics for Hurricane Bonnie for stationarity data segments with respect to the mean and variance of each wind component.

	Stationary	
	Airport	Transitional
No. 5-min. Segments	230	71
Min. Longitudinal TI	12.2%	17.3%
Mean Longitudinal TI	17.7%	28.0%
Max. Longitudianl TI	24.4%	40.7%
Stnd. Dev. Longitudinal TI	0.020	0.049
Min. Lateral TI	12.3%	16.0%
Mean. Lateral TI	16.3%	26.0%
Max. Lateral TI	19.6%	34.7%
Stnd. Dev. Lateral TI	0.014	0.035
Min. Vertical TI	6.5%	9.2%
Mean. Vertical TI	8.5%	15.4%
Max. Vertical TI	10.4%	22.3%
Stnd. Dev. Vertical TI	0.007	0.026

5.1.2 Turbulence Intensity Ratios

Combining these different TI components by constructing ratios, one can make a comparison to values that are thought to exist in neutrally stratified surface layers (Cermak et al., 1983). For a neutral surface layer (constant flux layer) with homogeneous roughness, the momentum flux becomes independent of height and only depends on the friction velocity. Employing this similarity hypothesis, the following ratios between the TI's can be derived.

$$\frac{\sigma_v}{\sigma_u} = \frac{I_v}{I_u} = 0.76 \tag{5.1}$$

$$\frac{\sigma_w}{\sigma_u} = \frac{I_w}{I_u} = 0.52 \tag{5.2}$$

$$\frac{\sigma_w}{\sigma_v} = \frac{I_w}{I_v} = 0.75 \tag{5.3}$$

The TI ratios determined from the 10.7 m WEMITE wind speed data are shown in Figure 5.6. For the airport exposure during the first portion of the hurricane record, the mean ratios between the lateral and longitudinal TI's, vertical and longitudinal TI's, and vertical and lateral TI's are 0.92, 0.47, and 0.52, respectively. The time histories indicate the ratios are very consistent throughout the storm, and vary only slightly with the change in upstream terrain conditions; however, the lateral-to-longitudinal ratio is substantially different than the expected value for a neutrally stable BL.

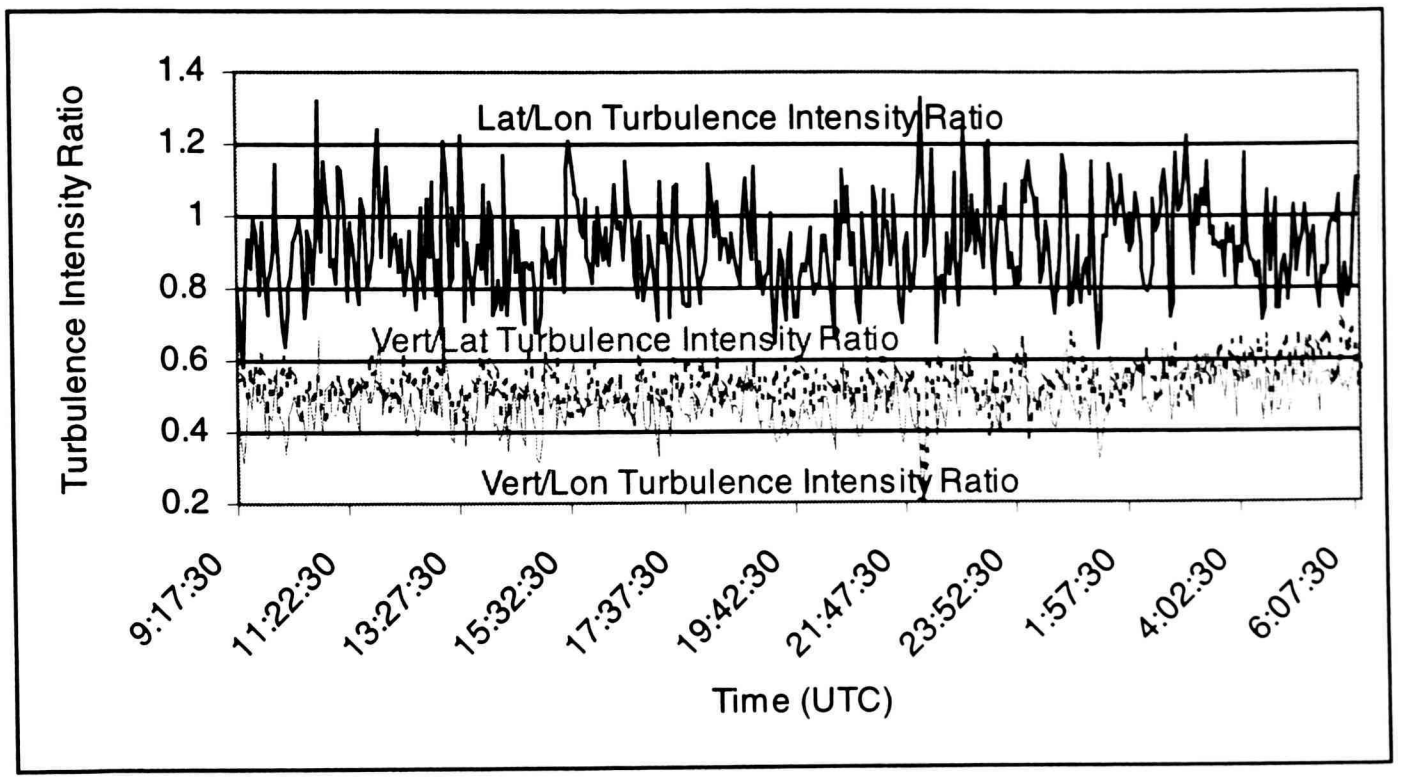

Figure 5.6. Turbulence intensity ratios as determined from 10.7 m WEMITE wind speed data collected during Hurricane Bonnie.

5.1.3 Comparison to Meteorology

Comparisons of the generated longitudinal TI time history to the radar reflectivity, and precipitation time histories are shown in Figures 5.7, and 5.8, respectively. These plots indicate only minor changes with time in the parameters; no obvious change in TI can be observed with changes in storm structure. Scatter plots of the parameters indicate no recognizable dependence; these are not provided in this document.

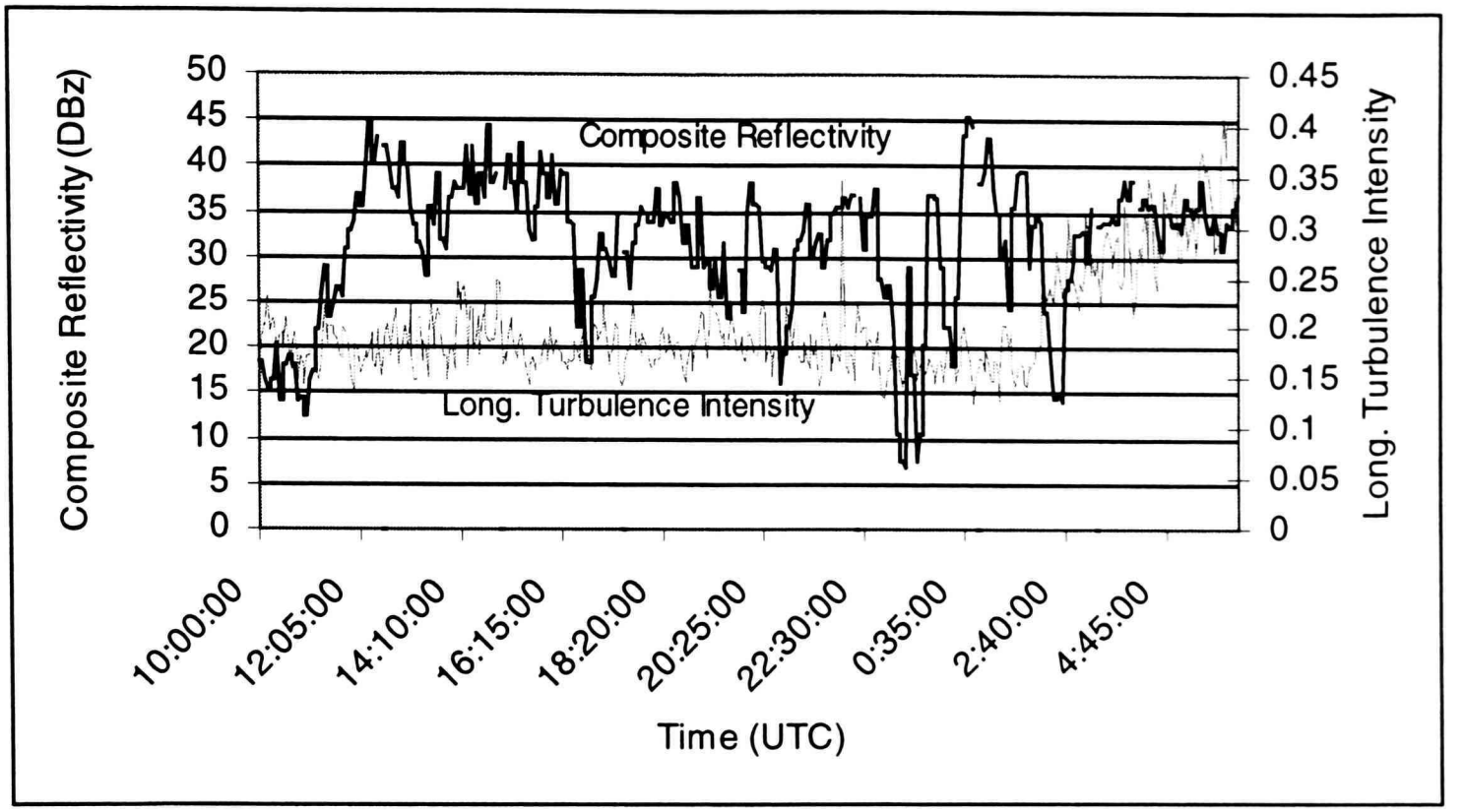

Figure 5.7. Longitudinal turbulence intensity and radar reflectivity time histories collected during Hurricane Bonnie.

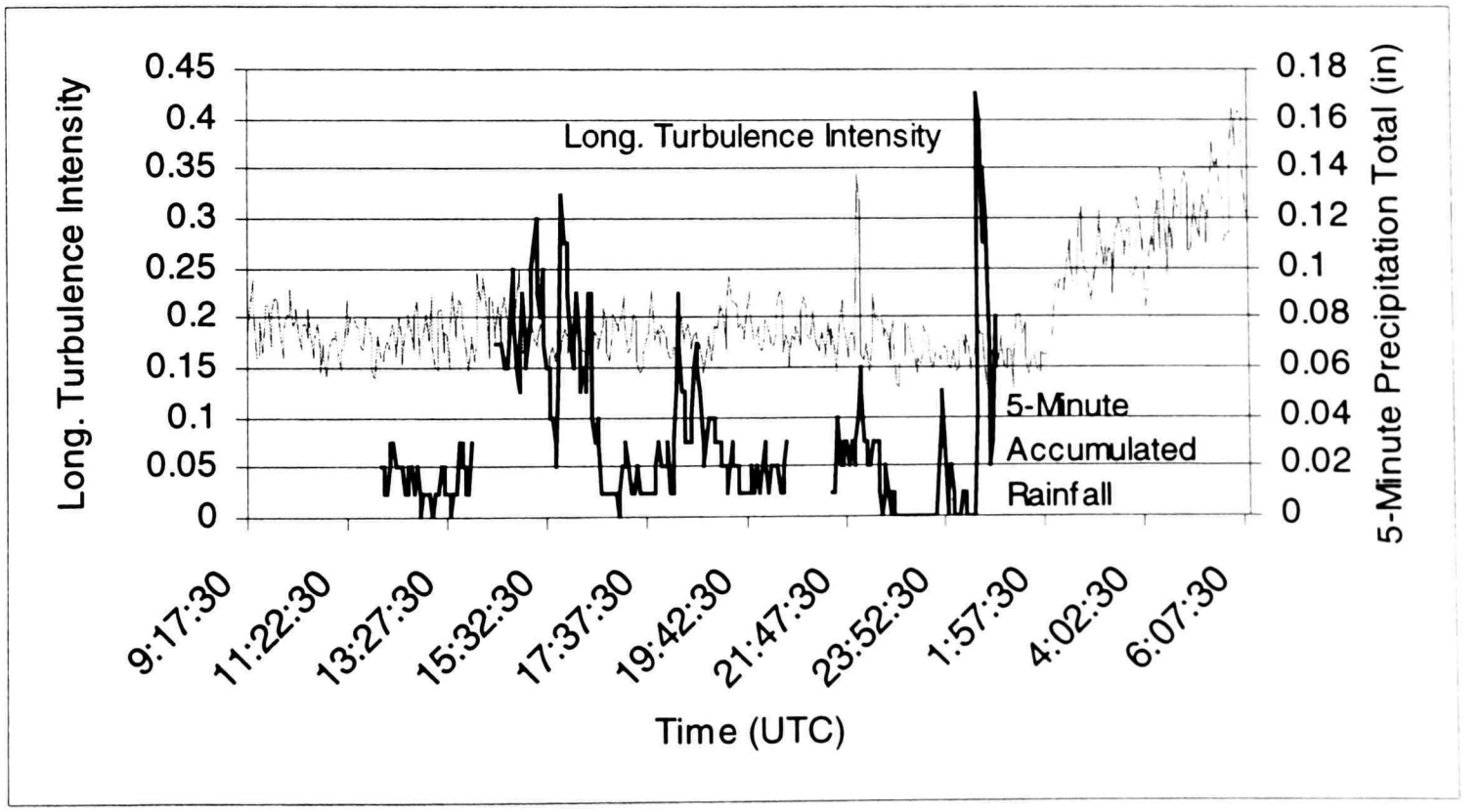

Figure 5.8. Longitudinal turbulence intensity and 5-minute precipitation total time histories from nearby NWS ASOS station collected during Hurricane Bonnie.

5.1.4 Comparison to ASCE 7-98

In ASCE 7-98, the methodology for the determination of the gust effect factor is discussed. This factor accounts for wind-structure interaction, and is dependent on several factors including TI and integral scales that yield a representation of the average turbulent state of the wind. The ASCE 7-98 determined TI at the 10.7 m (35 ft) equivalent height level is dependent on exposure and yields the magnitudes shown in Table 5.8

Table 5.8 ASCE 7-98 determined TI's for various exposures.

Exposure	Description	TI at 10.7 m (%)
A	Large City Center	44.6
B	Suburban	29.7
C	Open Terrain	19.8

The WEMITE deployment in Hurricane Bonnie was in an "airport" exposure for the first portion of the record. This exposure yielded a mean longitudinal TI of 18.2% with a standard deviation of 2.5%; the histogram is provided in Figure 5.9. Given this exposure would be classified as exposure C in ASCE 7-98, the actual TI compares well its ASCE 7-98 counterpart. Assuming a normal distribution (given the large sample size) and using a 95% confidence interval (2 standard deviations) the highest turbulence intensity one might expect to measure within a 5-minute period is 23.2%.

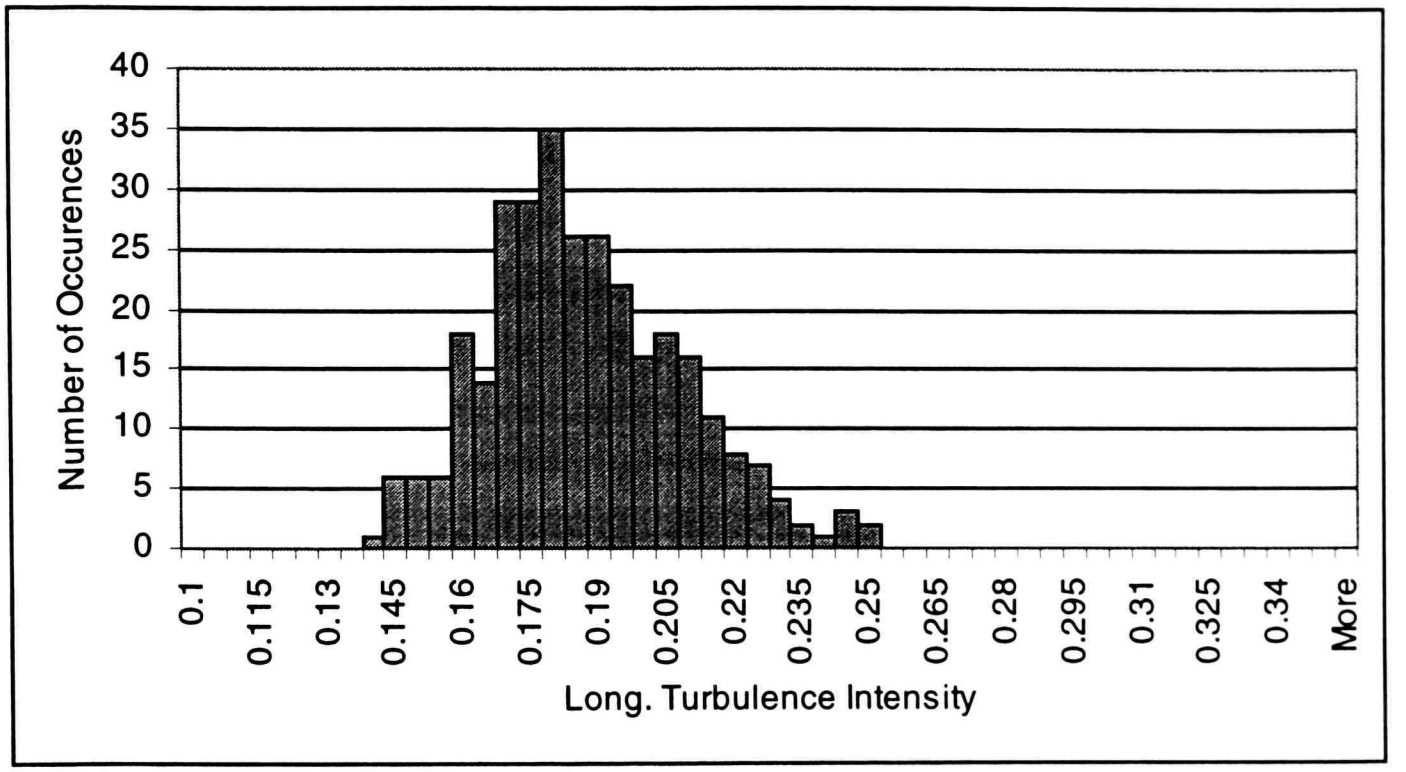

Figure 5.9. Histogram of longitudinal turbulence intensities collected during Hurricane Bonnie with airport exposure only.

5.1.5 Turbulence Intensity Summary and Commentary

As other researchers have indicated, TI's do not show much indication of changing as different portions of the storm pass by. This initial work (see Chapter 5, Section 6 for more information) indicates there is essentially no or very little dependence of TI's on storm-scale processes, or at least none that can be statistically proven by comparing the original 5 minute time histories within Hurricane Bonnie. This may not be all that revealing, because as previously discussed, the turbulence field can change dramatically but still yield the same TI.

As with previous research, sharp peaks in the longitudinal and lateral TI records are caused by wind directional nonstationarities in the record. Although in general, only minimal increases in TI were noted for

nonstationary segments relative to stationary data segments. Comparisons to ASCE 7-98 indicate little difference in mean values of TI. However, comparison to what is expected in a neutrally stratified BL flow in high wind situations indicates that the turbulence field may be different than what is expected as the ratio between lateral and longitudinal TI is inflated. One relevant explanation is that the difference is inherent in the particular characteristics of the anemometer. Different response characteristics for the propeller and vane could lead to differences in the lateral and longitudinal wind speed records, and the determined TI ratios. To investigate this possibility, a comparison was made between a 3-component propeller (UVW) anemometer and the propeller-vane anemometer employed on WEMITE #2. The anemometers are mounted above the top of the tower so no interference effects are expected. This comparison, made over a 1 hour time period in hurricane conditions (Hurricane Dennis, 1999), is detailed in Table 5.9.

Table 5.9 Comparison of generated TI's from different anemometers.

	Long. TI	Lat. TI	Mean Lat/Long TI Ratio	% Difference Longitudinal TI	% Difference Lateral TI
UVW	17.5%	15%	0.87	11%	41%
Propeller-Vane	19.5%	21.2%	1.10		

Results indicate differences in the TI statistics between the anemometers. The UVW and propeller-vane anemometer separated by a approximately 1.82 m (6-ft) both registered the same longitudinal wind speed, but the propeller-vane anemometer measured an increase in TI of approximately 11% longitudinally and 41% laterally relative to the UVW anemometer. Another inspection of 5 hours of data taken at minimal wind

speeds (<7 m/s) with the same exposure indicates the UVW anemometer with essentially constant TI's for the same exposure, but the TI's determined from the propeller-vane anemometer are reduced. This lends support to the argument that the overshoot problem (at high wind speeds) and reduced response (at low speeds) of the propeller-anemometer affect the determined TI's. Using the UVW anemometer as the benchmark, the calculated TI's can be overestimated by the propeller-vane anemometer by as much as approximately 40% laterally, while the longitudinal TI's are much more accurate. Therefore short-term fluctuations in the wind direction record of a propeller-vane anemometer should be questioned, and at intense wind speeds the overshooting problem may result in overestimated lateral TI's. To rectify this problem a combination of UVW, sonic and propeller-vane anemometers should be used for future research, and indeed on the second WEMITE tower to be used during the 1999 hurricane season a UVW anemometer was added to the arsenal. One interesting note is that even the UVW registered longitudinal-to-lateral ratios that are above the expected values based on a neutrally stratified BL, indicating the BL within a hurricane is not neutrally stratified, or the nature of turbulence changes in extreme winds.

5.2 Gust Factors

5.2.1 Gust Factor Statistics

From the 10.7 m Hurricane Bonnie wind speed data collected with WEMITE, 2-second/10-minute GF's were calculated, and the time history is shown in Figure 5.10. An average GF of 1.6 was determined for the airport exposure with a standard deviation of 0.11. A maximum value of 2.3 was found for the airport exposure. The second, rougher (transitional) exposure at the end of the data record contributed to GF's as high as 2.7 with an average value of approximately 2.0. These values fall more in line with the results of

Krayer and Marshall (1992) which indicated a 2-second/10-minute average of 1.55 in hurricanes. The time history indicates there is little change in the magnitude of the determined GF's throughout the storm, and only one brief time period with an airport exposure that yields GF's over 2.0.

Another comparison to previous research can be made if we generate a curve of GF's based on a mean hourly wind speed and peak gusts of variable duration. This curve (Figure 5.11) was constructed by employing a 20-minute offset between the 1-hour data segments and using only data from the first portion of the collected record (airport exposure). Comparison to the Marshall/Krayer curve indicates a similar result with only a minimal amount of deviation. The histogram of the determined GF's for airport exposure is shown in Figure 5.12.

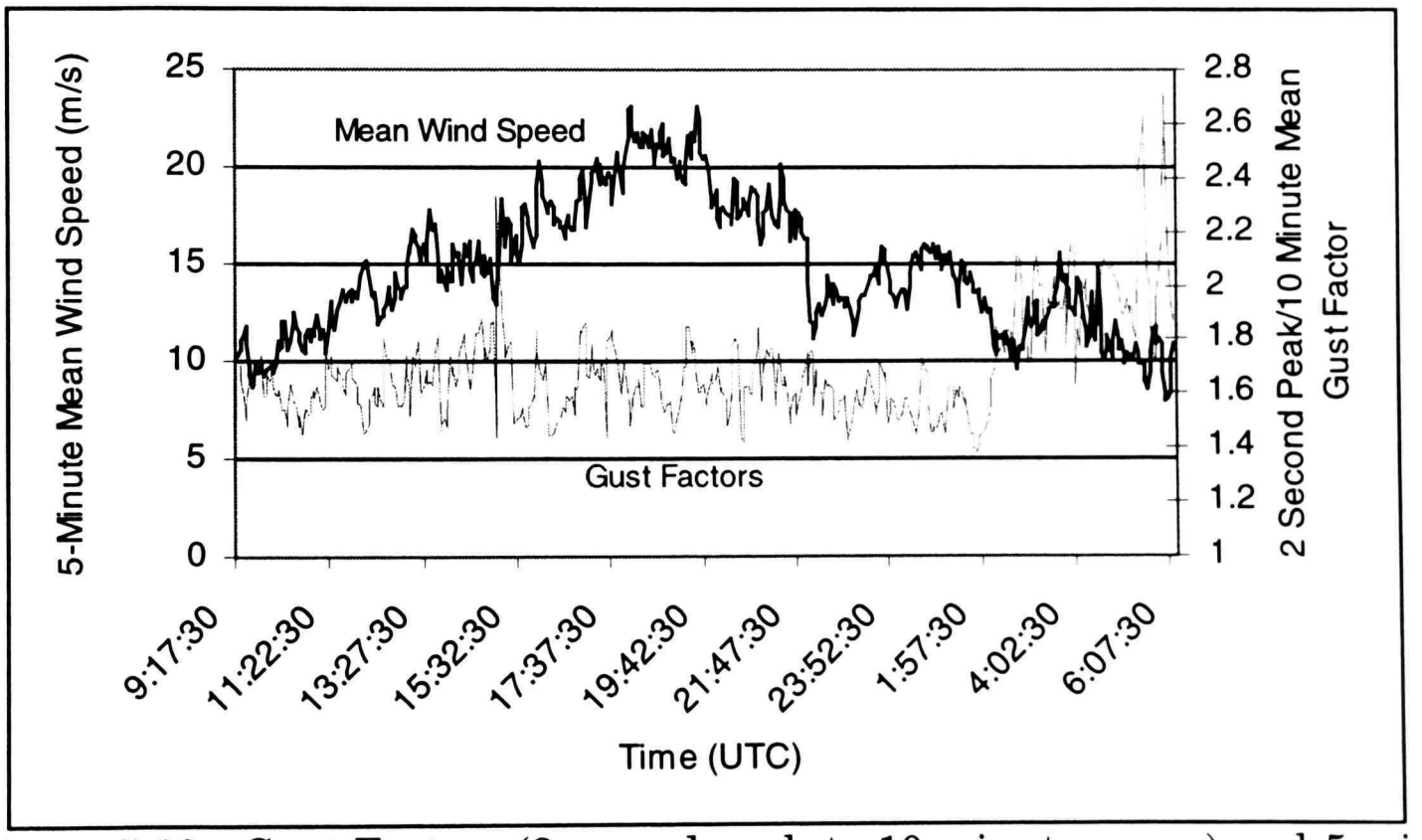

Figure 5.10. Gust Factors (2-second peak to 10-minute mean) and 5-minute mean longitudinal wind speed time histories collected by WEMITE during Hurricane Bonnie.

5.2.2 Comparison to Meteorology

Comparing the determined GF's to the composite radar reflectivity yields no observational correlation as shown in Figure 5.13. The same is true

for the GF's and the 5-minute accumulated rainfall (not shown). However, upon closer examination of the barometric pressure record, along with the horizontal wind speed, wind direction, and vertical wind speed data collected during the short time period of elevated GF's (>2.0) for airport exposure, some interesting features are indicated (Figures 5.14 and 5.15).

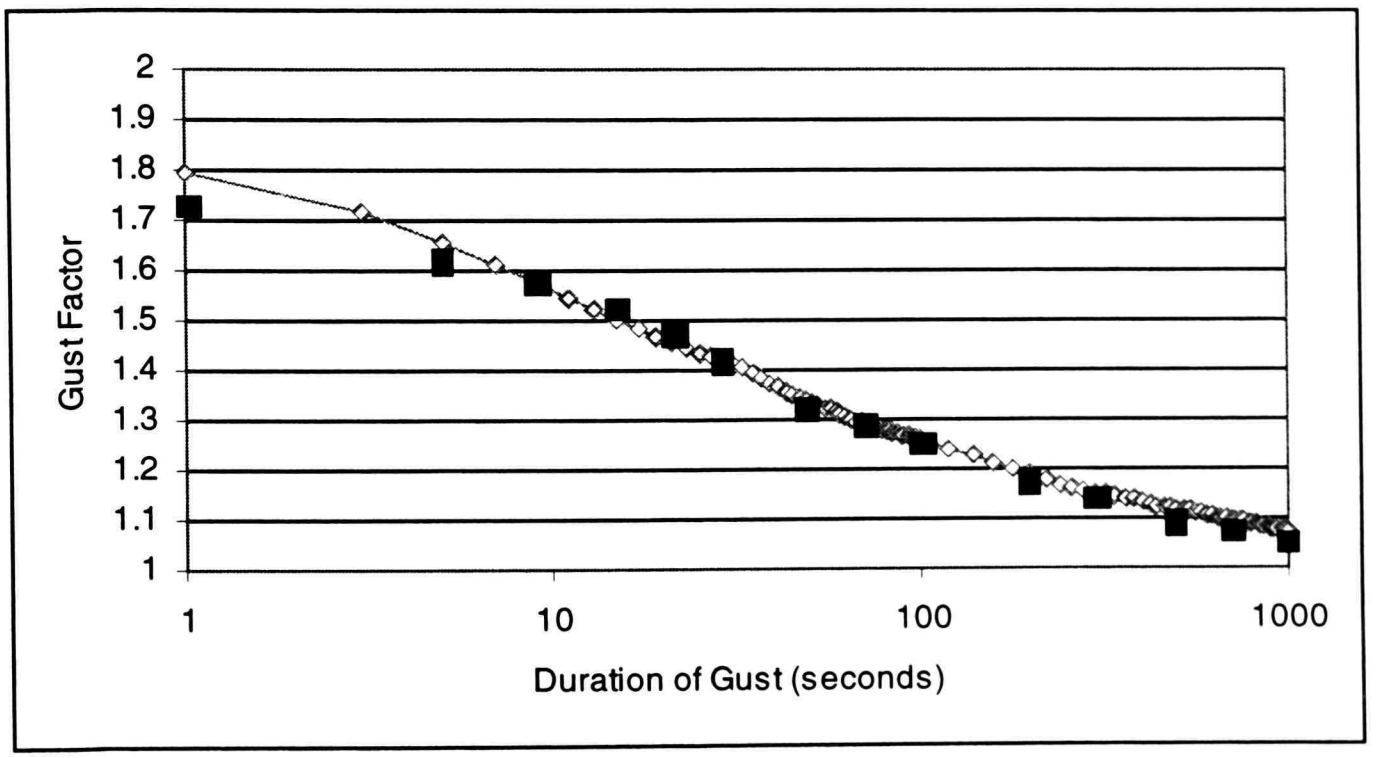

Figure 5.11. Gust Factor curve based on mean hourly wind speeds and average gust factors determined by using Hurricane Bonnie data with airport exposure (with open data points) compared to Marshall/Krayer (with filled data points).

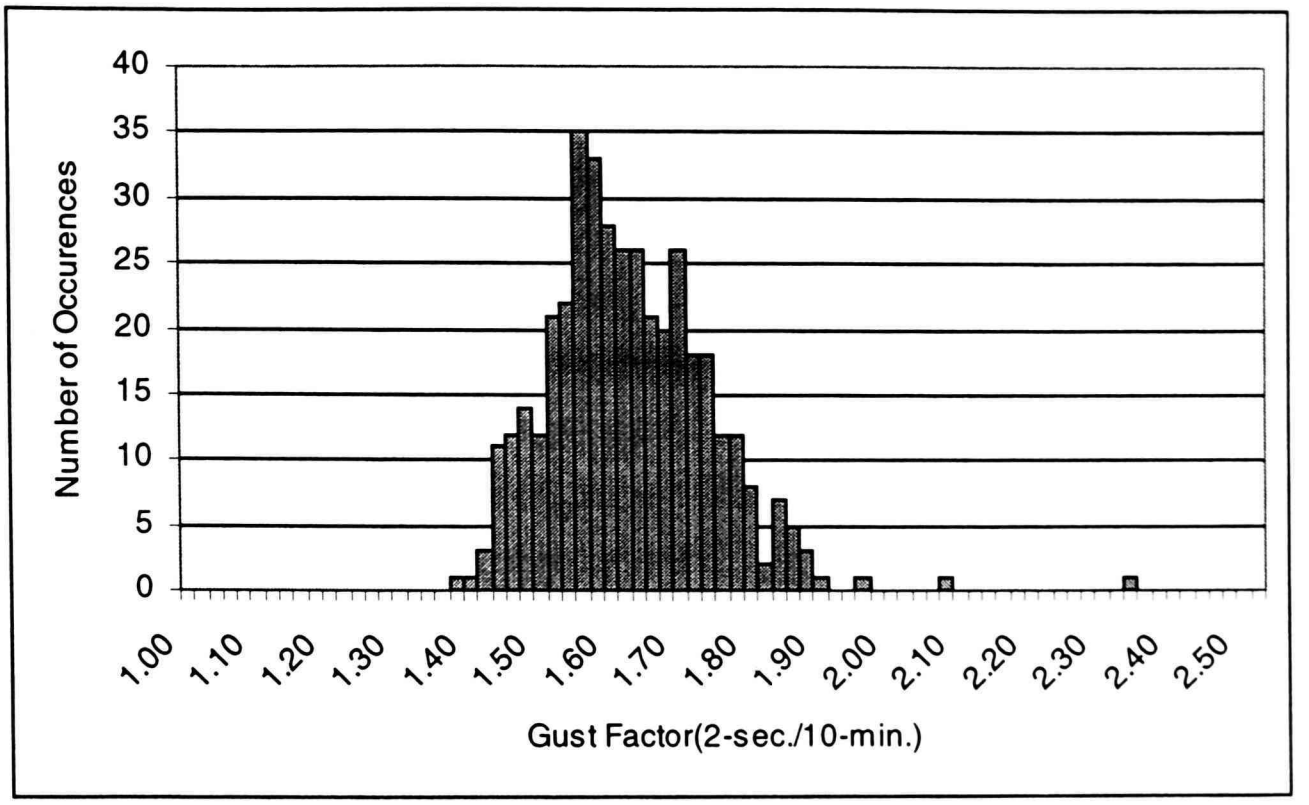

Figure 5.12. Histogram of 2-second to 10-minute GF's collected from the passage of Hurricane Bonnie during airport exposure.

As can be observed in Figure 5.14, the high values of the GF are caused by one peak in the wind speed that occurred at approximately 15:08:45 UTC. Accompanying this change in wind speed is a 40° change in wind direction (Figure 5.14), a 4 m/s to –5 m/s vertical wind speed change (Figure 5.15), and a 1 mb drop in barometric pressure followed by a sharp rise (Figure 5.15). If the event is associated with a storm-scale feature, given the duration of the event (15-20 seconds) and a mean wind speed of approximately 40 m/s at cloud level (estimated from doppler radar), this feature would be about 600-800 m in size, or for a wind speed of 20-25 m/s at 10 m level the feature would be about 400-500 m in size. This is not likely associated with the passage of a meso-vortex which would be of a larger scale (1-3 km), but the correlated pressure drop and changes in wind direction raise the question whether it corresponds to a convective gust within a downdraft of a rainband.

At the time of the intense gust, a plan view of the radar reflectivity (Figure 5.16) indicates the major axis of a rainband has just passed by the site. This rainband passage is also confirmed by looking at the radar reflectivity time history (Figure 5.13) as the reflectivity decreases for a short amount of time between the departing and approaching bands. It is in this location within a rainband (Powell, 1990) that the interface between the updraft and any downdraft would most likely occur. The change in wind direction and drop and rise in pressure may be associated with a downdraft axis or boundary.

While this hypothesis may fit the available data, it is impossible to statistically prove this is what really occurred. Another complication results from the fact that the closest functioning radar was in Morehead City, NC, resulting in no radar data being available in the lowest 1500 m (5000 ft) of the atmosphere. Beyond this, further examination of the record indicates a similar pressure drop and wind direction change occurred within a minute earlier in the record, but no associated gust can be found in the wind speed record.

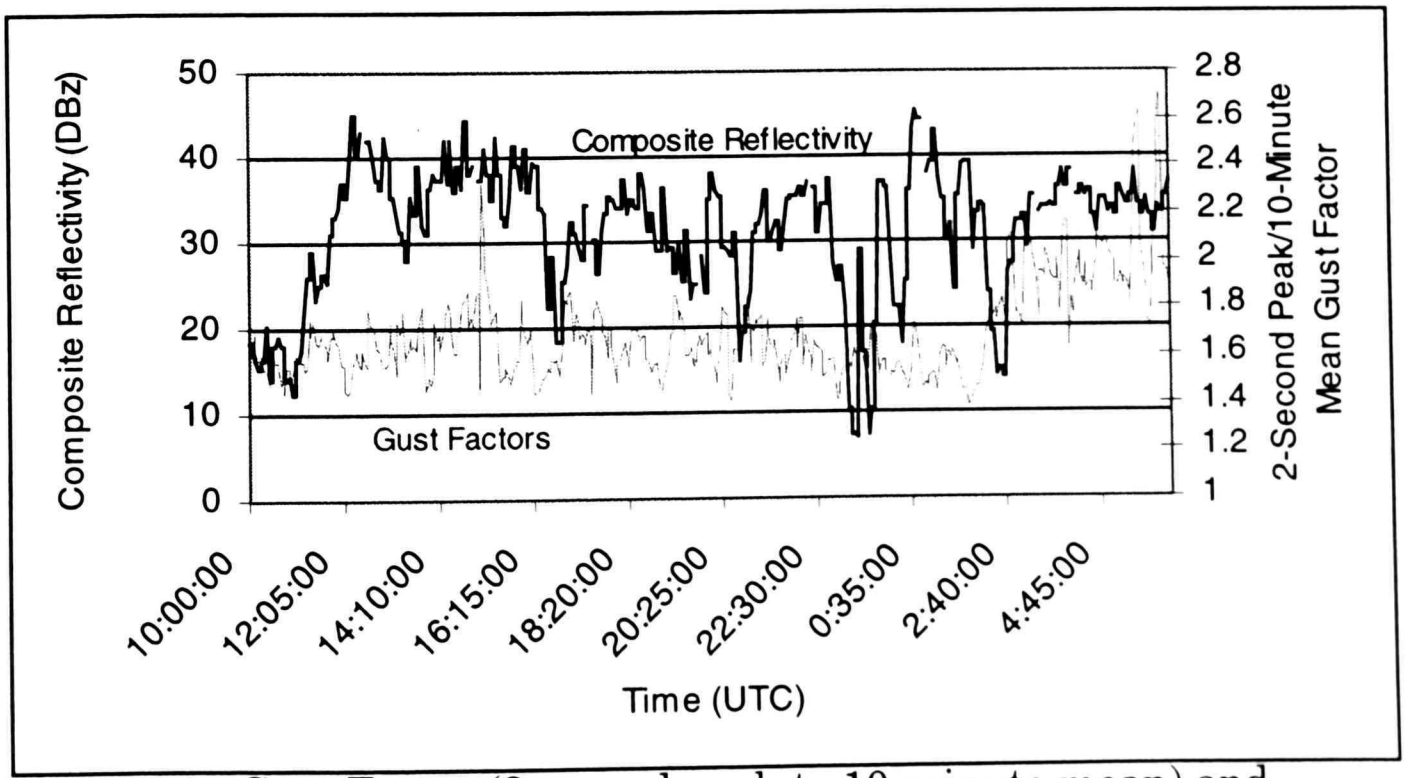

Figure 5.13. Gust Factor (2-second peak to 10-minute mean) and composite reflectivity time histories for Hurricane Bonnie.

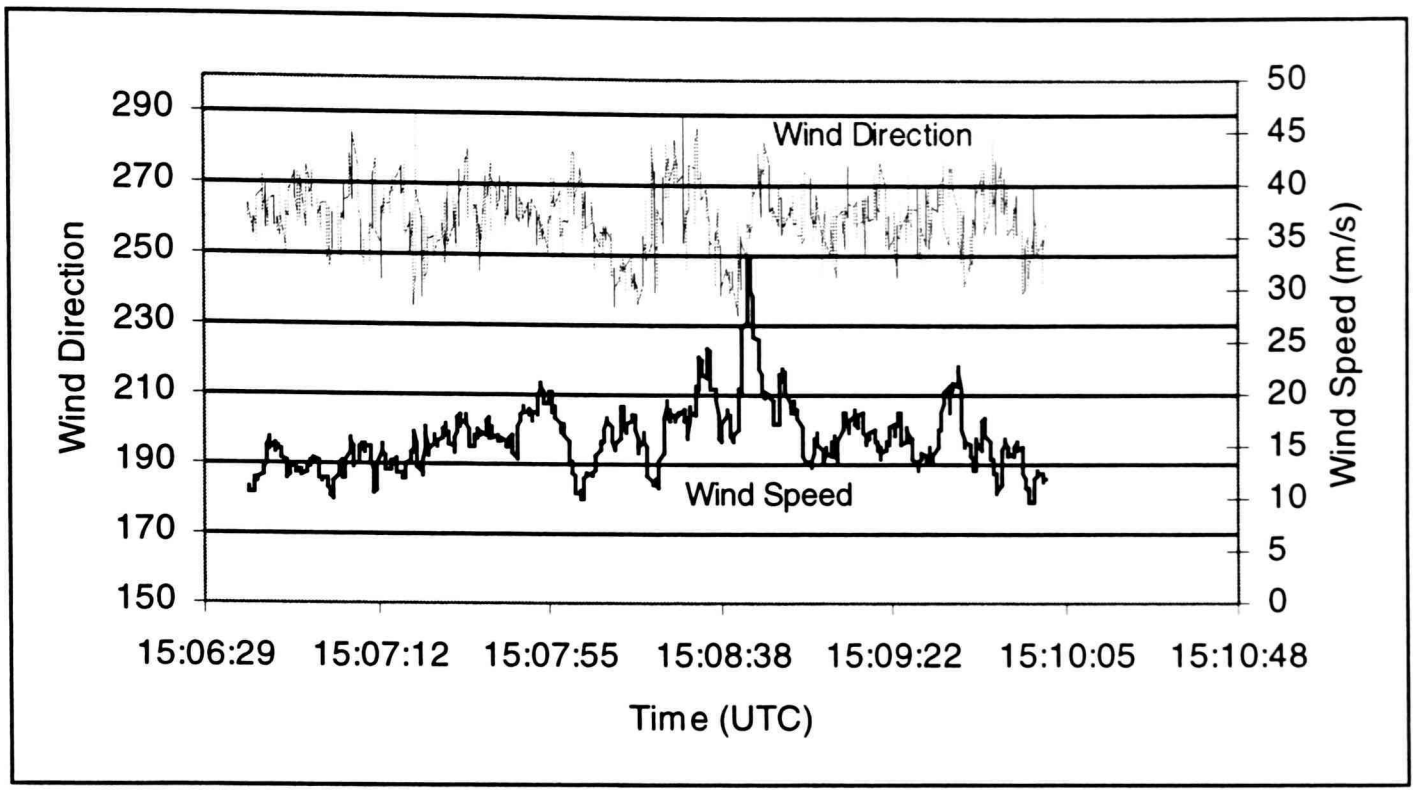

Figure 5.14. Horizontal wind speed and direction time histories from a small portion of the record collected from the passage of Hurricane Bonnie.

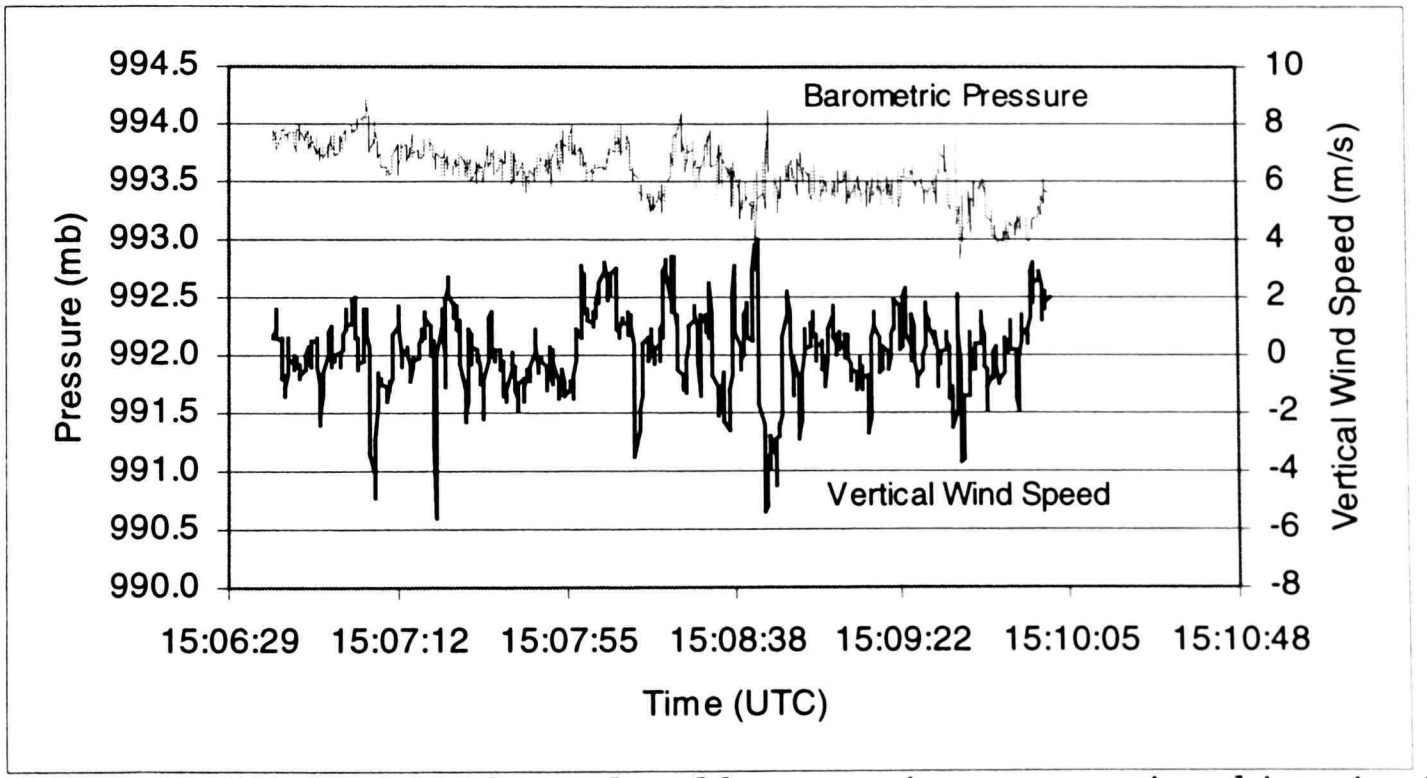

Figure 5.15. Vertical wind speed and barometric pressure time histories from a small portion of the record collected from the passage of Hurricane Bonnie.

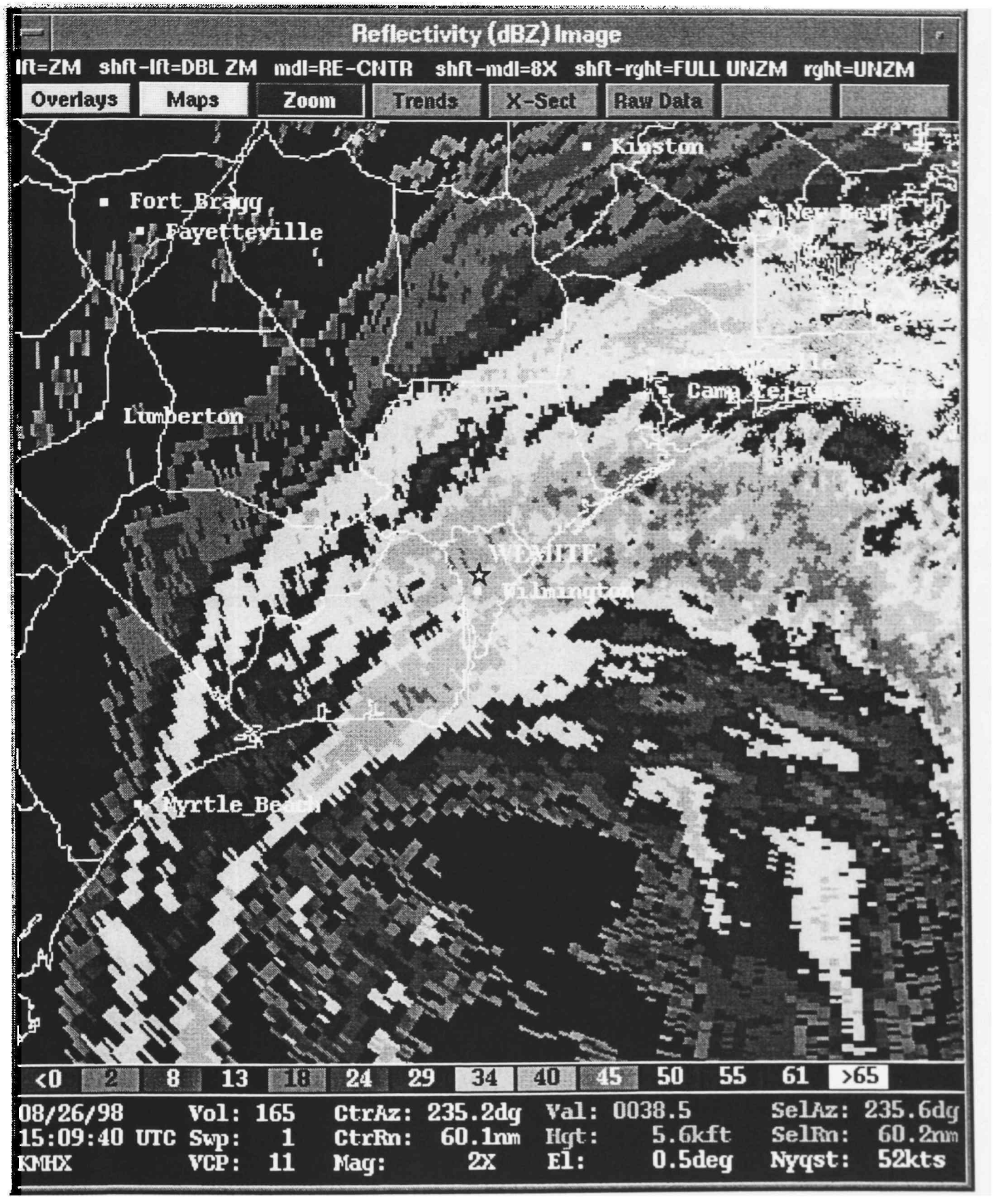

Figure 5.16. Plan view of radar reflectivity from the Morehead City NWS WSR-88D.

5.2.3 Gust Factor Summary and Commentary

It is impossible statistically to draw significant correlation between the GF's determined from the WEMITE data and other meteorological time histories such as radar reflectivity or precipitation time series. For most of the time history, very few "extreme" values in GF's are found for the airport exposures. However, it has been shown that the most extreme value of the determined GF's occurred in a region where the barometric pressure changed abruptly, and vertical wind speed and wind direction also deviated. These changes may be associated with storm-scale motions, but it cannot be proven with the data at hand.

In general from Figure 5.11, it appears that GF values are very consistent within a given exposure. This observation would lead one to the hypothesis that Marshall and Krayer's findings of elevated GF's within hurricanes compared to Durst's extratropical work may indeed be due to slight changes in exposure as predicted by Sparks, and not due to convective gusts. Upon closer examination (elaborated in Chapter 5, Section 6) GF's do indeed show some variation that can be attributed to convective scale motions. With this in mind one might expect that, if GF's increase due to convective gusts as Marshal and Krayer hypothesize, these higher GF's would be more prevalent in other more active hurricanes, and would cause localized enhancement in favored areas such as the interior half of rainbands, or within the eyewalls. This effect may be more prevalent in more intense hurricanes.

5.3 Integral Scales

The longitudinal integral scale simply represents the average along-wind dimension of the wind gusts in a given data segment. Thus, integral scales (longitudinal, lateral, and vertical) are related to the total static load on a structure. As the integral scale increases, the gust size increases, along with its total influence on a structure. Therefore, integral scales are inherent in building standards and are "matched" by wind tunnel operators in order to properly model the wind and collect realistic building pressure data. Only a limited amount of analysis (Schroeder et al. 1998; Chuen 1971) has been conducted on the integral scales present within the HPBL due to a lack of high-resolution wind speed data.

5.3.1 Integral Scale Statistics

The results presented in this case study are determined by calculating the ACF for 5-minute data (using 50% offset) segments of instantaneous longitudinal wind speed from the 10.7 m WEMITE data. Then an exponential curve is fitted to the data up to where the derivative of the ACF curve is zero. This represents the location in the ACF where the correlation starts to increase with longer lag duration. Once the exponential curve is fitted, it is integrated from zero to infinity to obtain the time integral scale. The time integral scale is then multiplied by the mean longitudinal wind speed over the same 5-minute data segment to obtain the longitudinal integral scale. Just as with the determination of the TI's, the time period used to calculate the ACF curve will affect the final integral scale calculated. This effect can be seen in Figure 5.17; with increasing time periods the area under the ACF curve increases, thereby effectively increasing the integral scale.

The results from Hurricane Bonnie, shown in Table 5.10, indicate a mean longitudinal integral scale of 99 m for stationary data segments (with respect to the first moment) within the airport exposure with a maximum of 255 m noted. Results from the nonstationary data segments indicate an increase in mean longitudinal integral scale to 145 m with a maximum value of 376 m found. This represents an increase of 46% in the average longitudinal gust size for the nonstationary data relative to the stationary data. Examination of the longitudinal integral scales determined from data within the transitional flow regime indicate a decrease in the average longitudinal gust size to 68 and 90 m for stationary and nonstationary data segments, respectively.

Upon examination of the longitudinal integral scale time history (Figure 5.18) two different integral scale regimes can be observed which are not associated with changes in surface roughness. One regime never has integral scales over 150 m, while the other regime has multiple peaks over 200 m. This phenomenon includes spectral methods and employing ACF curves generated from longer data segments. These two different regimes are evident regardless of the method used to calculate the integral scales. Therefore, the two different regimes are inherent to the flow and not dependent on the method of calculation. This is evident in the histogram of longitudinal integral scales determined for airport exposure (Figure 5.19) as there are hints of a secondary peak in the distribution from about 150 to 180 m, and the right hand tail is much longer than that expected for a normal distribution.

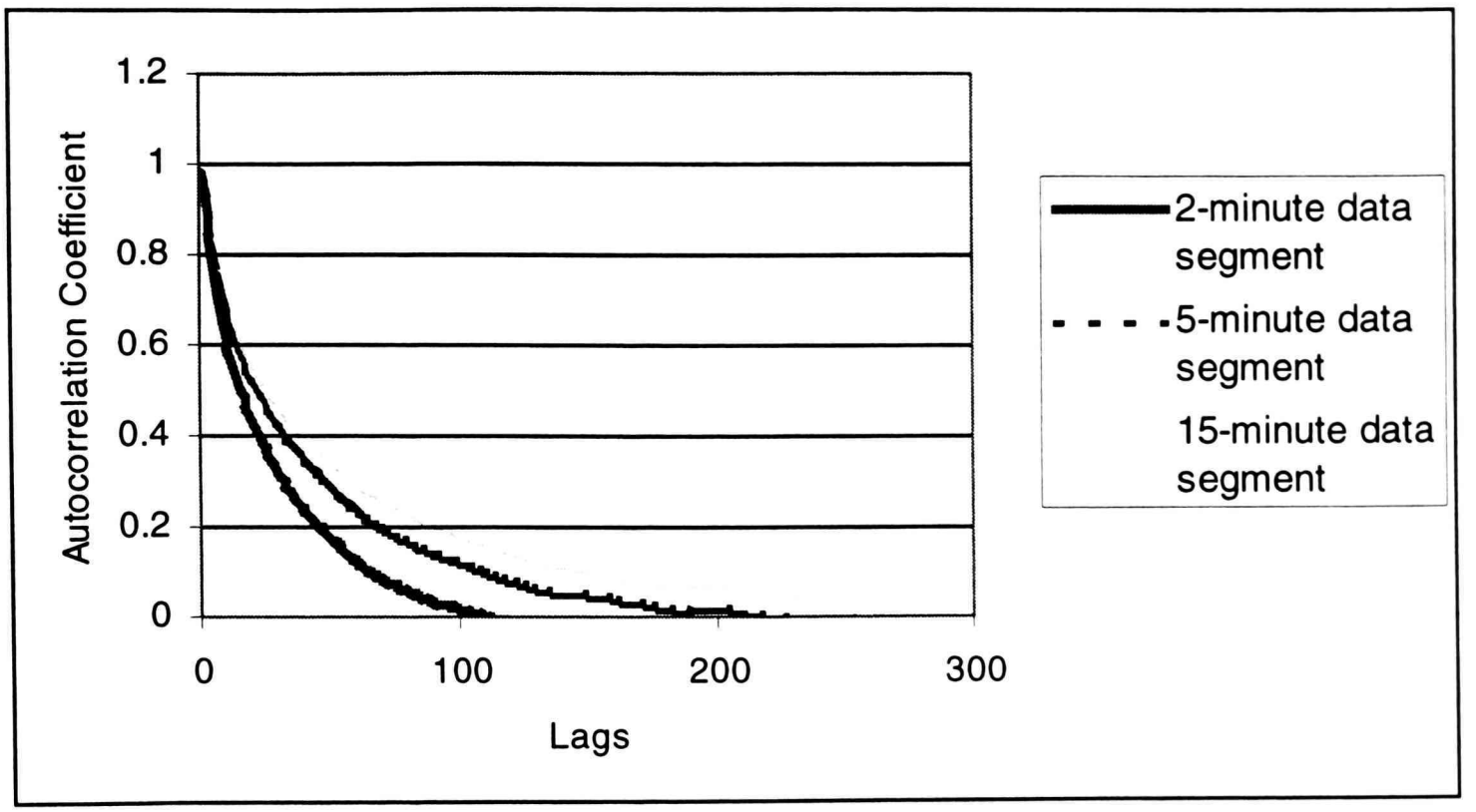

Figure 5.17. Mean ACF's determined from Hurricane Bonnie using various data segment lengths.

Table 5.10 Longitudinal integral scale statistics for Hurricane Bonnie classified in terms of stationarity with respect to the longitudinal mean wind speed.

	Stationary		Nonstationary	
	Airport	Transitional	Airport	Transitional
No. 5-min. Segments	269	74	133	27
Mean (m)	99.9	68.4	144.9	90.2
Maximum (m)	254.6	179.5	376.3	175.8
Minimum (m)	37.6	31.3	36.9	32.4
Standard Deviation	37.3	24.5	64.4	34.4

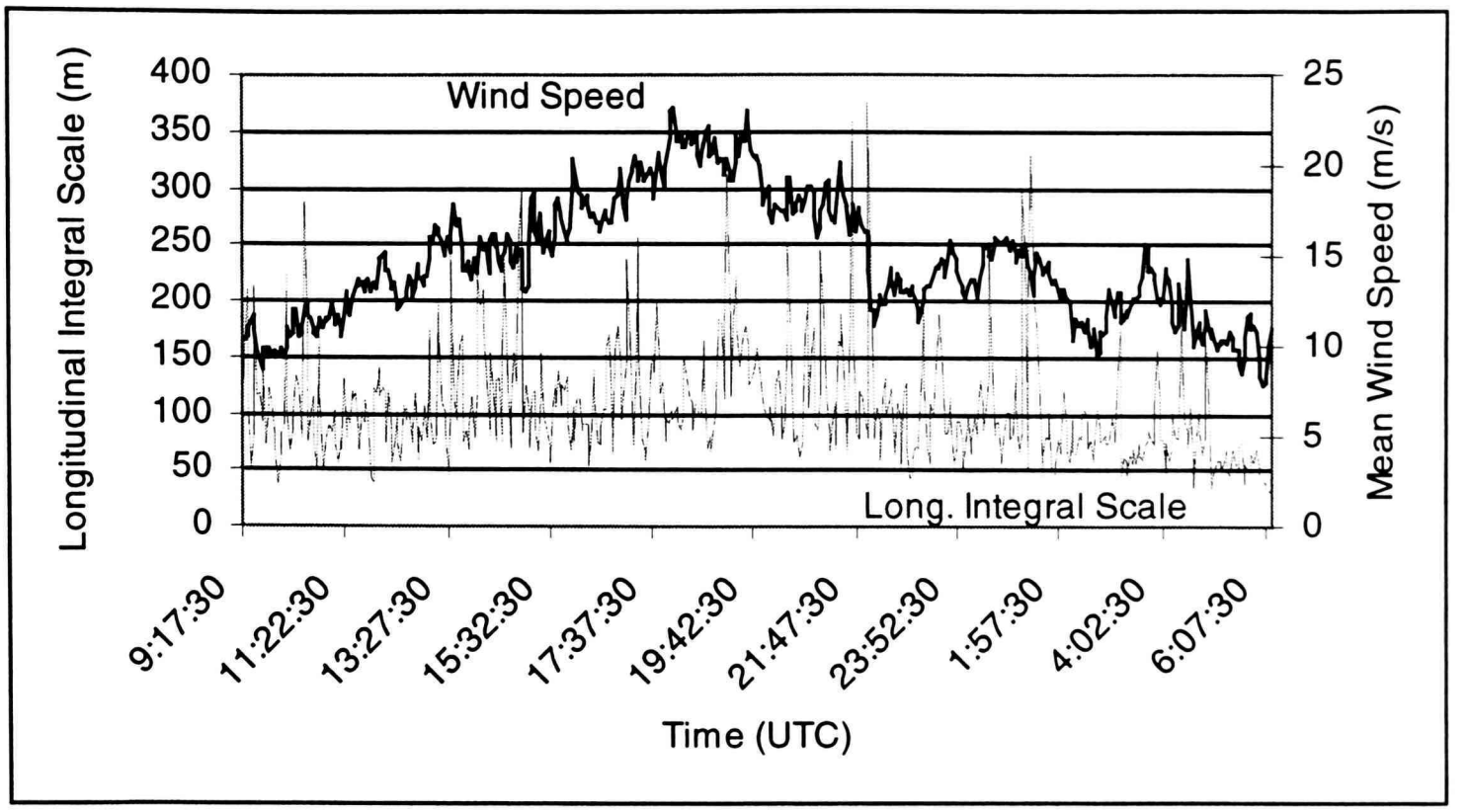

Figure 5.18. Time history of longitudinal integral scales as determined from the 10.7 m WEMITE data during the passage of Hurricane Bonnie.

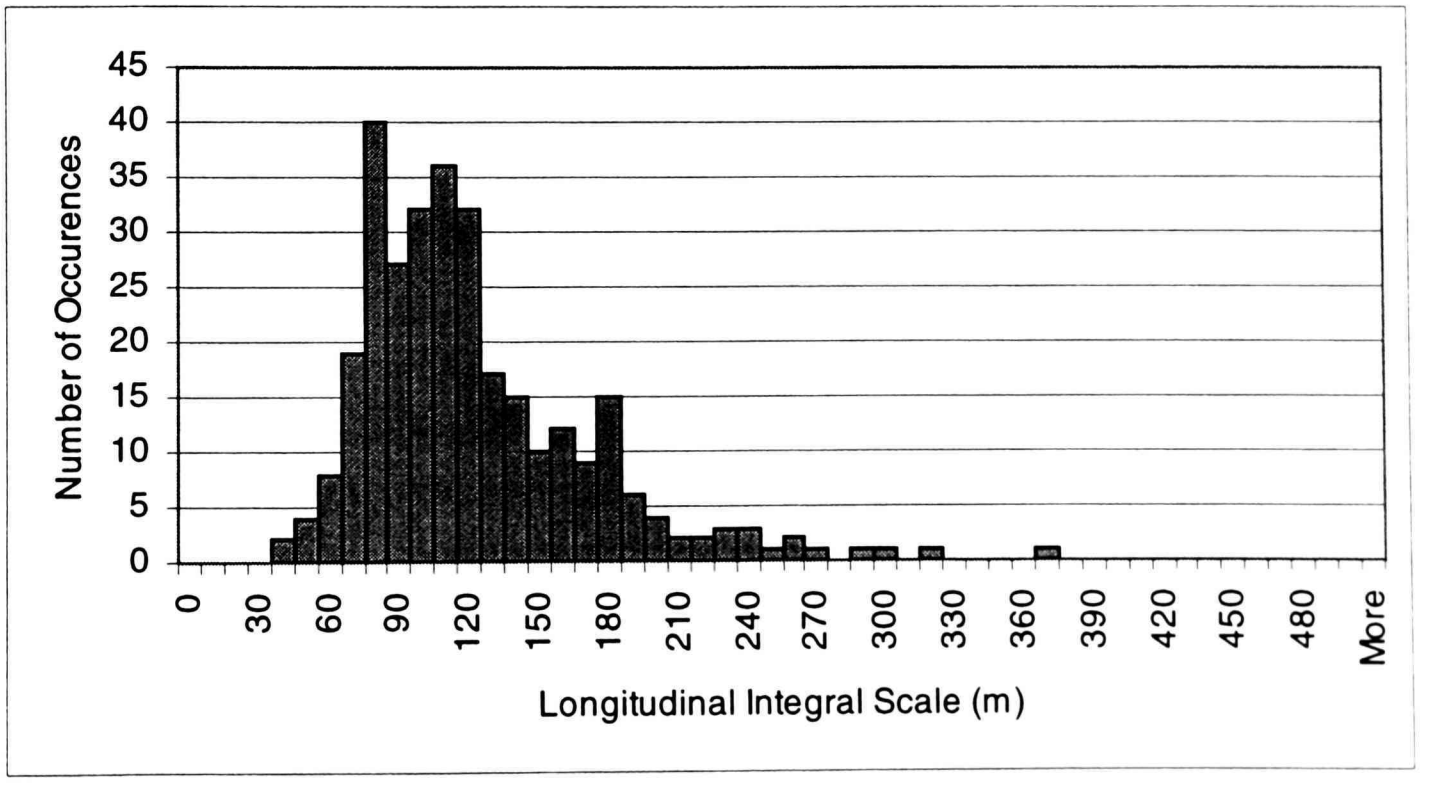

Figure 5.19. Histogram of longitudinal integral scales.

5.3.2 Comparison to Meteorology

Comparison of the generated longitudinal integral scale time history to the radar reflectivity time history (Figure 5.20) shows some observational correlation, especially when a moving average filter is used to remove high frequency fluctuations. Rarely do the large integral scales occur in time periods centered with high reflectivity; this is especially true in the outer rainbands. In fact, in most cases they seem to occur at adjacent locations just prior to or following the "center" of the high reflectivity. This can be seen at numerous times in the time history such as at 13:30-14:45, 16:30-17:30, and 19:15-20:15 UTC. While this is evident visually in the time history, if a scatter plot is made of reflectivity and longitudinal integral scales (Figure 5.21) the correlation is impossible to find. Both signals are very noisy and fluctuate rapidly.

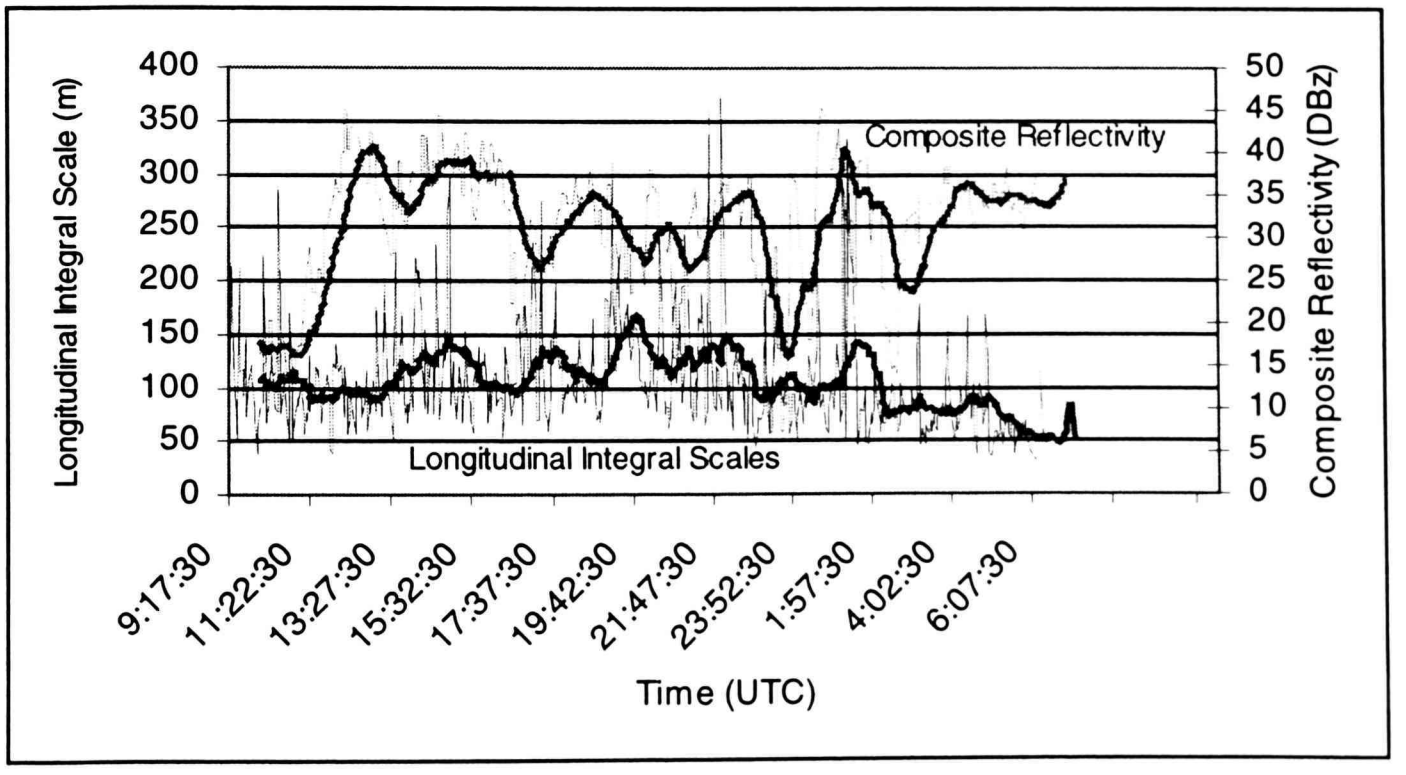

Figure 5.20. Time history of longitudinal integral scales and composite reflectivity as determined from the 10.7 m WEMITE data and the Morehead City NWS WSR-88D during the passage of Hurricane Bonnie.

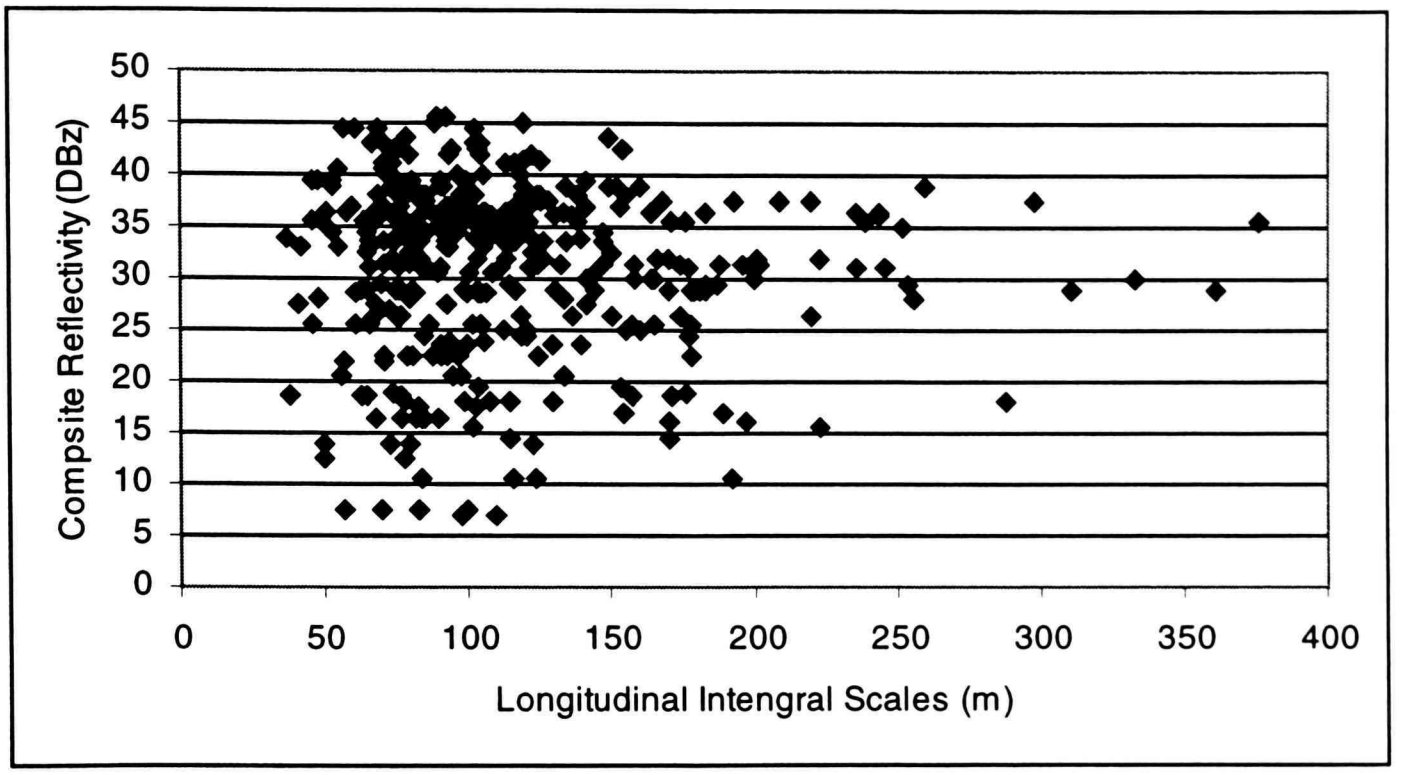

Figure 5.21. Scatter plot of longitudinal integral scales and composite reflectivity as determined from the 10.7 m WEMITE data and the Morehead City NWS WSR-88D during the passage of Hurricane Bonnie.

Close examination of the record indicates that the largest sustained integral scales occurred at approximately 19:30 UTC. This event corresponds to the passage of the first eyewall (Figure 5.22). At this time the convection in the eyewall was not very intense, as indicated by the lack of high reflectivity in the radar image, but the site is located along the inside edge of the eyewall. The largest peak integral scales occur about one hour later at 20:20 UTC, with the passage of another eyewall feature. At this time forced convection along the coastline has aided in the development of an intense convective cell that passes just south of the deployment site (Figure 5.23). These two radar images depict several features. The storm was moving extremely slowly to the north, and the eyewalls (inner and outer) are not steady state. They have changed rapidly in appearance and relative location

within the hour between the two radar images. In fact, the latter image indicates the two eyewalls have combined to the northwest of the center of circulation near Wilmington.

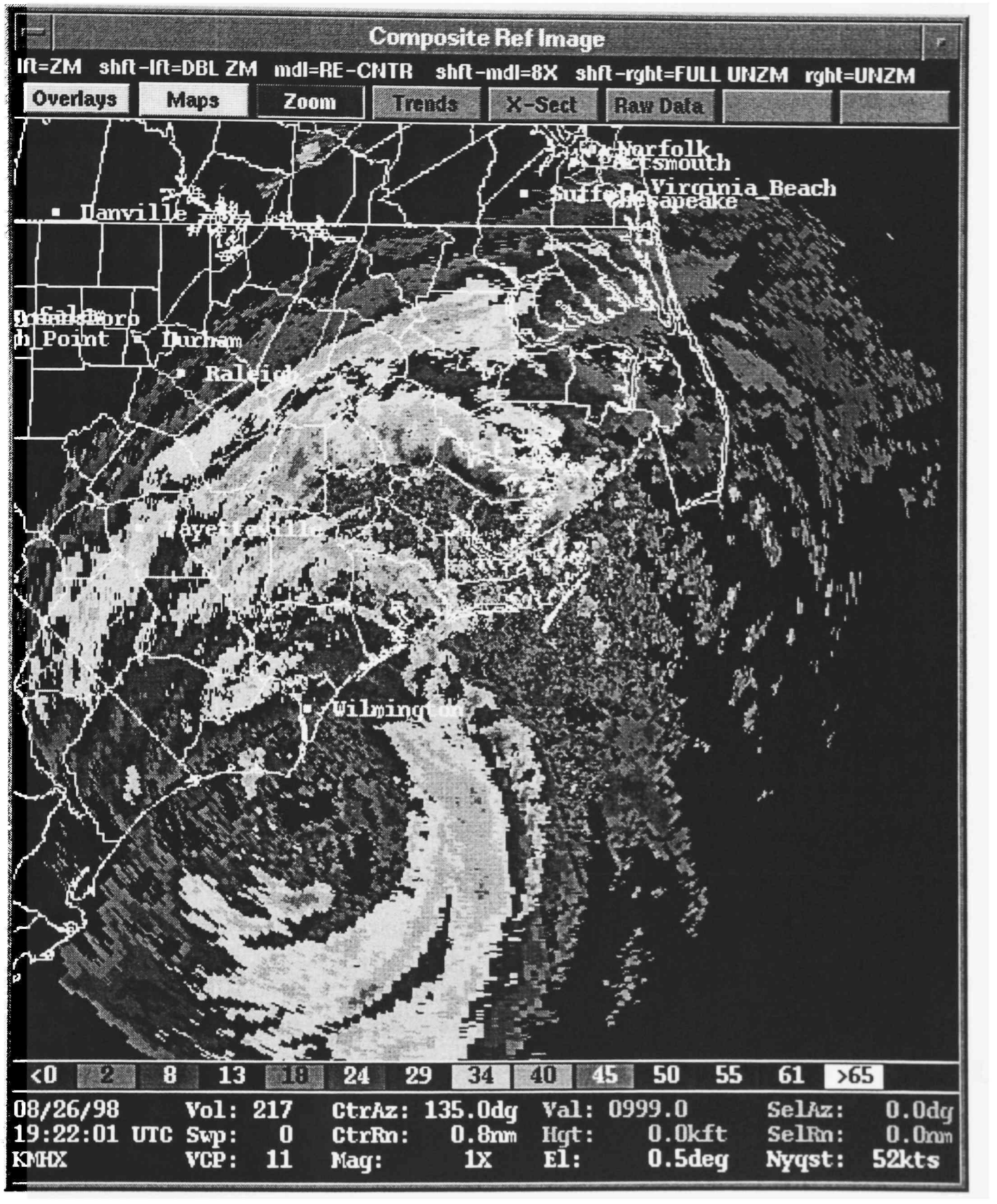

Figure 5.22. Morehead City NWS WSR-88D reflectivity image for 19:22 UTC.

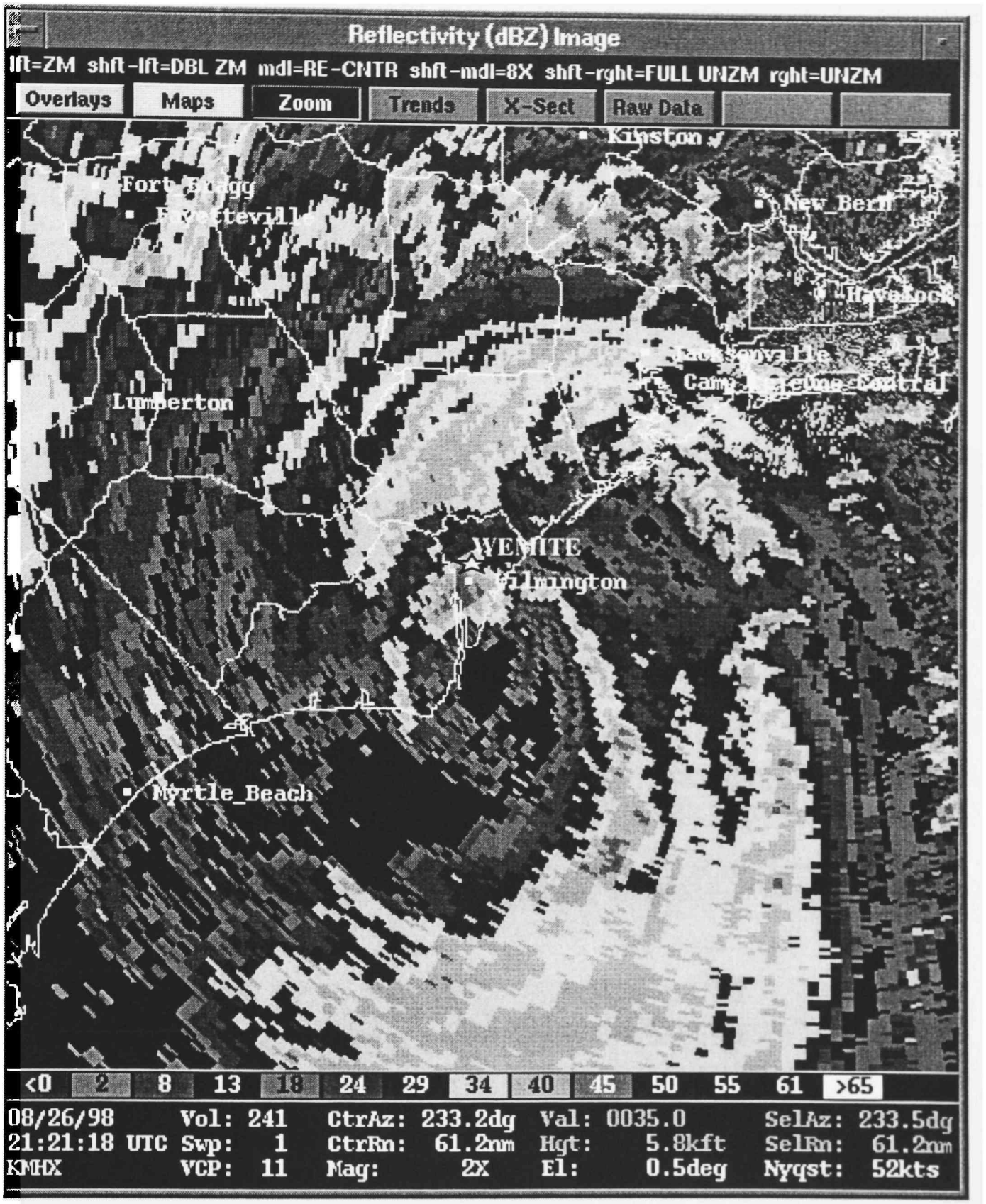

Figure 5.23. Morehead City NWS WSR-88D reflectivity image for 21:21 UTC.

A cross-section of the radar reflectivity at 21:21 UTC is also provided in Figure 5.24. The deployment site is located at about the 15 nautical mile marker along the horizontal axis. It is adjacent to the convective cell located just to the south the site. This cross-section shows the complications of simply relating a time history of radar reflectivity to turbulent characteristics of the wind. Some rainbands may have a maximum reflectivity of 35 DBz while other intense convective cells may have reflectivities as high as 45-50 dBZ.

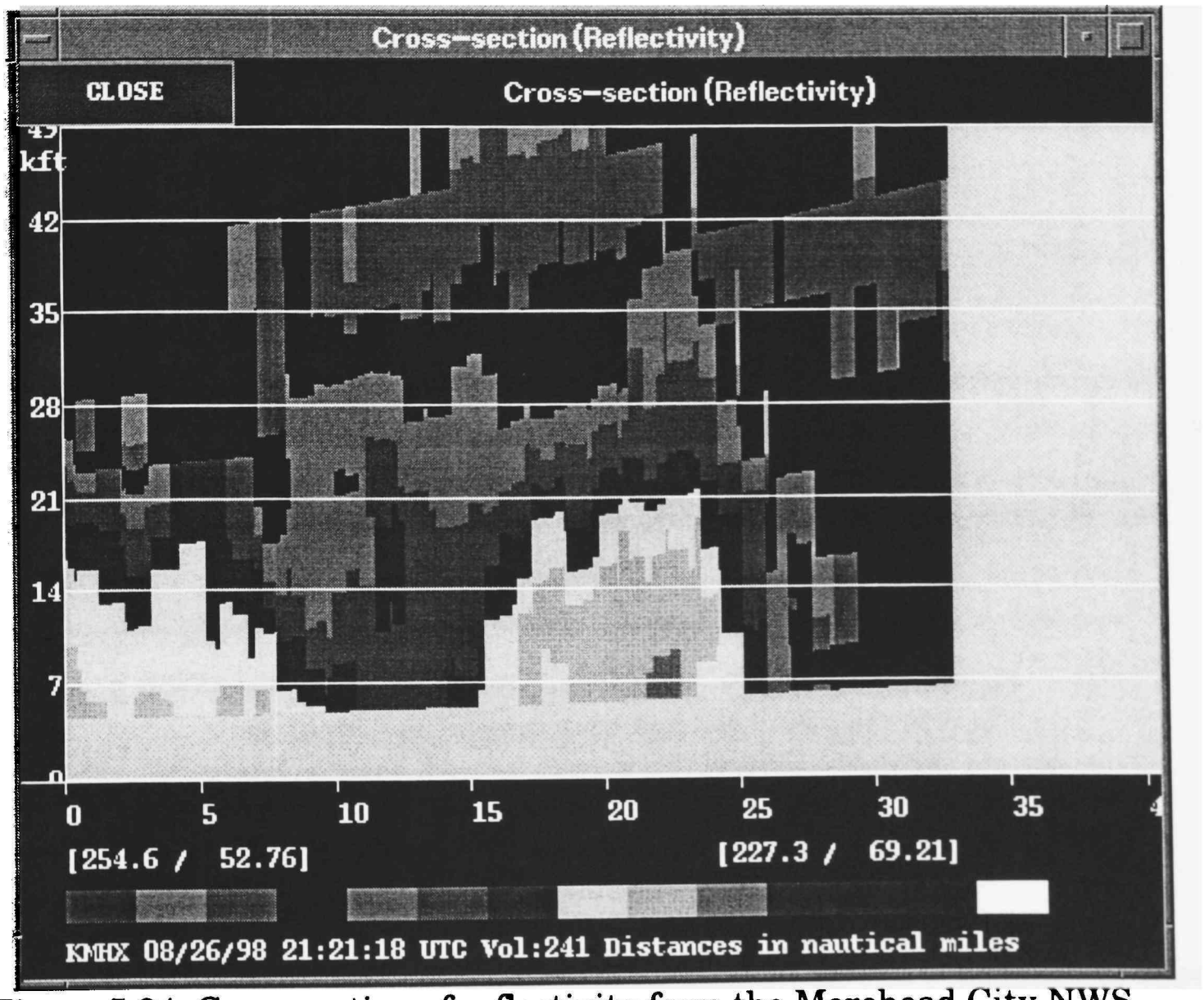

Figure 5.24. Cross-section of reflectivity from the Morehead City NWS WSR-88D at 21:21 UTC.

Another revealing comparison can be made to vertical wind (Figure 5.25). It can be seen that the majority of the largest integral scales occur when the 5-minute average vertical wind speed is negative. While some downward motion is expected with time, negative values of vertical wind speeds from –0.2 to –0.4 m/s averaged over a 5-minute period seem to indicate more that just turbulent BL mixing. In a neutral BL the vertical wind speed averaged over several minutes should be very close to zero. Again, if a scatter plot is made the correlation cannot be found.

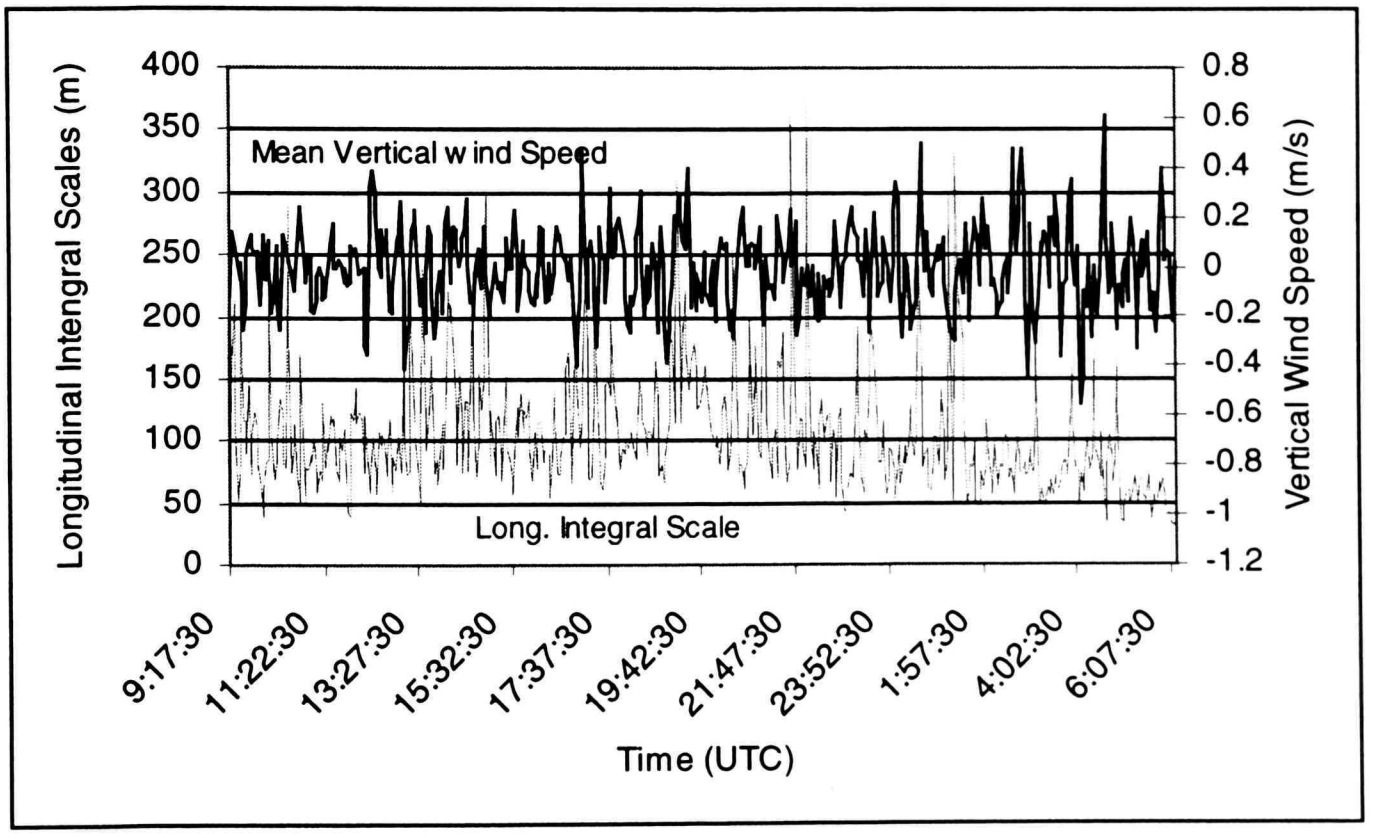

Figure 5.25. Vertical wind speed and longitudinal integral scale time histories recorded by the 10.7 WEMITE anemometer during the passage of Hurricane Bonnie.

5.3.3 Comparison to ASCE 7-98

Longitudinal integral scales are present in ASCE 7-98 and are used in the determination of the gust effect factor. Just as with the TI's, integral scales are assigned for each different exposure (Table 5.10). The values given are determined for an equivalent height of 10.7 m.

Table 5.11 ASCE 7-98 determined integral scales for various exposures.

Exposure	Description	Integral scales at 10.7 m (m)
A	Large City Center	56
B	Suburban	99
C	Open Terrain	155

The WEMITE deployment in Hurricane Bonnie was in an "airport" exposure for the first portion of the record. This exposure yielded a mean longitudinal integral scale of 115 m with a standard deviation of 52.4 m. Because this exposure would be classified as exposure C in ASCE 7-98, the actual mean integral scale is smaller than its ASCE 7-98 counterpart. However, from the time history, we know that integral scales as large as 200 m occurred at several locations within the storm and for sustained time periods, and thus the standard deviation is substantial. For wind speed data with the transitional exposure, the mean longitudinal integral scale is 74 m with a standard deviation of 29 m.

5.3.4 Integral Scale Summary and Commentary

It has been shown that integral scales vary widely throughout the passage of Hurricane Bonnie. Most interesting is the presence of two different regimes that are not associated with changes in surface roughness. The one regime is usually located adjacent to the central portion of a rainband or eyewall, and produces substantially larger integral scales relative to the other regime. So in contrast to TI's and GF's, integral scales show some promise and may indeed be influenced by convective scale

motions, with storm-scale processes (downdrafts, etc.) producing turbulence of a larger scale than a neutral BL counterpart.

Another visual correlation can be made with vertical wind speeds, as larger integral scales usually are accompanied by 5 minute mean vertical wind speeds that are negative. These correlations cannot be found by using scatter plots on the original data; however when a moving average filter is applied to the data to remove high frequency fluctuations the correlations become apparent. Since no two rainbands are identical though, and peak reflectivity values contained within each band are different, it is difficult to compare one rainband/eyewall to another.

A close examination of the TI's and integral scales indicates some dependence (Figure 5.26). Within the same terrain conditions, TI's increase with increasing integral scales, indicating that the largest gusts also produce a fair amount of variance in the wind speed record. Thus we would expect to find a moderate amount of energy at larger scales in the PSD. Reducing the data to only stationary data segments does not improve the correlation.

Comparing integral scale values provided by ASCE 7-98 to those found in Hurricane Bonnie indicates the mean gust size found within Hurricane Bonnie was smaller than expected. However, since the standard deviation of the integral scale statistic is fairly large, it is likely that a structure within Hurricane Bonnie would have seen 5-minute mean integral scales as large as 200-300 m several points through the storm.

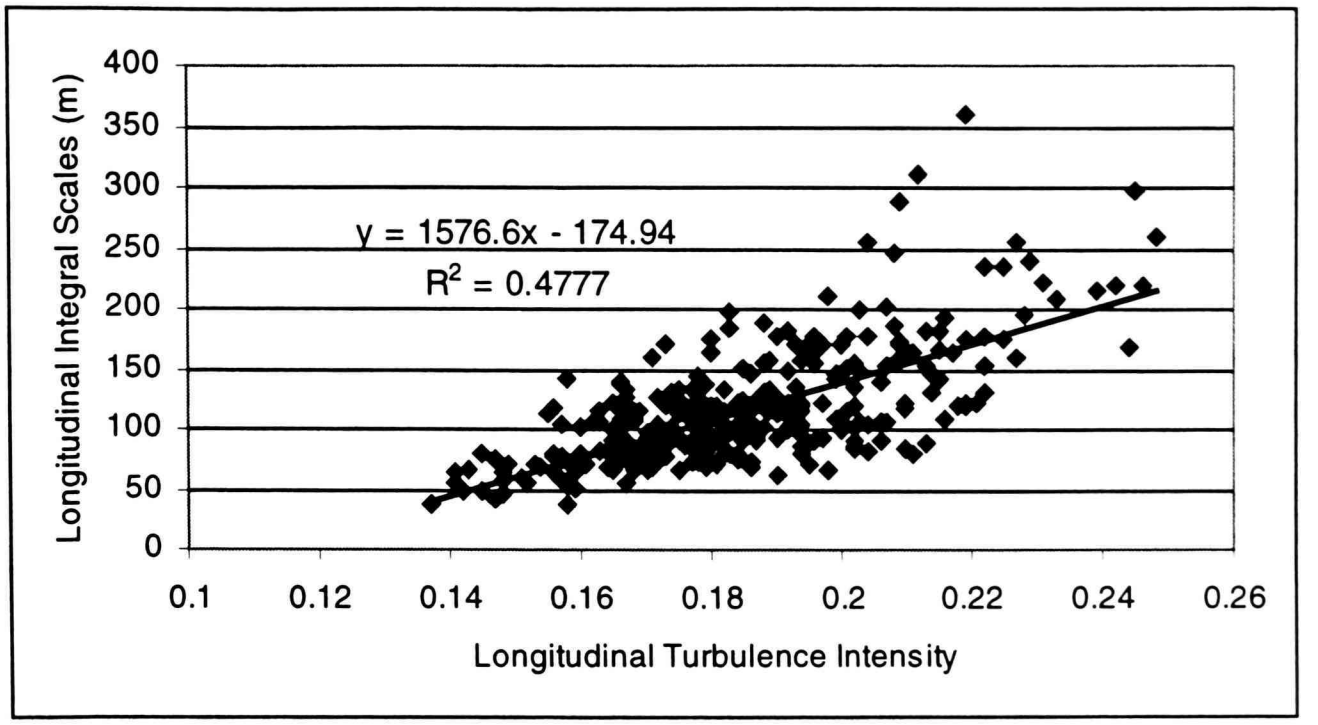

Figure 5.26. Longitudinal integral scales and turbulence intensities.

5.4 Power Spectral Density and Spectrograms

5.4.1 Power Spectral Density

A PSD estimate of the longitudinal wind speed record was made for a 2-hour data segment near the peak of the storm. For this 2-hour time period from 17:50 to 19:50 UTC, the wind speed averaged approximately 21.3 m/s (average of 5-minute mean wind speeds), and was fairly consistent (stationary). The longitudinal PSD estimate is shown in Figure 5.27. Reduced frequency is employed as the horizontal axis and normalized power (power spectrum divided by the variance) multiplied by the frequency is used for the vertical axis. The Nyquist frequency is 2.5 Hz, given the sampling rate of 5 Hz. The original two hours of time series data was segmented into 10-minute data segments (with a 50% offset) that were used to calculate individual PSD's. The final presented PSD was taken as the average of these individual PSD's.

Comparisons between the acquired data and expected models such as the perturbed terrain or flat-smooth-uniform (FSU) models (Tieleman, 1995)

indicate the longitudinal wind speed data lacks high frequency energy and contains more low frequency than expected. In general the peak frequencies are in reasonable agreement, and the lack of high frequency energy is thought to be due to the minimal response characteristics of the Wind Monitor anemometer used for the WEMITE application. The additional low frequency energy in the estimate is most likely from the "storm" environment and is in agreement with previous research completed by Powell (1996a) which indicates more low frequency energy in the spectrum.

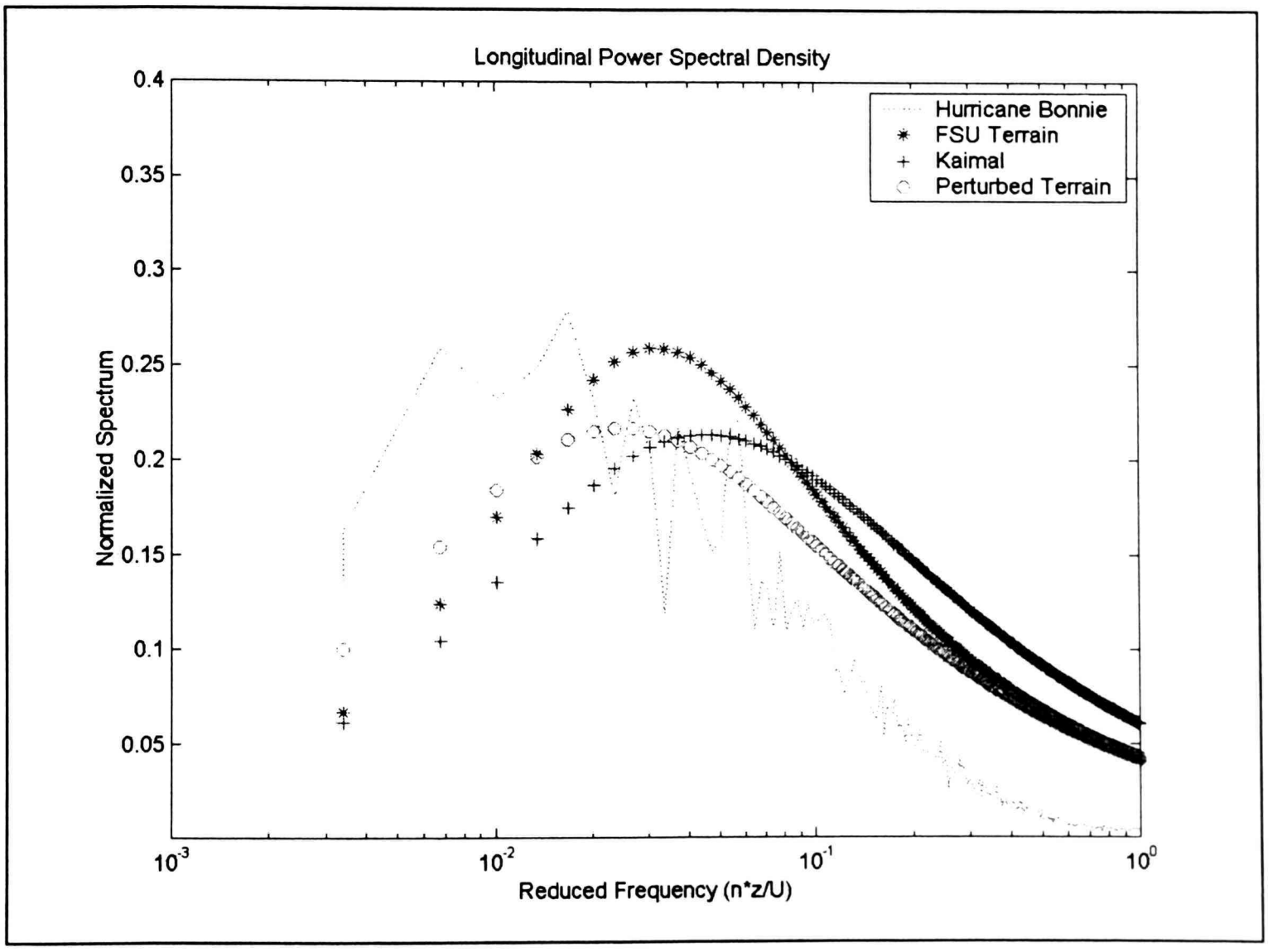

Figure 5.27. Longitudinal power spectral density estimate from WEMITE data compared to theoretical model spectra.

Comparing longitudinal PSD estimates (Figures 5.28 and 5.29) generated from UVW and Wind Monitor anemometers reveals a remarkably good similarity. In these figures, the Nyquist frequency is increased to 5 Hz due to employment of a 10 Hz sampling rate in Hurricane Dennis (the source of the data). Again the reduced response of the Wind Monitor and UVW anemometers can be noted as the high frequency energy content of the longitudinal wind record does not compare well to the model spectra.

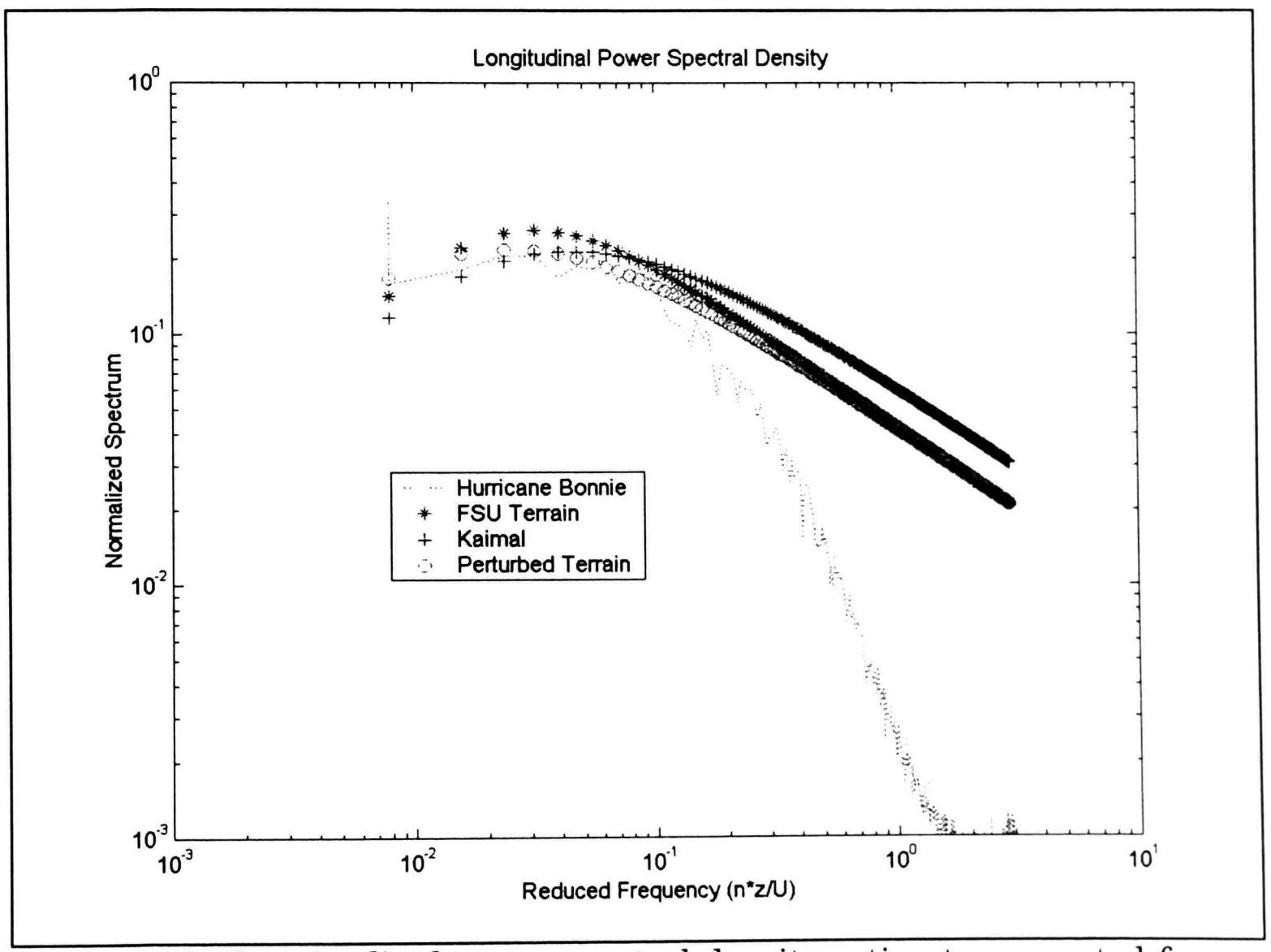

Figure 5.28. Longitudinal power spectral density estimate generated from a Wind Monitor anemometer in Hurricane Dennis (1999).

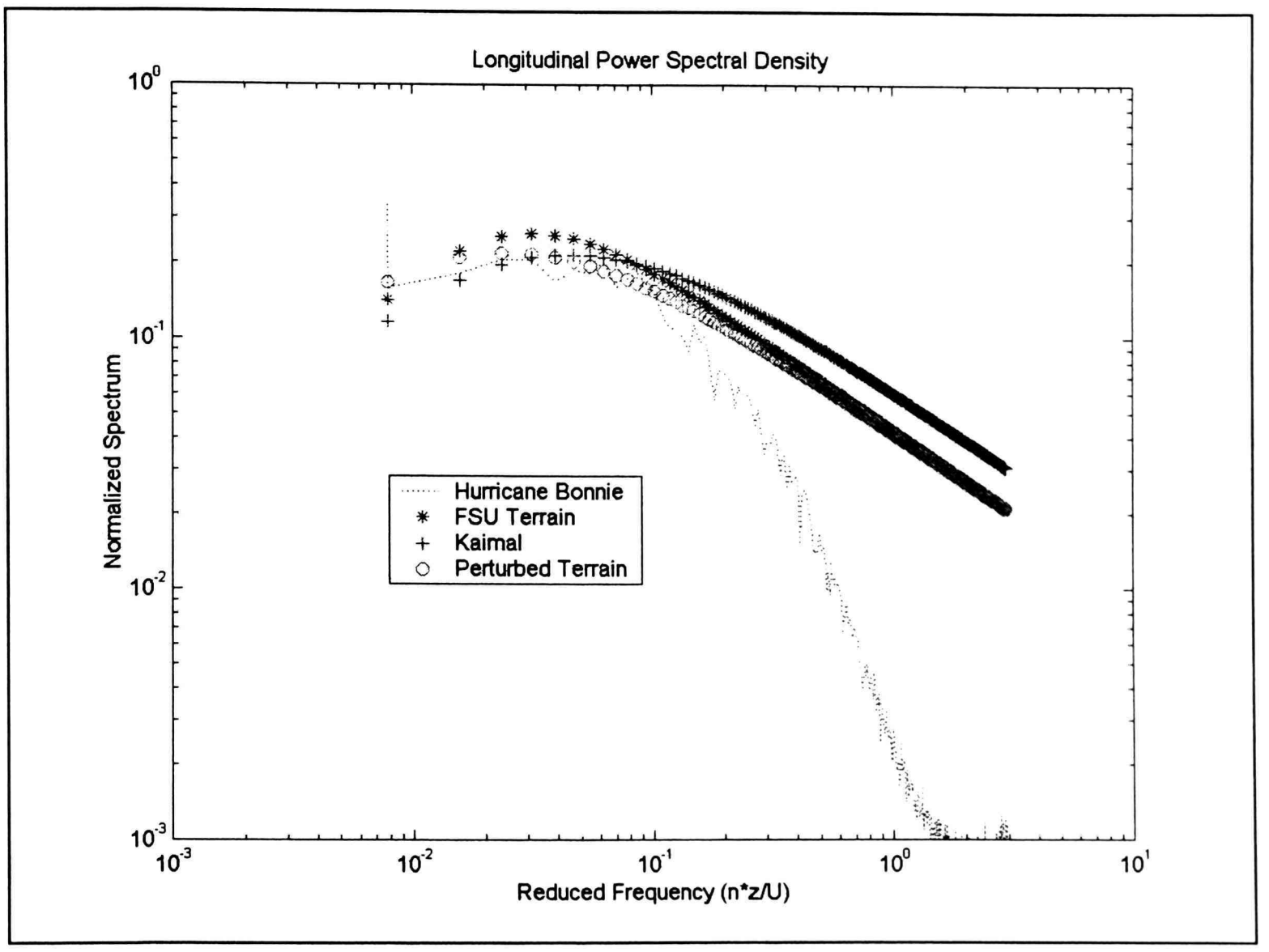

Figure 5.29. Longitudinal power spectral density estimate generated from a UVW anemometer in Hurricane Dennis (1999).

5.4.2 Spectragram

A spectragram is a more useful tool for trying to evaluate changes in energy content throughout the storm. Changes in time are not lost through averaging over the entire event or several hours. So if one is searching for an event which occur over a period of minutes, then the spectragram offers a more valuable tool to highlight such changes.

A spectragram of the wind record recorded by the 10.7 m anemometer of WEMITE during Hurricane Bonnie is shown in Figure 5.30. It was calculated by separating the record into 10-minute data segments that are subsequently used to calculate the local PSD using the AR(50) and nonparametric methods. These individual estimates are stacked into a time history of PSD's that represents the presented spectragram. In this figure, the vertical axis is the logarithm (base 10) of the frequency, the horizontal axis is time, and the brighter colors indicate higher amounts of normalized power (power multiplied by frequency divided by variance).

From the figure it can be seen that the peak frequency and peak amplitudes do indeed change with time. Changes in peak frequency can result from increasing wind speed or actual changes in the process. Time histories of peak frequency and normalized peak frequency are provided in Figures 5.31 and 5.32. These can be used to separate the effects of increasing winds speeds.

Given the process remains constant in time, the normalized peak frequency would not change. Therefore one can observe that there are substantial differences in normalized peak frequency throughout the storm due the natural variability or changes in process of the wind. The variability in normalized peak frequency (period) for airport exposure ranges from 0.06 Hz (17 seconds) to less than 0.01 Hz (100 seconds). This represents a 600% variation in normalized peak frequency from one location in the storm to

another. One can also note the change in normalized peak frequency associated with the change in exposure found at the end of the record. Higher frequency energy (smaller scales) becomes more active with the rougher transitional exposure.

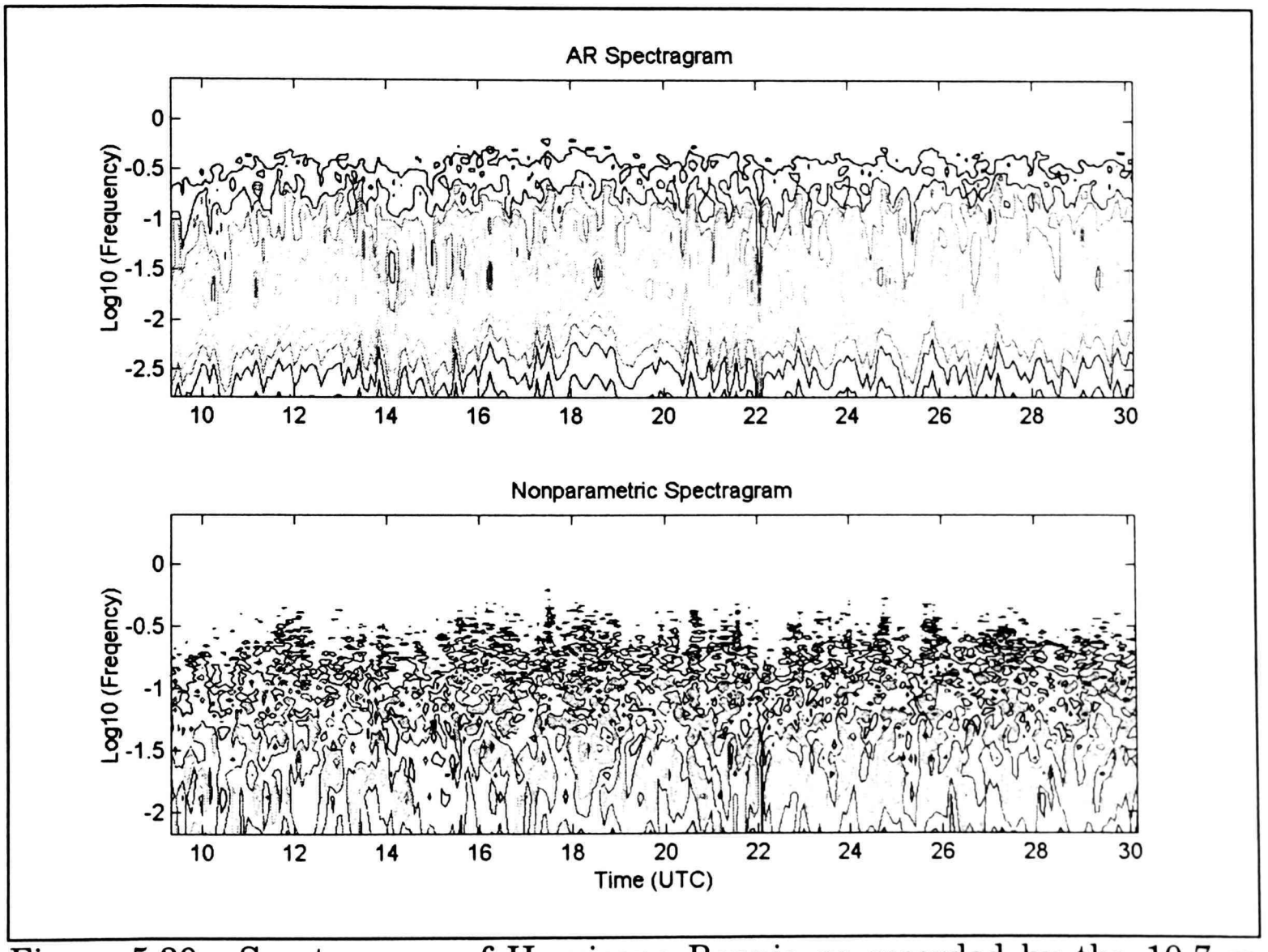

Figure 5.30. Spectragram of Hurricane Bonnie as recorded by the 10.7 m WEMITE anemometer.

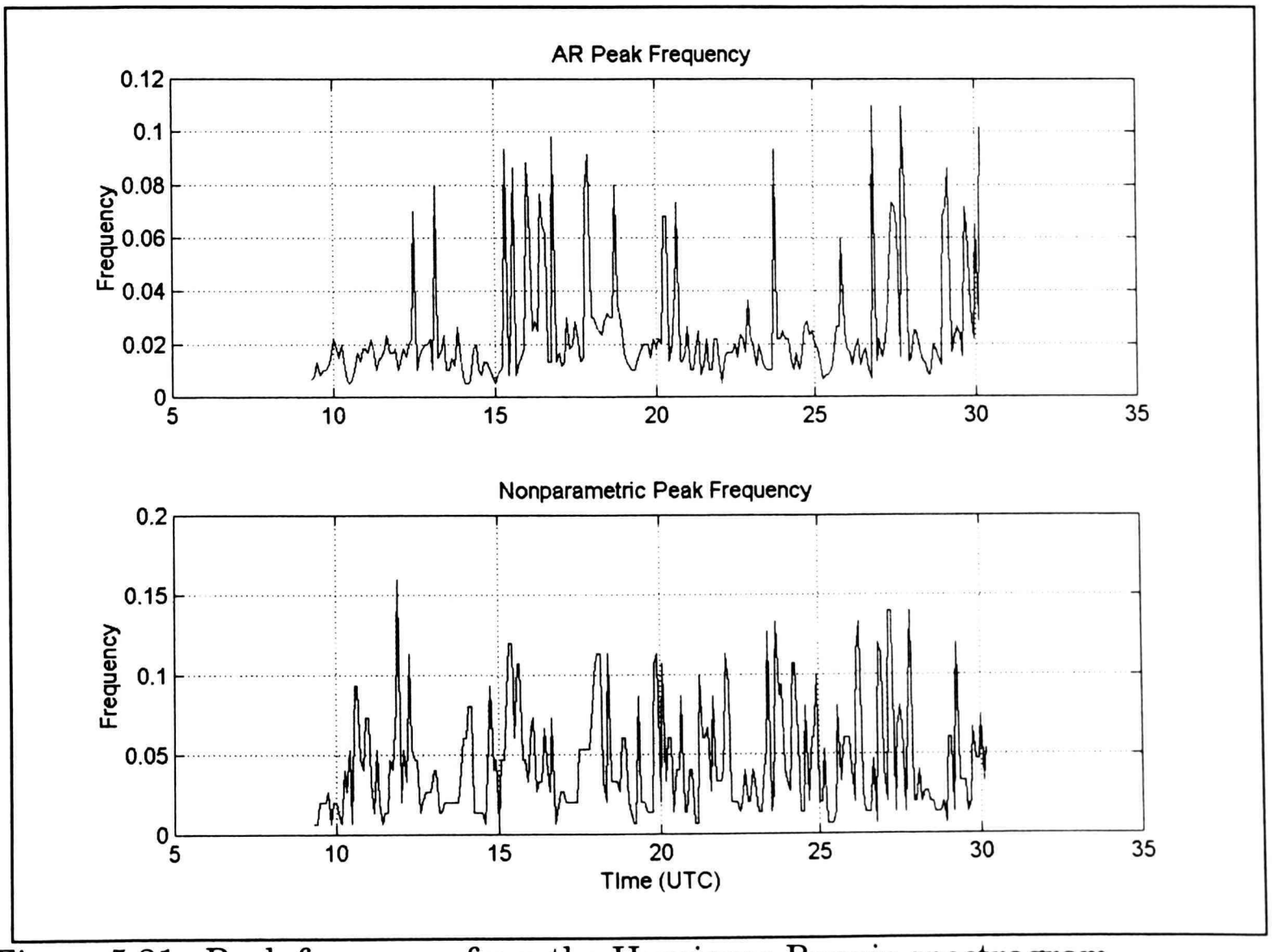

Figure 5.31. Peak frequency from the Hurricane Bonnie spectragram.

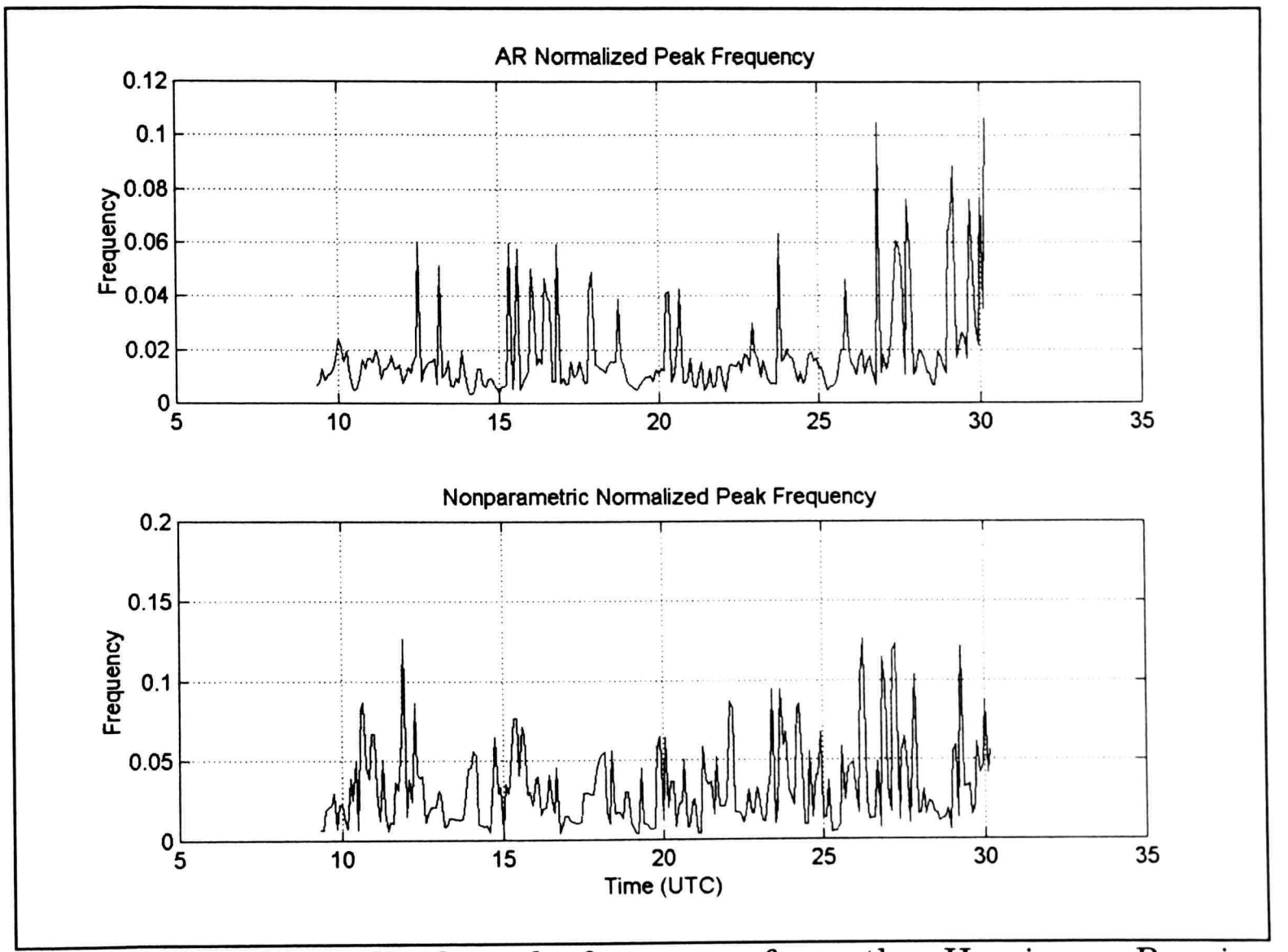

Figure 5.32. Normalized peak frequency from the Hurricane Bonnie spectragram.

Changes in normalized peak frequency should also correspond to changes in longitudinal integral scale due to the relationship between the ACF and PSD. This can be proven through examination of Figure 5.32 and Figure 5.18; when the peak frequency decreases, the integral scales increase. This shows that on average there is more energy at larger scales at these time periods.

There are many locations in the record that show concentrations of energy at certain frequencies usually between 0.03 and 0.015 Hz. These locations such as 16:10 UTC and a frequency of approximately 0.03 Hz (Log_{10} = -1.5) are interesting, but have little relationship to TI's, or GF's. However, the majority of the highest concentrations occur in locations near the center of rainbands and eyewalls where relatively high reflectivity cores exists, along with smaller integral scales and higher frequency energy.

5.4.3 Summary and Commentary

The reduced frequency response of the Wind Monitor anemometer used on WEMITE is evident in the determined PSD's. While in general this is not beneficial, it does not adversely affect the goal of relating storm-scale processes to wind characteristics, because the rate at which convective processes operate should be on the order of seconds to minutes and not at the high frequency end of the determined PSD's.

Energy at the low end of the PSD was found to be substantially higher than expected and is related to the larger integral scales found in the record. However, just as with the previously discussed turbulent characteristics, the larger integral scales and active low frequency energy at certain locations is not statistically significant. If one generates exemplar time histories based on model spectra by using inverse FFT's, it does not take many exemplars to find integral scales as large as those found in Hurricane Bonnie. So while the

spectragram offers some interesting variability it does not comprehensively lend statistical support to the fact the Hurricane Bonnie was "different" from that which was expected within the realm of a normal wind.

In general, the variability of energy is large, and the storm cannot be well represented by using one averaged PSD for the entire event. The peak of the energy content is usually related to time scales on the order 100 seconds, but concentrations in energy exist periodically at 15-30 second time scales.

5.5 Wavelet Analysis

Applying a wavelet transform to the wind speed record produces a time series of wavelet coefficients representing the correlation between the mother wavelet and the wind record. Different scales are evaluated by stretching the mother wavelet. Therefore, the shape of the mother wavelet is important because it is essentially used as a matched filter. Once the wavelet coefficients are determined, the CSD method is employed to identify statistically significant coherent structures.

5.5.1 Morlet Wavelet Analysis of Wind Speed Record

To look for areas of increased "turbulence" in the wind speed record the Morlet mother wavelet is used. The Morlet wavelet (Figure 2.14) can be matched at any scale, so small- and large-scale variations in the wind can be detected. In this case study, a 7-hour data segment from 13:15 to 20:15 UTC was used for the analysis. This data segment contains numerous locations of large longitudinal integral scales, one extreme peak in gust factor (15:08 UTC), and the passage of several storm-scale features.

The analysis produced plots (e.g., Figure 5.33) for the time period between 15:00 and 15:15 UTC. During this 15-minute time segment several coherent structures passed through the CSD using a false alarm rate of 0.2.

Although the plots are not provided in this document, throughout the 7-hour evaluation period coherent structures were found in every 15-minute data segment. The p-value generated from the entire 7-hour time period indicates that there are statistically significant coherent structures detected at a variety of scales. The plot of the p-value as a function of frequency is provided in Figure 5.34. One can see that the detection rate is higher for high frequency activity.

5.5.2 Haar Wavelet Analysis of Wind Direction Record

To identify areas of sustained wind direction changes the Haar mother wavelet is employed. These changes have been shown to occur in previous research (Schroeder et al., 1998), and have recently been found in the wind speed record obtained by TTU in Hurricane Dennis. The overshoot phenomenon, and resonant response of the Wind Monitor's directional vane complicate this analysis, but large-scale changes would indeed represent a coherent structure.

The same 7-hour data segment was used for this analysis as for the Morlet analysis. Again coherent structures are detected in each 15-minute time segment such as those shown in Figure 5.35. These structures are more prevalent at higher frequencies, but also do exist periodically at lower frequencies. The overall p-value determined from the 7-hour data set is shown in Figure 5.36. Although there are numerous statistically significant coherent structures, the detection rate is not quite as high as that produced by using the Morlet and wind speed records.

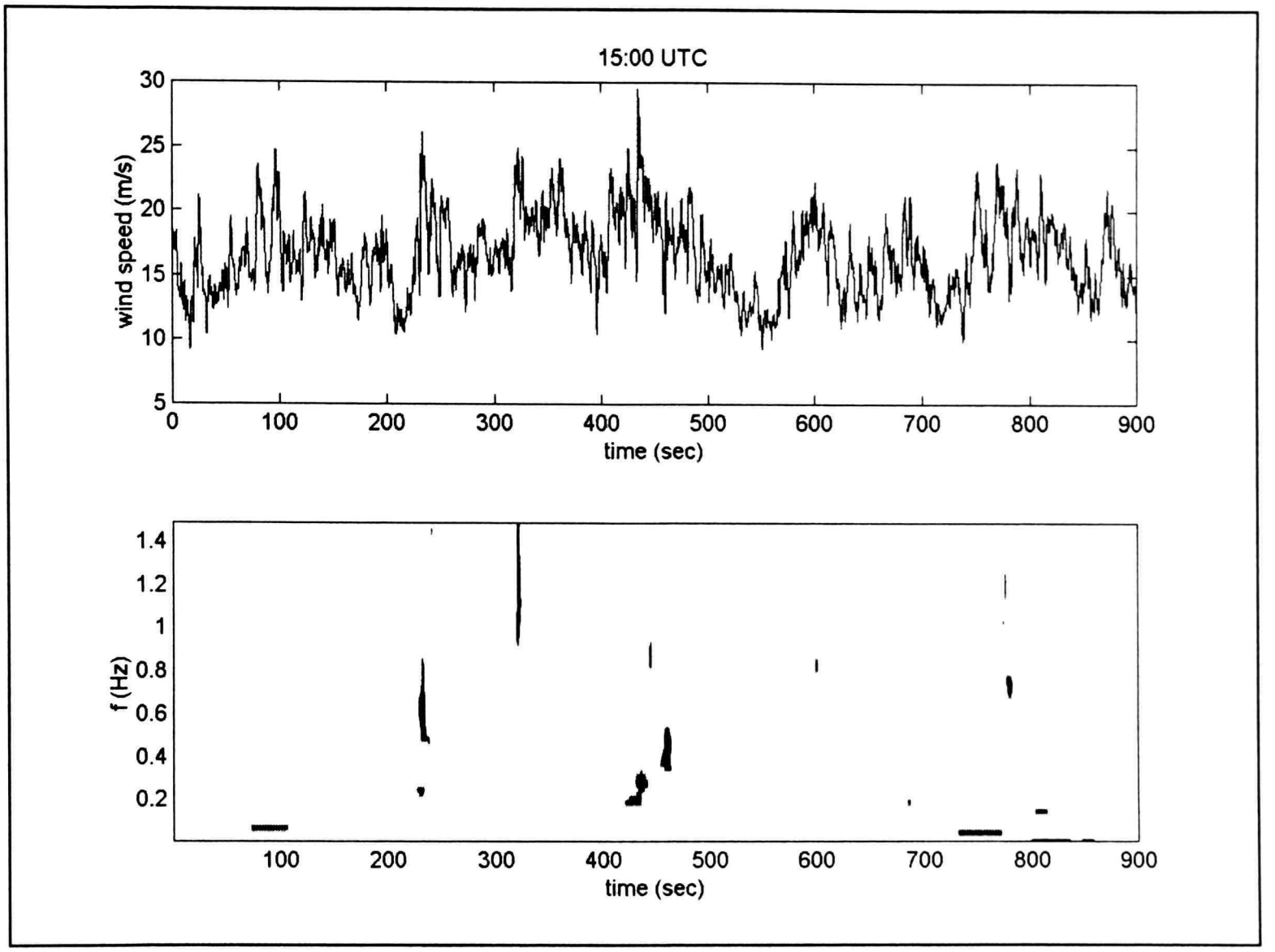

Figure 5.33. Fifteen-minute wind speed data segment starting at 15:00 UTC obtained from WEMITE during the passage of Hurricane Bonnie and the associated CSD thresholded Morlet wavelet transform.

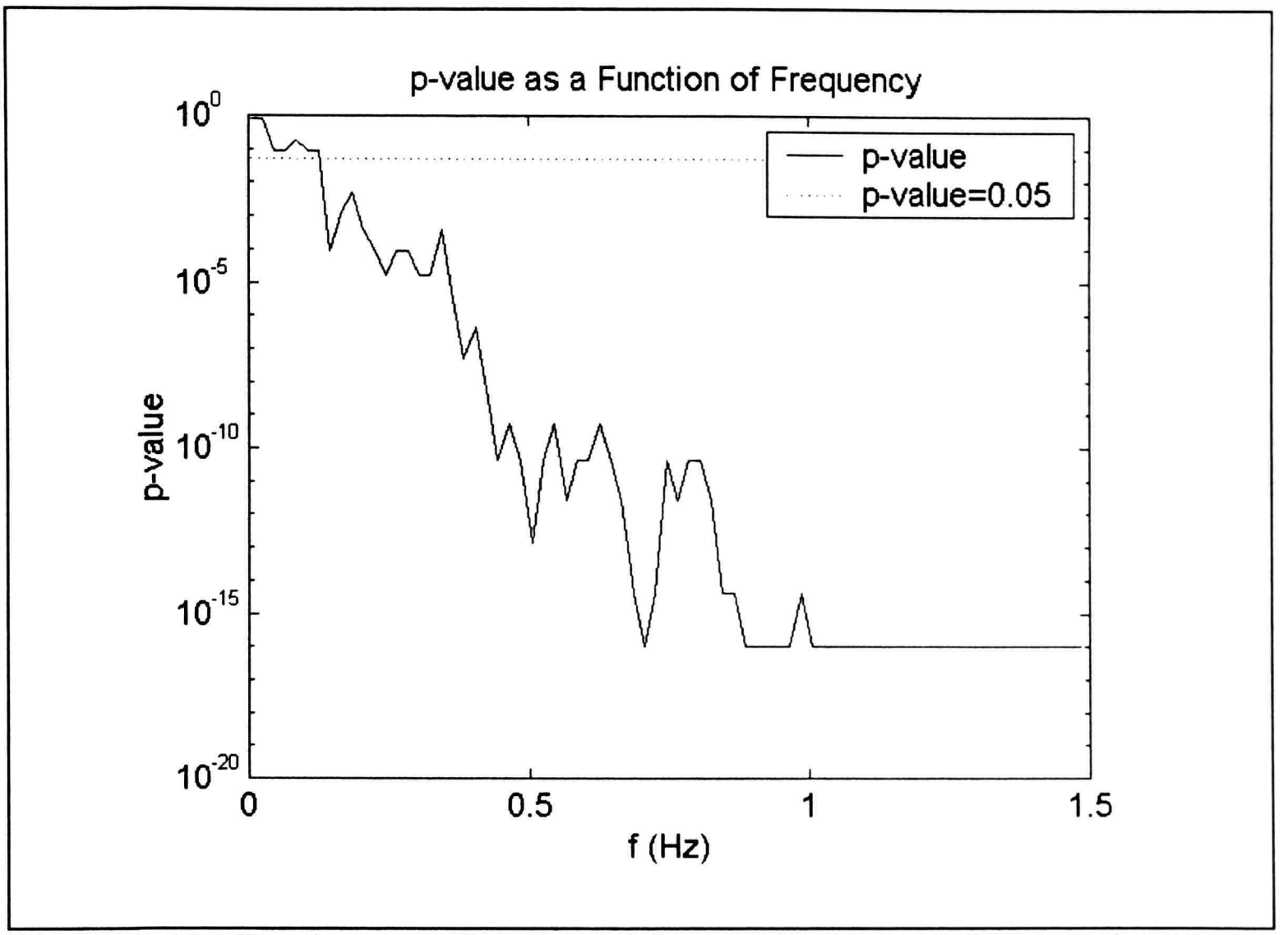

Figure 5.34. P-value as a function of frequency generated using the Morlet wavelet and CSD for the 7-hour wind speed record from 13:15 to 20:15 UTC collected by WEMITE during the passage of Hurricane Bonnie.

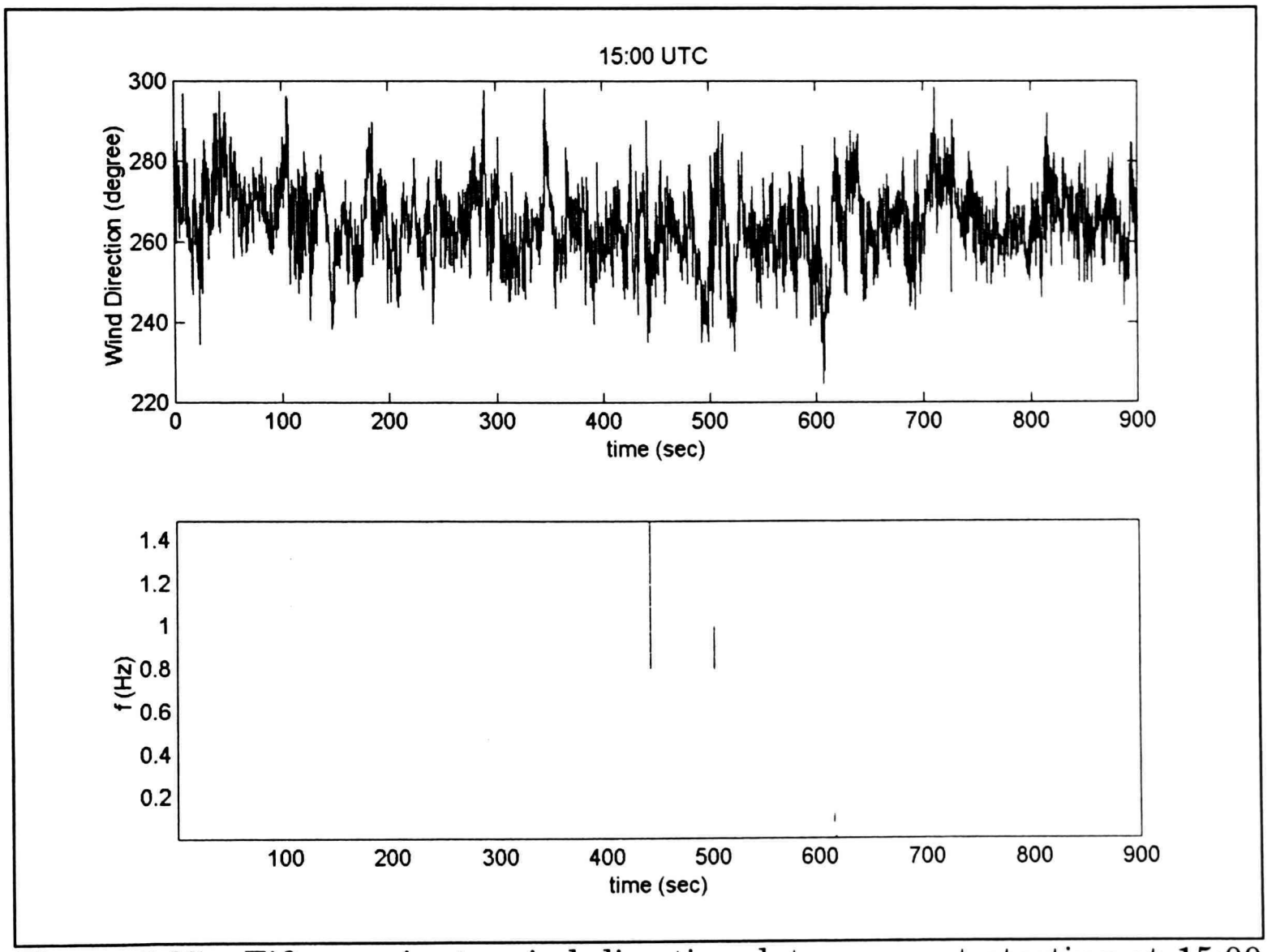

Figure 5.35. Fifteen-minute wind direction data segment starting at 15:00 UTC obtained from WEMITE during the passage of Hurricane Bonnie and the associated CSD thresholded Haar wavelet transform.

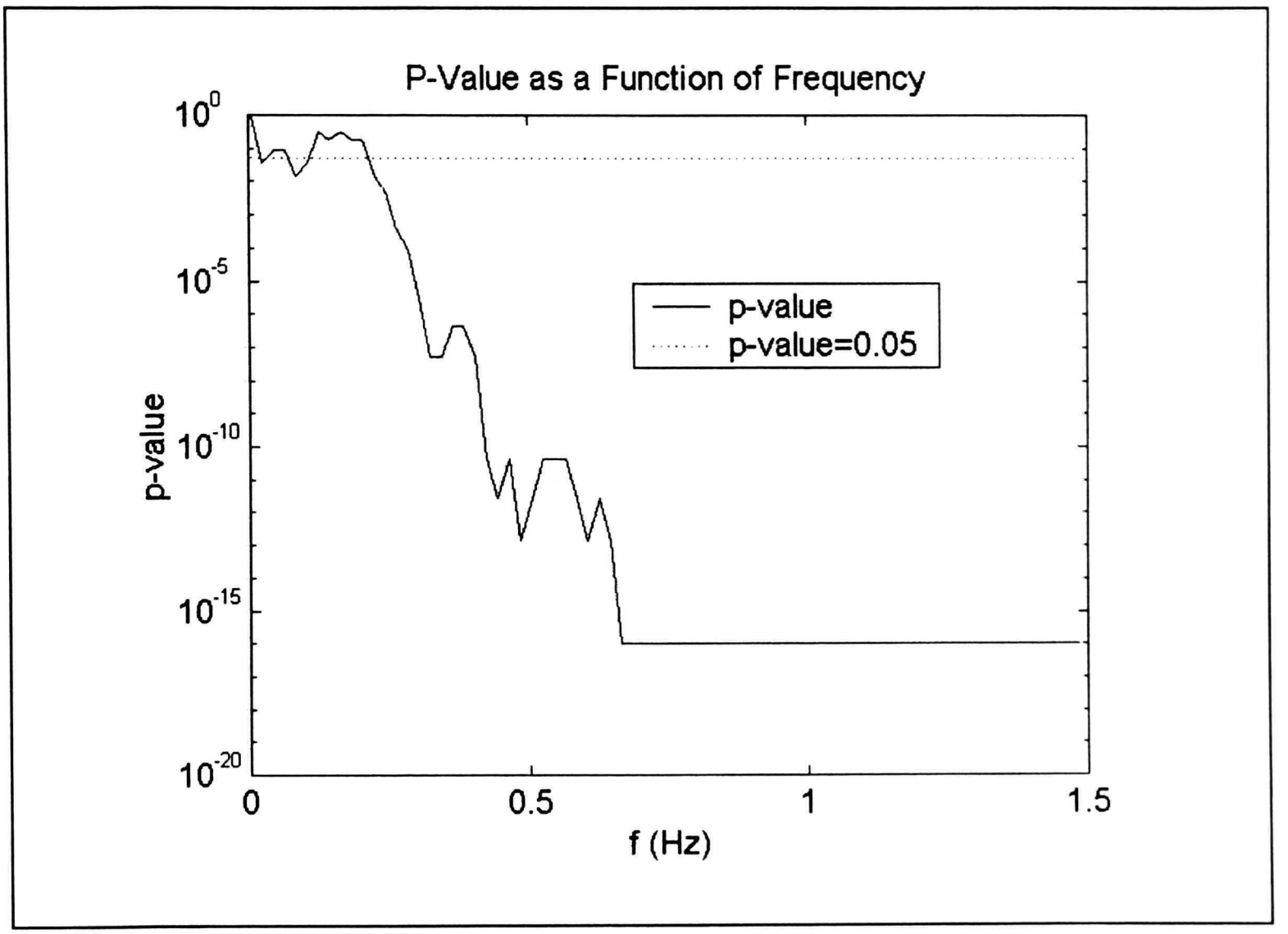

Figure 5.36. P-value as a function of frequency generated using the Haar wavelet and CSD for the 7-hour wind direction record from 13:15 to 20:15 UTC collected by WEMITE during the passage of Hurricane Bonnie.

5.5.3 Summary and Commentary

The output from the wavelet transforms after thresholding using the CSD indicate the wind speed and direction records contain coherent structures. These coherent structures are distributed throughout the analyzed 7-hour time series, and do not seem to be correlated with the passage of rainbands, the location of higher integral scales or TI's, nor are they more prevalent in higher wind speeds. Specifically, at 15:08 UTC coherent structures were identified in both the wind speed and wind direction records. As previously discussed the highest gust factor in the record for airport exposure was also found at this location. Therefore it can be concluded that a coherent structure leads to the extreme gust factor. This leads to concern that determining TI's averaged over a specific time period or employing PSD's does not provide a complete description of the extremes contained in the wind as concentrations of energy (phase dependent) may exist in the record.

5.6 Localized Correlation

As discussed several times in this manuscript, there is some visual correlation between the occurrence of larger integral scales and slightly higher turbulence intensities with the passage of rainbands. However, trying to establish a statistically meaningful correlation (scatter plot, correlation coefficient, regression, etc.) between the parameters is difficult for several reasons, including:

1. Rainbands contain different intensities of reflectivity. One rainband may contain 45 dBZ along its central axis, while the next may only contain 35 dBZ; therefore, it is difficult to correlate across multiple rainbands.

2. The larger integral scales and higher turbulence intensities do not occur when the reflectivity is most intense, nor do they occur when the reflectivity is weakest. Most activity occurs with moderate values of reflectivity.
3. The storm is not steady state at landfall, especially the eyewalls. Its forward motion is changing, and new convective activity is developing near the coastline due to forced convergence.
4. The exposure changes as the wind direction varies.
5. The 5-minute time histories are cluttered with high frequency fluctuations (noise).

To rectify these problems, a smaller segment of the storm was selected (12:40 – 18:30 UTC) for evaluation. Within this segment, the exposure for the approaching wind and the storm's forward motion remained approximately constant. This segment also does not contain any interaction with the rapidly changing eyewalls of Hurricane Bonnie. A moving average of 60 minutes (low-pass filter) was applied to the original 5-minute averaged time histories to remove the high frequency fluctuations (noise) in the signals. Then to help reveal the correlation the radar reflectivity time history was shifted forward in time by 55 minutes. This shift in time allows for the peaks in the longitudinal integral scale, and TI time histories to align with the peaks in the radar reflectivity time history (Figures 5.37 and 5.38).

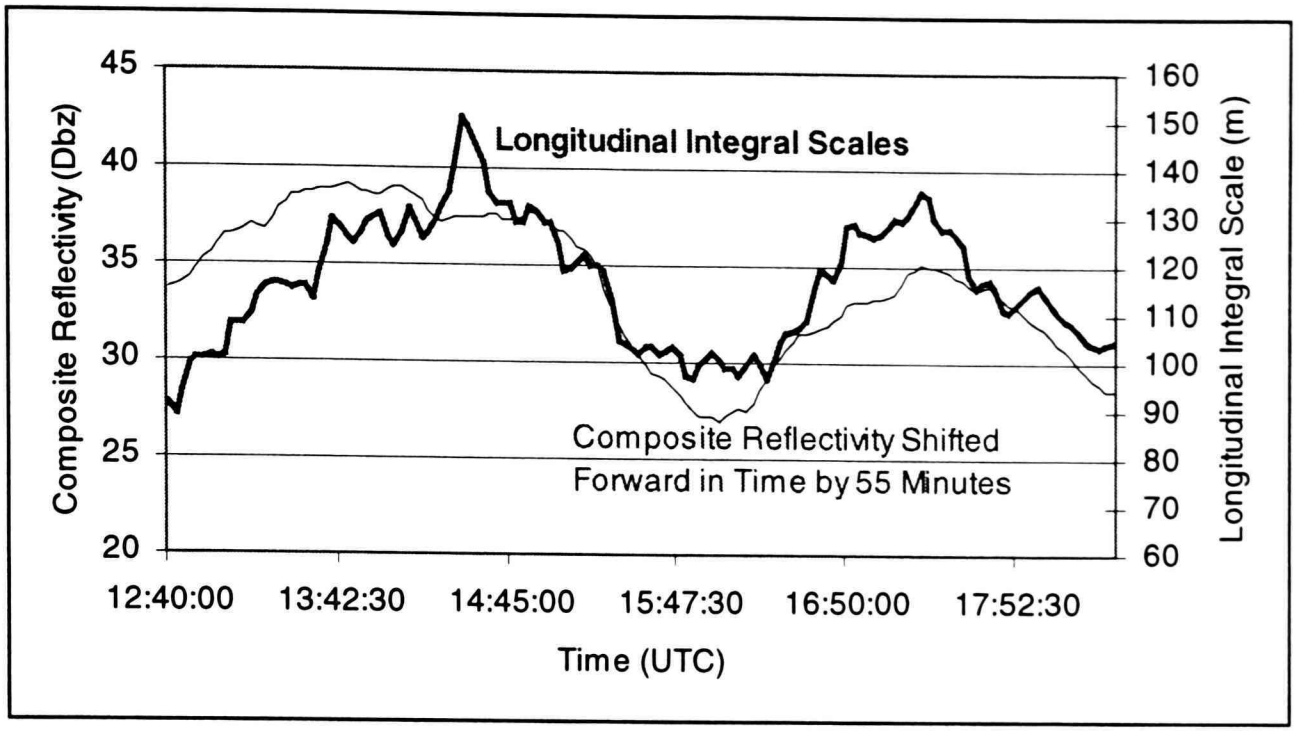

Figure 5.37. Time history of shifted composite radar reflectivity and longitudinal turbulence intensity from Hurricane Bonnie.

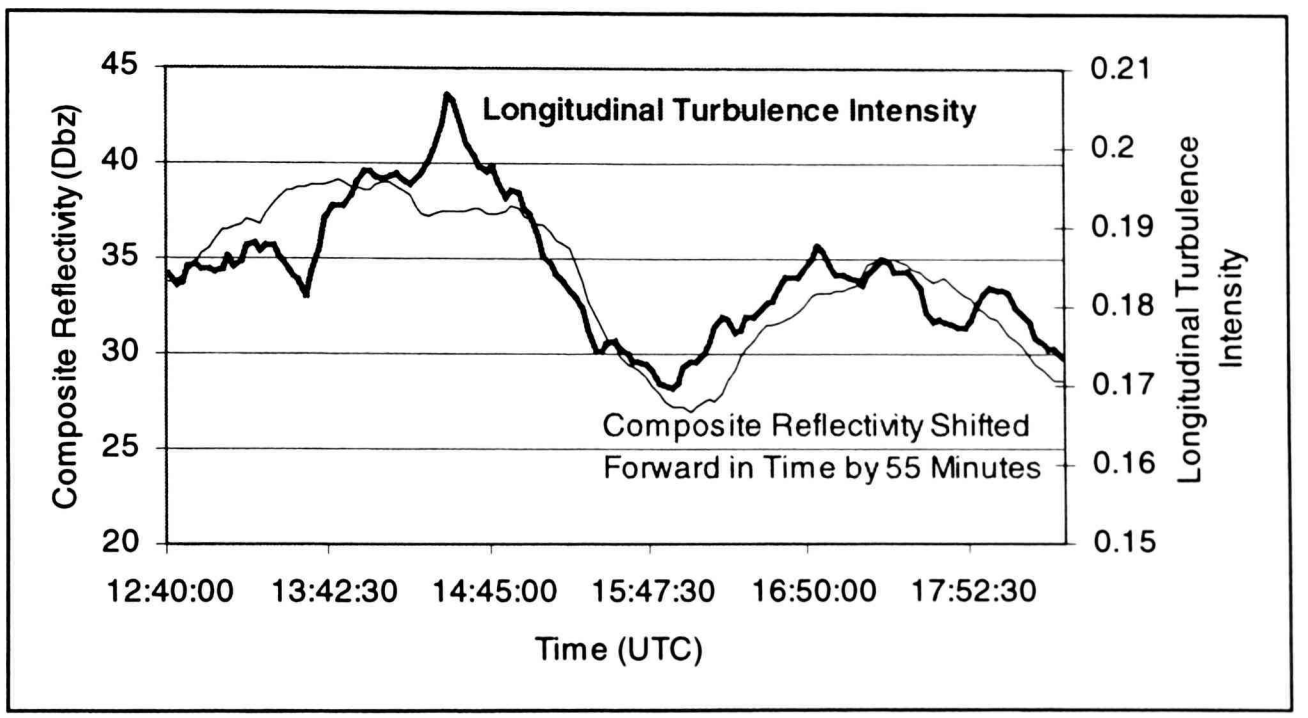

Figure 5.38. Time history of shifted composite radar reflectivity and longitudinal integral scale from Hurricane Bonnie.

The correlation between the time histories is obvious. The correlation coefficient between the composite radar reflectivity and the longitudinal TI is 0.83. For the radar reflectivity and the longitudinal integral scale, the coefficient is 0.68. As the time series progresses the wind speed is increasing,

while the pressure is decreasing, seemingly unaffected by the passage of the bands, at least once the data is smoothed to this degree. There is also a high degree of correlation between the TI's and integral scales, leading to a coefficient of 0.81. Even a correlation of 0.63 exists between the shifted composite reflectivity and the GF time history (Figure 5.39).

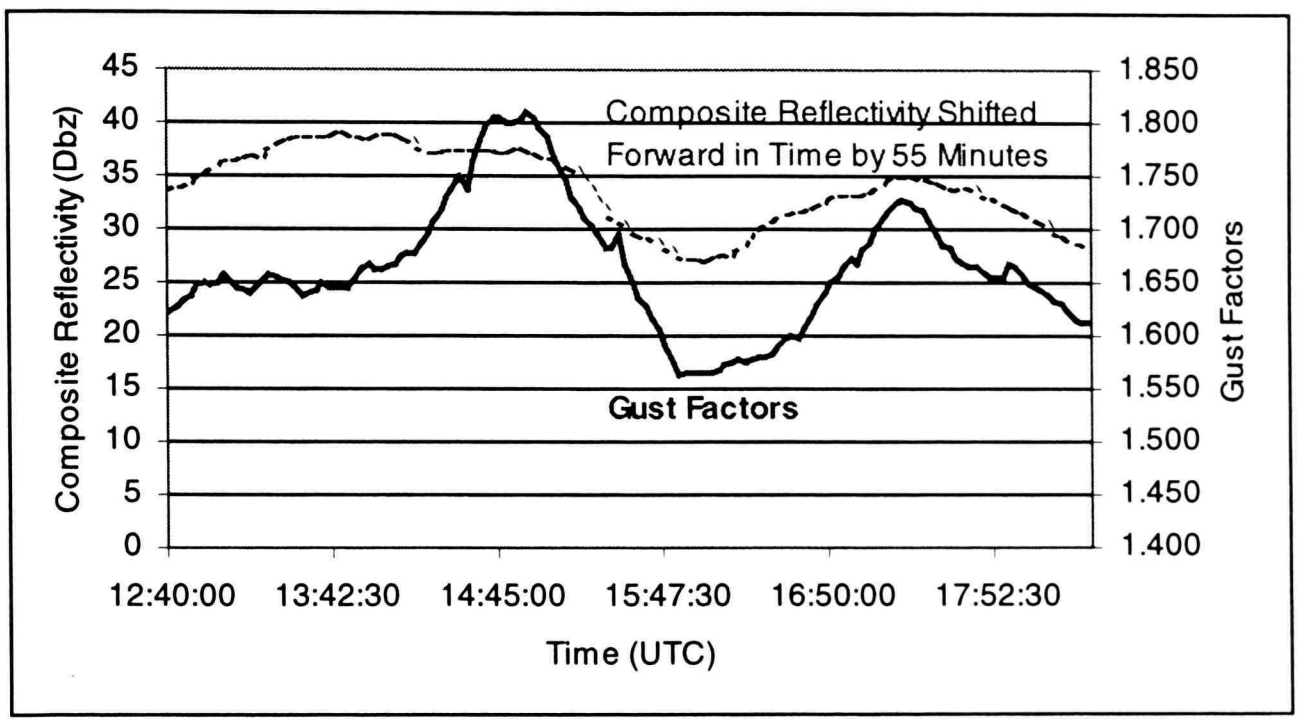

Figure 5.39. Time history of shifted composite radar reflectivity and gust factors from Hurricane Bonnie.

Therefore, it has been shown there are slow variations in the TI and longitudinal integral scale time histories that can be linked to convective activity (rainbands) with the use of radar data. The time shift of 55 minutes is related to the position, size, and movement of the rainband (convective) activity relative to the deployment site. The larger scaled turbulence is likely associated with areas of gentle downdraft which in this case are separated in time by about 55 minutes. This will be different in every hurricane and location. These downdrafts would then provided larger scale turbulence into the BL. As the central portion (beyond 18:30 UTC) of the storm makes landfall, the convective activity becomes much more complicated, as Hurricane Bonnie's eyewalls are not steady state. It seems plausible that the

intensity of convection, anemometer site proximity to landfall location and the coastline, forward motion of the storm, eyewall structure, and several other factors would affect this dependence of the TI's, GF's, and integral scales on the convection. However, in Hurricane Bonnie areas adjacent to the central axis of a rainband seem most likely to have inherently larger integral scales (50%), increased TI's (25%), and larger GF's (10-15%). As one can observe from Figures 5.37, 5.38, and 5.39, the peak averaged values in the integral scale, and TI (14:30-14:45 UTC) are approximately 150 m, and 20%, respectively. These values are still very close to the exposure C ASCE 7-98 values discussed earlier.

CHAPTER VI

CONCLUSIONS AND RECCOMENDATIONS

6.1 Summary

Due to a lack of high-resolution data from within hurricanes, little is known about the HPBL. This limited knowledge includes a lack information surrounding the wind flow characteristics that are inherent to some building standards and codes and used in wind tunnel experimentation. Of particular interest is how the storm-scale processes present in hurricanes and other severe wind events affect these wind flow characteristics. To better evaluate these characteristics WEMITE was designed and constructed.

WEMITE was designed to collect high-resolution data from within hurricanes. The 10.7 m (35 ft) tower was built to withstand sustained wind speeds of approximately 67 m/s (150 mph) and collect data continuously at sampling rates of 5-10 Hz for days without the aid of an outside power source. The system was successfully constructed and deployed by a group of undergraduate students, and graduate students from TTU. There were four deployments during the 1998 hurricane season including Hurricane Bonnie that made landfall near Cape Fear, NC, on 26 August 1998.

Unfortunately, Hurricane Bonnie was a mainly stratiform event, and thus convective activity was minimal. Nevertheless, the case study focused on examining changes in wind flow characteristics throughout the storm; thereby, highlighting the effect, if any, of storm-scale processes such as the passage of rainbands, interaction of updrafts and downdrafts, influence of meso vortices, etc. TI's, GF's, and integral scales were evaluated and contrasted to wind speed, wind direction, barometric pressure, vertical wind speed, rainfall rates, and radar reflectivity. The records were also evaluated and separated into exposure categories, and stationary and nonstationary data segments.

The longitudinal power spectral density and spectragram were developed and compared to the same meteorological characteristics. Wavelet analysis was also completed using the Morlet and Haar mother wavelets to evaluate coherent structures that may exist in the wind speed and direction records. Again the generated time series was compared to other meteorological data.

Comparisons were made to ASCE 7-98 where applicable, and the incoherent model assumption was scrutinized. Finally, conclusions were drawn and recommendations were made.

6.2 Conclusions

The conclusions drawn from this case study are based on Hurricane Bonnie alone and may be vastly different than what is found in other hurricanes. Regardless, several important conclusions can be drawn from the case study including:

1. Examination of the turbulence intensity 5-minute averaged time histories indicates that they were seemingly unaffected by the passage of rainbands and other storm-scale processes. However, close examination of the record after low pass filtering indicates that indeed higher turbulence intensities occurred in areas adjacent to the central portion of rainbands. Correlating the filtered turbulence intensity and radar reflectivity time histories proved this; the calculated correlation coefficient was 0.83. The increase in turbulence was as much as 25% for the 6-hour data segment studied in detail. This increase occurred in areas adjacent to the central axis of rainbands.
2. The mean value (18.2%) of the determined longitudinal turbulence intensity (airport exposure) matches well with the value found in ASCE 7-98 for exposure category C.

3. Nonstationarities that exist in the record do not affect the determined turbulence intensity, unless the segment contains a sharp change in direction coupled with a change in wind speed. This type of nonstationarity can artificially inflate the longitudinal and lateral turbulence intensity values.
4. Gust factors, after a low pass filter was employed, were correlated with the passage of rainbands via the use of shifted composite reflectivity. The correlation coefficient was 0.63 for the 6-hour segment and indicated increased gust factors of 10-15% for areas located adjacent to the central axis of rainbands.
5. The one exception is a peak in time history near 15:08 UTC which contained a gust factor of over 2.0 for airport exposure. The explanation of this increased localized gust factor is a 20-second peak in wind speed. This peak in wind speed is coupled with a pressure drop and subsequent rise, vertical wind speed changes, wind direction changes, and embedded in a region of larger integral scales. The size of the feature is too small to be associated with a meso-vortex, but may be associated with the boundary of a downdraft, BL induced vortex, or convective gust within a downdraft.
6. Integral scales vary widely throughout the storm. The time history suggests that there are two separate regimes of longitudinal integral scales that are not correlated with changes in exposure. One of these regimes produced integral scales that are substantially larger (50%). These larger scales usually occurred in areas adjacent to the center of rainbands. The 5-minute time history of integral scales cannot be directly statistically correlated with the radar reflectivity time history. However, following the use of a moving average filter on the 5-minute

integral scale and radar reflectivity time histories, significant correlation is revealed 0.68.

7. Nonstationarities that exist in the wind record affect the magnitude of the calculated integral scales. The result of nonstationarities in the first moment (trends) of the wind speed record is inflation of the calculated integral scales by as much as 46% due to the fact that low frequency is induced into the ACF producing more correlation at longer time periods, effectively increasing the integral scales.
8. The calculated longitudinal power spectral density indicated the Wind Monitor anemometer used on WEMITE lacks high frequency response.
9. The longitudinal power spectral density indicates there is more low frequency energy in the wind record than expected by various model spectra.
10. The spectragram indicates there are tremendous variations in the energy content of the record throughout the passage of the storm. Normalized peak frequencies vary by as much as 600%. Time periods with excesses of low frequency energy correlate to larger integral scales due to the relationship between the auto correlation function and the power spectral density. These locations cannot be proven to be statistically significant when compared to model spectra.
11. Wavelet analysis of the wind record (speed and direction) using the Morlet and Haar mother wavelets indicate the record is largely incoherent, but that it contains a statistically significant amount of coherent structures. More localized coherent structures are identified with the Morlet wavelet for the wind speed record compared to the Haar wavelet and the wind direction record.
12. The detected coherent structures cannot be correlated with any storm-scale processes via radar or reflectivity time histories. The structures

are distributed fairly evenly throughout the records. In general, they cannot be correlated with peak integral scales, TI's or GF's. Although one exception does exist, the largest peak in GF is correlated locally with a coherent structure in the wind speed and direction time history.

6.3 Recommendations

Based on the completed project and case study, several recommendations can be made, these include:

1. Since Hurricane Bonnie was a fairly stratiform storm at landfall, the same efforts should be repeated for another storm(s). Increased convective activity may further enhance the increase in longitudinal integral scales, turbulence intensities, and gust factors over those seen in this event.
2. Additional high-resolution wind speed data should be collected. Assuming a larger data base can be constructed, the extreme values can be better evaluated for a variety of storm characteristics (intensity, forward motion, convective activity, etc.) Given recent finding in associated research, special attention should be paid to major hurricanes (category 3 and higher).
3. The collection effort should be coupled with a DOW to evaluate the effect of the recently documented boundary layer rolls.
4. The present instrumentation should be coupled with additional wind speed equipment including UVW and sonic anemometers. This will increase the high-frequency resolution of the data and allow for comparison of the high-frequency energy present in a hurricane wind to model spectra.
5. Conclusions about the interaction of storm-scale processes and boundary layer wind flow characteristics should not be made based solely on the evaluation of turbulence intensities and gust factors.

Additional information from evaluating integral scales and/or spectragrams, as well as other signal processing techniques, offers hope for a more comprehensive understanding of the turbulent nature of the wind.

LIST OF REFERENCES

Acevedo, O. C., D. C. Fitzjarrald, and R. K. Sakai, 1997: Detecting Coherent Structures in Water Vapor Series over a Deciduous and a Boreal Forest. Proc., 12th Conf. Boundary Layers and Turbulence, Vancouver, BC, 190-191.

Arya, S. P., 1988: Introduction to Micrometeorology. Academic Press, San Diego, 307 pp.

ASCE/ANSI 7-98, 1999: Minimum Design Loads for Buildings and Other Structures. American Society of Civil Engineers, New York, 168 pp.

Atkinson, G. D., 1974: Investigation of Gust Factors in Tropical Cyclones. U.S. Fleet Weather Central Tech. Note JTWC 74-1, 9 pp.

Avila, L. A., 1999: Highlights of the 1998 Atlantic Hurricane Season: Year of Landfalls. Preprints, 23th Tech. Conf. Hurricanes and Tropical Meteorology, Dallas, Amer. Meteor. Soc., 1282-1285.

Bendat, J. S., and A. G. Piersol, 1986: Random Data, Analysis and Measurement Procedures. John Wiley and Sons, New York, 566 pp.

Black, P. G., and F. D. Marks, 1991: The Structure of an Eyewall Meso-Vortex in Hurricane Hugo. Preprints, 19th Tech. Conf. Hurricanes and Tropical Meteorolgoy, Miami, Amer. Meteor. Soc., 579-582.

Black, P. G., 1992: Evolution of Maximum Wind Estimates in Typhoons. Proc. ICSU/WMO International Symposium on Tropical Cyclone Disasters, Beijing, 104-115.

Bradbury, W.M.S., D. M. Deaves, J. C. R. Hunt, R. Kershaw, K. Nakamura, M. E. Hardman, and P. W. Bearman, 1994: The Importance of Convective Gusts. Meteorol. Appl., 1, 365-378.

Box, G. E. P., and G. M. Jenkins, 1976: Time Series Analysis: Forecasting and Control. Holden Day, San Francisco, 553 pp.

Brockwell, P. J., and R. A. Davis, 1991: Time Series Theory and Methods. Springer-Verlag, New York, 577 pp.

Cermak, J. E., A. G. Davenport, E. J. Plate, and D. X. Vieges, 1983: Wind Climate in the City. Proc., NATO Advanced Study Institute on Wind Climate in Cities, Waldbronn, Germany.

Choi, E. C. C., 1978: Characteristics of Typhoons Over the South China Sea, J. Indust. Aerodynam., **3**, 353-365.

Choi, E. C. C., 1983: Gradient Height and Velocity Profile during Typhoons, J. Wind Eng. Indust. Aerodynam., **13**, 31-41.

Chuen, E. C., 1971: Correlation and Spectral Functions of Atmospheric Turbulence, Proc., 3rd Intern. Conf. Wind Effects on Buildings and Structures, Tokyo, 45-55.

Cohen, L., 1995: Time Frequency Analysis. Prentice-Hall, Englewood Cliffs, NJ, 299 pp.

Conder M. R., R. E. Peterson, J. L. Schroeder, and D. A. Smith, 1999: Comparison of Hurricane Wind Data from Hurricane Bonnie: The Texas Tech Wind Engineering Mobile Instrumented Tower Experiment (WEMITE) and the NWS Wilmington ASOS. Proc. 13th Symp. Boundary Layers and Turbulence, Dallas, 484-487.

Cook, N. J., 1985: The Designer's Guide to Wind Loading of Building Structures – Part 1. Butterworths, London, England, 371 pp.

Dunyak, J., X. Gilliam, and D. A. Smith, 1999: Intermittent Turbulence in Near-Gound Wind, submitted to: J. Wind Eng. Indust. Aerodynam.

Durst, C. S., 1960: Wind Speeds over Short Periods of Time. Meteor. Mag., **89**, 181-187.

Emanuel, K. A., 1988: Toward a General Theory on Hurricanes. American Scientist, **76**, 370-379.

ESDU, 1974: Characteristics of Atmospheric Turbulence near the Ground, Part 1: Definitions and General Information. Item No. 74030, Engineering Sciences Data Unit, London, England, 14 pp.

ESDU, 1982: Strong Winds in the Atmospheric Boundary Layer. Item No. 82026, Engineering Sciences Data Unit, London, England, 51 pp.

Franklin, J. L., M. L. Black, and S. E. Feuer, 1999: Wind Profiles in Hurricanes Determined by GPS Dropwindsondes. Preprints, 23th Tech. Conf. Hurricanes and Tropical Meteorology, Dallas, Amer. Meteor. Soc., 167-168.

Fujita, T. T., 1980: In Search of Mesoscale Windfields in Landfalling Hurricanes. Preprints, 13th Tech. Conf. Hurricanes and Tropical Meteorology, Miami Beach, Amer. Meteor. Soc., 43-57.

Fujita, T. T., 1992: Damage Survey of Hurricane Andrew in South Florida. Storm Data, **34**, 25-30.

Garrat, J., 1992: The Atmospheric Boundary Layer. Cambridge University Press, New York, 316 pp.

Gilliam, X., 1998: Statistical Techniques for Identification of Coherent Structures by Wavelet Analysis. Doctoral Dissertation, Texas Tech University, Lubbock, Texas, 92 pp.

Guertz C. P. W, 1997: Wind-Induced Pressure Fluctuations on Building Facades. Technische Universiteit Eindhoven, Faculteit Bouwkunde, Vakgroep Constructief Ontwerpen, 255 pp.

Gumbel, E. J., 1958: Statistics of Extremes. Columbia University Press, New York, 375 pp.

Hall, C. D., Hunt, J. C. R. Radford, A .N. Carruthers, D. J., and W. S. Weng, 1992: Forecasting Tropical Cyclones and Near Surface Wind Conditions. Proc., ICSU/WMO International Symposium on Tropical Cyclone Disasters, Beijing, 232-257.

Holmes, J. D., 1989: Course Notes: Random Processes with Applications in Wind Engineering. Department of Civil Engineering, Texas Tech University, Lubbock, Texas, 89 pp, (unpublished).

Houze, R.A., 1993: Cloud Dynamics. Academic Press, Inc., San Diego, 573 pp.

Ishizaki, H., 1983: Wind Profiles, Turbulence intensities, and Gust Factors for Design in Typhoon-Prone Regions. J. Wind Eng. Indust. Aerodynam., **13**, 55-66.

Maeda, J., 1996: Gusty Wind Observations Utilizing a Measurement Array of High Density. Proc. 3rd, Ann. Intl. Colloq. Bluff Body Aerodynam. and Applied Fluid Mechanics, C IV 1-C IV 4.

Maloney, S. P., 1994: The Effect of Atmospheric Stability on Characteristics of Surface Flows, Master's Thesis, Texas Tech University, Lubbock, Texas 90 pp.

Krayer, W. R., and R. D. Marshall, 1992: Gust Factors Applied to Hurricane Winds. Bull. Amer. Meteor. Soc., **73**, 613-617.

Meyers, S. D., B. G. Kelley, and J. J. O'Brien, 1993: An Introduction to Wavelet Analysis in Oceanography and Meteorology: with Application to the Dispersion of Yanai Waves. Mon. Wea. Rev., **2**, 2858-2866.

Mitsuta, Y., and O. Tsukamoto, 1989: Studies on Spatial Structure of Wind Gust. J. Appl. Meteor., **28**, 1155-1160.

Naito, G., 1988: Turbulent Properties and Spectral Behaviors of Ocean Winds Observed at an Offshore Tower. J. Wind Eng. Indust. Aerodynam., **28**, 51-59.

Pasch, R. J., and L. A. Avila, 1992: Atlantic Hurricane Season of 1991. Mon. Wea. Rev., **120**, 2671-2681.

Powell, M. D., 1987: Changes in the Low-Level Kinematic and Thermodynamic Structure of Hurricane Alicia (1983). Mon. Wea. Rev., **110**, 75-99.

Powell, M. D., 1990: Boundary Layer and Dynamics in Outer Hurricane Rainbands, Part I: Mesoscale Rainfall and Kinematic Structure. Mon. Wea. Rev., **118**, 891-917.

Powell, M. D., F. D. Marks, and P. G. Black, 1984: The Asymmetic Structure of Alicia's Windfield at Landfall. Proc., ASCE Specialty Conference: Hurricane Alicia: One Year Later, 40-54.

Powell, M. D., and P. G. Black, 1990: The Relationship of Hurricane Reconnaissance Flight-Level Wind Measurements to Winds Meastured by NOAA's Oceanic Platforms. J. Wind Eng. Indust. Aerodynam., **36**, 381-392.

Powell, M. D., P. P. Dodge, and M. L. Black, 1991: The Landfall of Hurricane Hugo in the Carolina: Surface Wind Distribution. Wea. Forecasting, **6**, 379-399.

Powell, M. D., S. H. Houston, and T. A. Reinhold, 1992: Standardizing Wind Measurements for the Documentation of Surface Wind Fields in Hurricane Andrew. Proc., ASCE Specialty Conference: Hurricanes of 1992, Miami, Florida, 52-68.

Powell, M. D., Houston, S. H. and Reinhold, T.A., 1996a: Hurricane Andrew's Landfall in South Florida. Part I: Standardizing Measurements for the Documentation of Surface Wind Fields. Wea. Forecasting, **11**, 304-328.

Powell, M. D., and Houston, S.H., 1996b: Hurricane Andrew's Landfall in South Florida. Part II: Surface Wind Fields and Potential Real-time Applications. Wea. Forecasting, **11**, 329-349.

Powell, M. D., T. A. Reinhold, and R. D. Marshall, 1999a: GPS sonde Insights on Boundary Layer Wind Structure in Hurricanes. Proc., 10th Int. Conf. Wind Eng., Copenhagen, 307-314.

Powell, M. D. and S. H. Houston, 1999b: Comments on " A multiscale Numerical Study of Hurricane Andrew (1992). Part I: Explicit Simulation and Verification, Mon. Wea. Rev., **127**, 1706-1710.

Reed, D. A., and R. H. Scanlan, 1984: Autoregressive Representation of Longitudinal, Lateral, and Vertical Turbulence Spectra. J. Wind Eng. Indust. Aerodynam., **17**, 199-214.

Schroeder, J. L., D. A. Smith, and R. E. Peterson, 1998: Variation of Turbulence Intensities and Integral Scales during the Passage of a Hurricane. J. Wind Eng. Indust. Aerodynam. **77 & 78**, 65-72.

Schroeder, J. L., and D. A. Smith, 1999: Hurricane Bonnie Wind Flow Characteristics as Determined from WEMITE. Proc., 10th Int. Conf. Wind Eng., Copenhagen, 329-335.

Simiu, E., and R. H. Scanlan, 1986: Wind Effects on Structures: An Introduction to Wind Engineering. John Wiley and Sons, New York, 589 pp.

Simpson, R.H., and H. Riehl, 1981: The Hurricane and Its Impact. Louisiana State University Press, Baton Rouge, 398 pp.

Smith, D. A., 1993: Stochastic Analysis of Wind Data, Doctoral Dissertation, Texas Tech University, Lubbock, Texas, 219 pp.

Sparks, P. R, and X. Yang, 1998: The Nature of Hurricane Wind Climate in the US. Proc., 8th US Nat. Conf. Wind Eng., Baltimore.

Sparks, P. R., and Z. Huang, 1999: Wind Speed Characteristics in Tropical Cyclones. Proc., 10th Int. Conf. Wind Eng., Copenhagen, 343-350.

Teunissen, H. W., 1980: Structure of Mean Winds and Turbulence in the Planetary Boundary Layer over Rural Terrain. Boundary-Layer Meteor., **19**, 187-221.

Thomas, G., 1996: Identification of Transfer Functions for Wind-induced Pressures on Prismatic Buildings, Doctoral Dissertation, Texas Tech University, Lubbock, Texas 222pp.

Tieleman, H., 1992: Wind Engineering Seminar Series, Seminar Notes, Dept. of Civil Engineering, Texas Tech University, Lubbock, Texas, (unpublished).

Tieleman, H., 1995: Universality of Velocity Spectra. J. Wind Eng. Indust. Aerodynam., **56**, 55-69.

Wakimoto, H. E., and P. G. Black, 1993: Hurricane Andrew in Florida: Dynamics of Disaster. Bull. Amer. Meteor. Soc., **77**, 543-549.

Willis, G. E., and Deardorff, J. W., 1976: On the Use of Taylor's Translation Hypothesis for Diffusion in the Mixed Layer. Quart. J. Roy. Meteor. Soc., **102**, 817-822.

Wurman, J., and J. Winslow, 1998: Intense Sub-Kilometer Boundary Layer rolls in Hurricane Fran. Science, **280**, 555-557.

Zao, J., 1992: Analysis of Low-Level Thunderstorm Winds, Master's Thesis, Texas Tech University, Lubbock, Texas, 145 pp.

Zhang D., L. Yabao, and M. K. Yau, 1999: Surface Winds at Landfall of Hurricane Andrew (1992) -- A Reply, Mon. Wea. Rev., **127**, 1711-1721.